福井県立恐竜博物館
FUKUI PREFECTURAL
DINOSAUR
MUSEUM

Osteology of *Fukuivenator paradoxus*: a bizarre maniraptoran theropod from the Early Cretaceous of Fukui, Japan

Soki HATTORI, Soichiro KAWABE, Takuya IMAI, Masateru SHIBATA, Kazunori MIYATA, Xing XU and Yoichi AZUMA

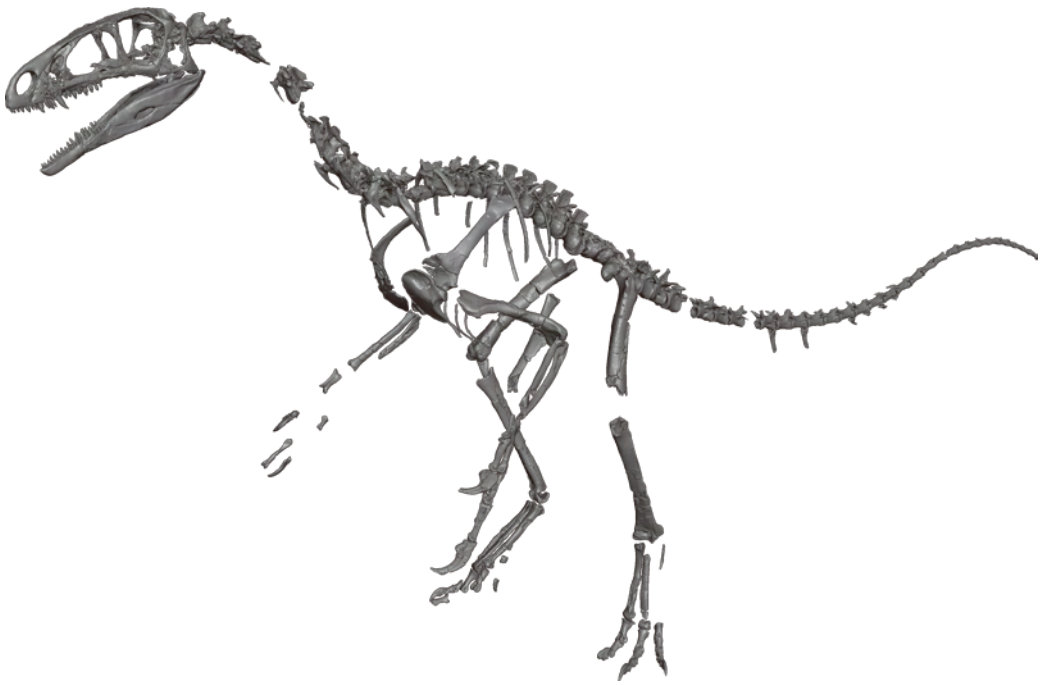

Reprinted from

Memoir of the Fukui Prefectural Dinosaur Museum 20: 1–82, December 2021

Memoir of the Fukui Prefectural Dinosaur Museum 20: 1–82 (2021)

ARTICLE

OSTEOLOGY OF *FUKUIVENATOR PARADOXUS*: A BIZARRE MANIRAPTORAN THEROPOD FROM THE EARLY CRETACEOUS OF FUKUI, JAPAN

Soki HATTORI[1,2], Soichiro KAWABE[1,2], Takuya IMAI[1,2], Masateru SHIBATA[1,2], Kazunori MIYATA[2], Xing XU[3] and Yoichi AZUMA[1,2]

[1]Institute of Dinosaur Research, Fukui Prefectural University, 4-1-1 Matsuoka Kenjojima, Eiheiji, Fukui 910-1195, Japan
[2]Fukui Prefectural Dinosaur Museum, 51-11 Terao, Muroko, Katsuyama, Fukui 911-8601, Japan
[3]Key Laboratory of Vertebrate Evolution and Human Origins, Institute of Vertebrate Paleontology and Paleoanthropology, Chinese Academy of Sciences, Beijing 100044, China

ABSTRACT

A bizarre coelurosaurian theropod *Fukuivenator paradoxus* is known only from the holotype specimen preserving majority of the skeleton from the Kitadani Dinosaur Quarry of the Lower Cretaceous Kitadani Formation, Tetori Group, Fukui, Japan. With aids of computed tomography techniques, a re-examination of the holotype specimen reveals additional features of *Fukuivenator* which was unobservable in the original description, such as the presence of parietals and a quadrate, and the fusion of the posteriormost caudal vertebrae. The thorough description in this study results in the emendation of diagnosis including the retraction of the large promaxillary fenestra subequal in size to maxillary fenestra, and the addition of the large maxillary fenestra expanded well dorsally above the suprantral strut. Expansion of morphological information elaborates the phylogenetic dataset, resulting in locating *Fukuivenator* as an unambiguous member of Maniraptora at the basalmost position of Therizinosauria. This phylogenetic position of *Fukuivenator* is supported by several therizinosaurian synapomorphies such as the subotic recess on the braincase, 11 cervical vertebrae some of which having two pneumatic foramina, and distal articular condyles on the anterior surface of the humerus. Among numerous diagnostic features, eight characters shared with some non-maniraptoran coelurosaurs and five shared with different clades within Maniraptora, highlighting the notably mosaic condition of *Fukuivenator* proposed in the original description. The combination of characters for herbivorous and carnivorous diets suggests the omnivory of *Fukuivenator*, projecting the dietary shift in the earliest evolutionary stage of Therizinosauria. Also, the large olfactory ratio revealed by the revised brain endocast highlights the unusually high olfactory acuity further developed than the plesiomorphic condition, implying that the acute sense of smell might be a characteristic of therizinosaurian theropods.

Key words: Maniraptora, Coelurosauria, Theropoda, Early Cretaceous, Kitadani Formation, Tetori Group, Fukui, Japan

服部創紀・河部壮一郎・今井拓哉・柴田正輝・宮田和周・徐星・東 洋一（2021）*Fukuivenator paradoxus* の骨学：福井県の下部白亜系から産出した特異なマニラプトル類．福井県立恐竜博物館紀要 20：1–82.

Fukuivenator paradoxus は，北谷恐竜化石発掘現場に露出する下部白亜系手取層群北谷層から発見された Coelurosauria の一種である．そのホロタイプについて CT スキャンを行ったところ，原記載では見出されなかった部位や特徴が明らかとなったため，改めて記載を行った．その結果，複数の標徴形質の見直しを行う必要性が生じた．また，様々な形質状態の再評価及び拡充を行い，改めて系統解析をしたところ，本種を Maniraptora の一種とし，さらに Therizinosauria の基盤に位置づける結果が得られた．ホロタイプには多数の固有派生形質が認められたが，様々なクレードとの同形形質が含まれていた．また，2 通りの食性を示す特徴の組み合わせは，本種の雑食性を示すとともに，Therizinosauria の進化史初期における食性の変化を物語っている．さらに，脳エンドキャストの形状から，本種の嗅球が他の獣脚類に比べて非常に大きいことがわかった．このことから，Therizinosauria には共通して鋭い嗅覚が備わっていたことが示唆される．

INTRODUCTION

Fukuivenator paradoxus is a small-sized theropod dinosaur from the Lower Cretaceous Kitadani Formation of the Tetori Group, Fukui, Japan (Azuma et al., 2016). It represents the fifth dinosaur species recovered in the Kitadani Dinosaur Quarry following *Fukuiraptor kitadaniensis* (Azuma and Currie, 2000), *Fukuisaurus tetoriensis* (Kobayashi and Azuma, 2003), *Fukuititan nipponensis* (Azuma and Shibata, 2010) and *Koshisaurus katsuyama* (Shibata and Azuma, 2015), increasing the known diversity of dinosaur fauna of the formation. The Kitadani Dinosaur Quarry is located in the bank of the Sugiyama River in the northern part of Katsuyama, Fukui (36 ° 7’ 17.9” N, 136 ° 32’ 41.4” E). The formation cropping out in the quarry represents alternating beds of coarse to fine sandstone and siltstone, which

Received June 30, 2021. Accepted October 11, 2021.
Corresponding author—Soki HATTORI
E-mail: s-hattori＊fpu.ac.jp

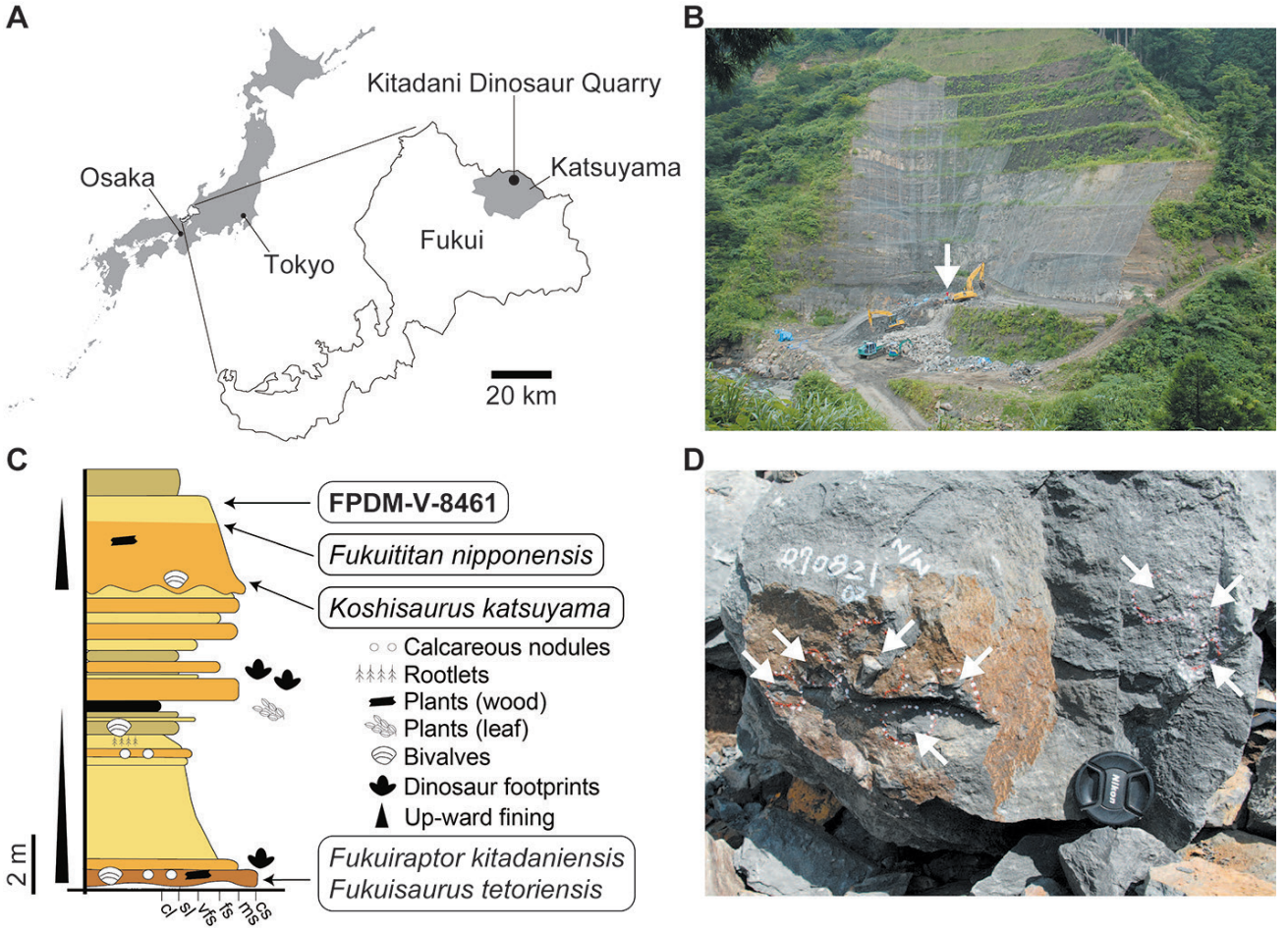

FIGURE 1. Locality and horizon for *Fukuivenator paradoxus*. **A**, regional map for the location of Fukui in Japan, and the Kitadani Dinosaur Quarry in Fukui; **B**, photograph of the Kitadani Dinosaur Quarry in 2007 with an arrowhead indicating the locality for FPDM-V-8461; **C**, stratigraphic section of the part of the Kitadani Formation in the Kitadani Dinosaur Quarry, representing the stratigraphic position of FPDM-V-8461; **D**, occurrence of FPDM-V-8461 in the field with arrowheads indicating exposed elements.

yield abundant plant, invertebrate, vertebrate, and trace fossils (Goto et al., 2002; Azuma, 2003; Shibata and Goto, 2008; Fig. 1). The Aptian age is inferred for the formation based on the co-occurrence of multiple species of charophyte gyrogonites (Kubota, 2005; Sano, 2015) as well as on the suggested stratigraphic correlations of the formations within the Tetori Group (Sano and Yabe, 2017). Furthermore, the tuff beds zircons U-Pb age of 121.2±1.1 Ma from the directly underlying Akaiwa Formation (Sakai et al., 2019) narrows the inferred age for the Kitadani Formation into middle to late Aptian.

While the holotype specimen of *Fukuivenator paradoxus* (FPDM-V-8461) was collected within a 50 by 50 cm area without any material identifiable to other animals and has been described in Azuma et al. (2016), subsequent preparations supplemented by computed tomography (CT) techniques has enabled us to observe additional morphological features and previously-unrecognized elements. Here, we provide a complete description of the holotype specimen and conduct a phylogenetic analysis taking previously unrecognized morphological features and elements into account. The present study confirms a peculiar set of features of *Fukuivenator*, as suggested by Azuma et al. (2016), and suggests an alternative phylogenetic position of the taxon as a basal maniraptoran.

MATERIAL

The material of *Fukuivenator paradoxus* described in this work is the holotype, FPDM-V-8461.

Institutional abbreviations: FPDM, Fukui Prefectural Dinosaur Museum, Fukui, Japan; IGM, Mongolian Institute of Geology, Ulaanbaatar, Mongolia; IPFUB, Institut für Geologische Wissenschaften, Fachrichtung Paläontologie, Freie Universität, Berlin, Germany; UMNH, Natural History Museum of Utah, Salt Lake City, Utah, USA.

METHODS

Computed tomography analyses

Individual skeletal elements of FPDM-V-8461 were analyzed using a veterinary X-ray CT, Latheta LCT-200 (Hitachi, Ltd, Tokyo, Japan) with the following parameters: voltage of 80 kV, current of 500 μA, and voxel size of 0.048–0.08 mm (x- and y-axes) and 0.096–0.16 mm (z-axis) at Institute of Dinosaur Research, Fukui Prefectural University. The complex including frontals, left parietal, left ectopterygoid, right atlantal neurapophysis, axis and fifth cervical vertebrae was also scanned using an industrial microfocus CT, TXS320-ACTIS (TESCO Co., Yokohama, Japan), at FPDM with the following parameters: voltage of 270 kV, current of 250 μA, and voxel size of 0.05 mm (x- and y-axes) and 0.05 mm (z-axis). We subsequently segmented all analyzed elements from the acquired CT images and exported polygon meshes using Amira (v 2020.1, Thermo Fisher Scientific; Waltham, MA, USA). Polygon meshes were then imported into Meshmixer (Autodesk, San Rafael, CA, USA) to observe, measure and capture images for figures under the orthographic projection view.

Anatomical terminologies

The anatomical terminologies used in this study are essentially based on the frequency of use in the referred literatures. However, some terminologies coined in previous studies are applied as follows; Hendrickx and Mateus (2014) for the maxilla, Hendrickx et al. (2015) for the dentition, Wilson (1999, 2012) for laminae of vertebrae, Wilson et al. (2011) for fossae of vertebrae, and Nicholls and Russell (1985) for the orientation of the pectoral girdle.

Phylogenetic analyses

To reassess the phylogenetic affinity of *Fukuivenator paradoxus*, FPDM-V-8461 was scored into the recent version of Theropod Working Group (TWiG) dataset (Brusatte et al., 2014), which is a large expansion of the one previously updated by Turner et al. (2012) and more recently updated by Nesbitt et al. (2019), with an additional set of morphological features described in this study. Although this specimen was previously scored for an older version of this dataset (Turner et al., 2012) by Azuma et al. (2016), scores on 106 characters were modified as a result of the present study. In addition, the derived state of character 90 was modified from "12 or more" to "11 or more" following Maryańska et al. (2002; character 98) so that *Fukuivenator* and other potential operational taxonomic units (OTUs) having 11 cervical vertebrae could be scored for this character. In addition, some scores for other OTUs on character 27, 28 and 318 were modified based on previously published literatures (see "Remarks on maniraptoran anatomy" in DISCUSSION for details). The final dataset compiled with Mesquite 3.6 (Maddison and Maddison, 2019) includes 155 taxa covering an extensive sample of coelurosaurs and outgroups scored for 853 discrete anatomical characters. The following characters were ordered following previous studies (Turner et al., 2012; Brusatte et al., 2014; Nesbitt et al., 2019): 3, 16, 17, 18, 19, 24, 25, 27, 38, 39, 40, 45, 63, 66, 72, 74, 89, 103, 108, 111, 114, 117, 119, 121, 123, 130, 146, 148, 152, 154, 161, 163, 166, 168, 169, 171, 175, 178, 179, 181, 195, 197, 200, 217, 222, 232, 234, 235, 238, 242, 250, 252, 255, 256, 261, 262, 265, 268, 270, 279, 287, 292, 299, 309, 316, 319, 321, 326, 328, 347, 351, 359, 364, 379, 384, 385, 387, 393, 397, 401, 409, 413, 415, 417, 420, 425, 426, 427, 428, 433, 434, 443, 445, 446, 459, 462, 475, 482, 485, 488, 494, 499, 520, 540, 545, 556, 557, 560, 578, 579, 605, 613, 622, 628, 631, 632, 635, 642, 648, 651, 665, 669, 670, 684, 694, 698, 702, 711, 712, 715, 727, 728, 763, 780, 805, 806, 807, 818, 823, 842 and 843. The dataset was analyzed with equally weighted parsimony in TNT 1.5 (Goloboff and Catalano, 2016). Following TWiG protocols, *Allosaurus* was used as an outgroup to root the tree. At first, the dataset was analyzed under the "New Technology" search options, using sectorial search, ratchet, tree drift and tree fuse options with default settings, and the minimum tree length was found in 10 replicates to recover as many tree islands as possible. Subsequently, the results were exposed to the branch-swapping algorithm of Tree Bisection Reconnection (TBR). Reduced strict consensus of MPTs was once constructed with a posteriori pruning of five wildcard taxa: *Kinnareemimus*, *Epidendrosaurus*, *Pyroraptor*, *Hesperonychus* and *Limenavis*, following previous studies (Turner et al., 2012; Brusatte et al., 2014; Nesbitt et al., 2019). The supporting values for each node were calculated as Bremer support (with retaining trees suboptimal by five steps) and bootstrapping score (with 10,000 replicates).

SYSTEMATIC PALEONTOLOGY

DINOSAURIA Owen, 1842
THEROPODA Marsh, 1881
COELUROSAURIA von Huene, 1914
MANIRAPTORA Gauthier, 1986
Fukuivenator paradoxus Azuma, Xu, Shibata, Kawabe, Miyata and Imai, 2016

Holotype

FPDM-V-8461, a disarticulated and closely associated skeleton composed of the following elements (Fig. 2): two isolated premaxillary teeth, both maxillae with four intact and one isolated teeth, both lacrimals, right jugal, both frontals, both parietals, braincase without laterosphenoid, both ectopterygoids, right palatine, posterior part of right dentary with two intact dentary teeth, 9 cervical, 11 dorsal, 5 sacral and 31 caudal vertebrae, several cervical and dorsal ribs, gastralia and chevrons, most of both forelimbs, right pubis, and nearly complete hindlimbs.

Modifications from the original description by Azuma et al.

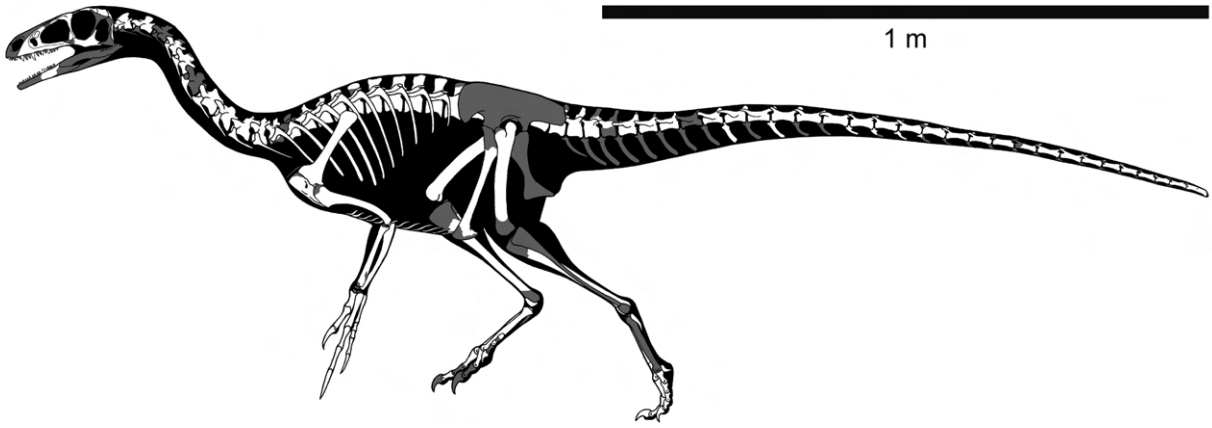

FIGURE 2. Reconstructed skeleton of *Fukuivenator paradoxus*. Elements missing in FPDM-V-8461 are illustrated in grey. Artwork by Genya Masukawa.

(2016) are summarized below. Re-identified elements: right maxilla, originally identified as right premaxilla; right lacrimal, originally identified as right postorbital; atlantal neurapophyses, originally identified as axial ribs; partial neural arch of fifth dorsal vertebra, originally identified as left squamosal; right manual phalanx III-1, originally identified as right pedal phalanx I-1; right pubis, originally identified as left pubis; left metatarsals II and V, originally identified as right metatarsals IV and V, respectively; left pedal phalanges II-1, II-2, III-2, IV-1 and IV-2, originally identified as right pedal phalanges IV-1, III-1, IV-2, II-1 and II-2, respectively. Additionally identified elements: right quadrate; both parietals; right ectopterygoid; centrum of 2nd dorsal vertebra; neural spine of 9th dorsal vertebra; partial neural arch of 4th caudal vertebra; prezygapophyses of 18th caudal vertebra; 29th caudal vertebra; several rib elements; distal end of right humerus; left manual phalanx I-2; left femoral head; distal part of right fibula; right distal tarsal III; left metatarsal III; right metatarsal IV; left pedal phalanx I-2. Withdrawn elements: left pterygoid; posterior caudal vertebra; left ischium.

Emended diagnosis

A maniraptoran theropod with following autapomorphies (Fig. 3): 1. large maxillary fenestra expanded well dorsally above the suprantral strut; 2. large oval lacrimal foramen on antorbital fossa medial wall; 3. jugal anterior ramus with thick and rounded dorsal margin continuous with the lateral surface; 4. bifid posterior end of ectopterygoid for contact with pterygoid; 5. highly heterodont dentition featuring robust unserrated teeth including small spatulate anterior teeth, large and posteriorly curved middle teeth, and small and nearly symmetrical posterior teeth; 6. mid-posterior cervical vertebrae with a complex lamina system surrounding the neural canal resulting in deep and wide grooves for interspinous ligaments and additional deep sockets; 7. anterior cervical vertebrae with intraprezygapophyseal, postzygodiapophyseal, prezygodiapophyseal, and intrapostzygapophyseal laminae connecting to each other to form an extensive platform; 8. middle and posterior cervical vertebrae with transversely bifid neural spines; 9. dorsal, sacral, and anterior caudal vertebrae with strongly laterally curved hyposphene and centropostzygapophyseal laminae that, together with the postzygapophyseal facet, form a socket-like structure for receiving the prezygapophysis; 10. dorsoventrally bifid sacral ribs; 11. caudal zygapophyseal facets expanded to be substantially wider than the zygapophyseal processes; and 12. middle caudal vertebrae with transversely and distally bifid prezygapophyses. The autapomorphies 2 and 5–12 follow Azuma et al. (2016). See also Emendation of diagnosis in DISCUSSION.

DESCRIPTION

Skull

Maxilla

The left maxilla is nearly complete, only missing the distal end of the dorsal ramus (Fig. 4A–F). On the other hand, the right maxilla, which was originally identified as the right premaxilla (Azuma et al., 2016) due to incomplete preparation, lacks the anterior ramus and most of the posterior ramus (Fig. 4G–L). The distal portion of the right dorsal ramus is preserved in contact with the lacrimal (Fig. 6G).

In lateral view, the anterior end of the maxillary body forms an acute angle, about 45 degrees (Fig. 4C). A small subnarial foramen is present on the anterior margin at the level of the ventral margin of antorbital fossa. The ascending ramus projects posterodorsally and is slightly recurved to enclose the antorbital fenestra ventral to it. Distally, the ascending ramus bears a

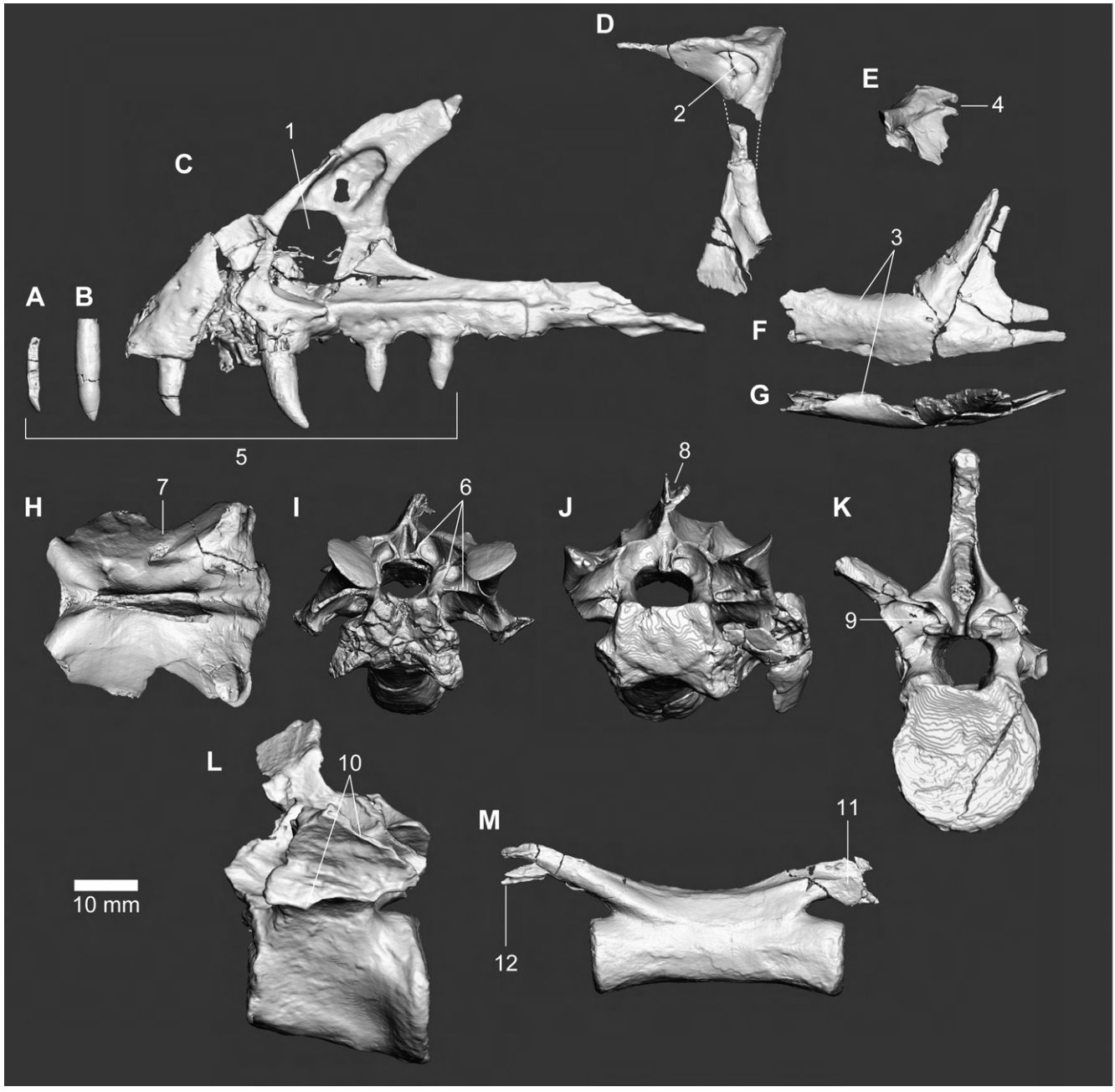

FIGURE 3. Selected elements of FPDM-V-8461 illustrating diagnostic features of *Fukuivenator paradoxus*. Mesialmost (**A**) and mesial (**B**) teeth, left maxilla (**C**), mirrored right lacrimal (**D**), mirrored right ectopterygoid (**E**), mirrored right jugal (**F**, **G**), 6th (**H**), 8th (**I**) and 9th (**J**) cervical vertebrae, 10th dorsal vertebra (**K**), 5th sacral vertebra (**L**) and 14th caudal vertebra (**M**) in mesial (A), labial (B), lateral (C–F, L, M), dorsal (G, H), anterior (I, J) and posterior (K) views. See Emended diagnosis in SYSTEMATIC PALEONTOLOGY for the numbers corresponding to each diagnostic feature.

concave dorsal surface for the contact with the lacrimal (Fig. 4G). The lacrimal contact surface bears an opening of a small pneumatic foramen present at the preserved distal end of the ascending ramus. The antorbital fossa is deeply excavated and extends to the anterodorsal margin of the ascending ramus, suggesting its possible expansion to the nasal (Fig. 4C) as in allosauroids (Rauhut, 2003) and avialans (Turner et al., 2012). The lateral wall of the antorbital fossa bears a large maxillary fenestra anteriorly and a large pneumatic excavation dorsal to it. Anterior to the antorbital fossa, several small foramina are observable on the lateral surface. Ventrally, the lateral surface exhibits a series of subtle and discrete foramina along the ventral margin approximately above the 5th–10th alveoli.

In the original description, a large fenestra in the antorbital

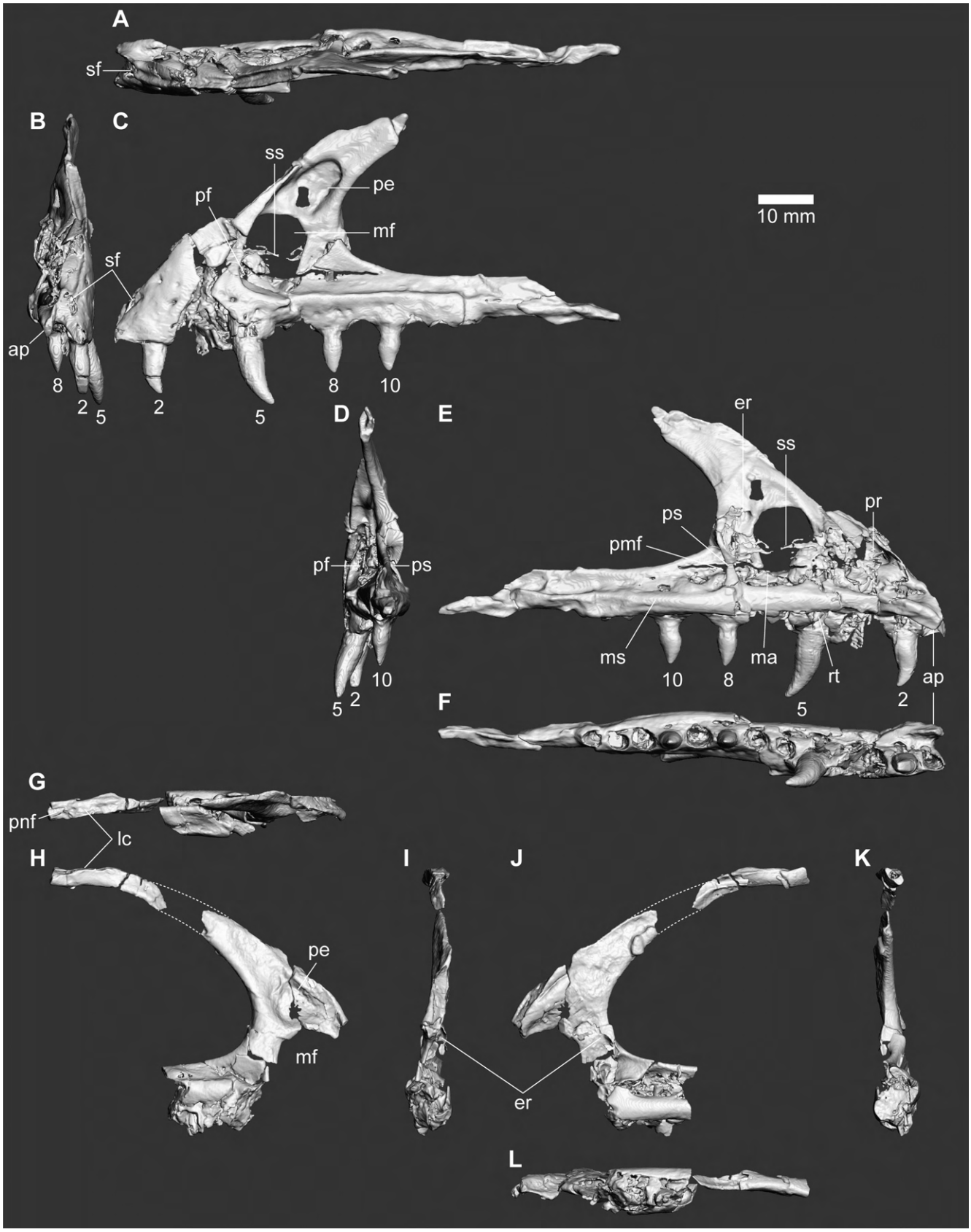

FIGURE 4. Maxillae of FPDM-V-8461. Left (**A**–**F**) and right (**G**–**L**) maxillae in dorsal (A, G), anterior (B, I), lateral (C, H), posterior (D, K), medial (E, J) and ventral (F, L) views. Abbreviations: 2–10, 2nd to 10th erupted teeth; ap, anteromedial process; er, epiantral recess; lc, lacrimal contact; ma, maxillary antrum; mf, maxillary fenestra; pe, pneumatic excavation; pf, promaxillary fenestra; pmf, posteromedial maxillary fenestra; pnf, pneumatic foramen; pr, promaxillary recess; rt, replacement tooth; sf, subnarial foramen; ss, suprantral strut.

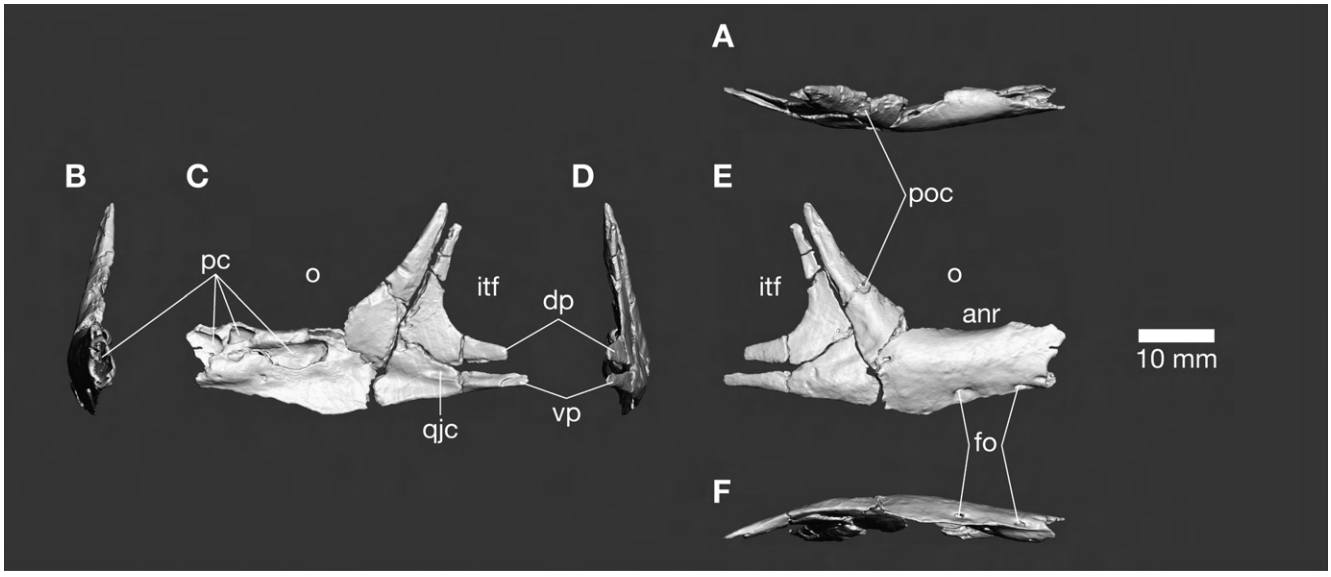

FIGURE 5. Jugal of FPDM-V-8461. Right jugal in dorsal (**A**), anterior (**B**), medial (**C**), posterior (**D**), lateral (**E**) and ventral (**F**) views. Abbreviations: anr, anterior ramus; dp, dorsal prong; fo, foramen; itf, infratemporal fenestra; o, orbit; pc, pneumatic cavity; qjc, quadratojugal contact; vp, ventral prong.

fossa is described as separated dorsoventrally into the maxillary and promaxillary fenestrae (Azuma et al., 2016). However, the rendered polygon mesh derived from CT images reveals that a faint bony bridge between them is situated medially to the lateral wall of the antorbital fossa (Fig. 4C, E). This bridge probably corresponds to the suprantral strut based on its continuous contact with the postantral strut, resulting in a single large maxillary fenestra expanded further dorsally above the suprantral strut, unlike that of *Allosaurus* (Hendrickx and Mateus, 2014). Although the maxillary fenestra abuts the anterior margin of the antorbital fossa as in *Tsaagan* (Norell et al., 2006; Turner et al., 2012), it never extends to the anteroventral corner unlike that of *Linheraptor* (Xu et al., 2015). The maxillary fenestra is expanded posteriorly to occupy slightly more than the half the length between the anterior margin of the antorbital fossa and that of the antorbital fenestra, as in troodontids (Currie and Varricchio, 2004). The maxillary fenestra is expanded dorsoventrally as well, while separated from the ventral margin of the antorbital fossa. Anteroventral to the maxillary fenestra, a true, small promaxillary fenestra excavates the anterior margin of the antorbital fossa anteromedially, slightly above its anteroventral corner.

In medial view, the jugal ramus and maxillary body are largely occupied by the medial shelf extending along the ventral margin (Fig. 4E). Anteriorly, the shelf becomes inflated to be a bar-like projection which extends to the short anteromedial process occupying only the area above to the first two alveoli (Fig. 4E) unlike more elongated ones of other coelurosaurs (Brusatte et al., 2014). The maxillary antrum is delimited ventrally by the medial shelf and dorsally by the suprantral strut. The postantral strut demarcates the posterior margin of the maxillary antrum and the anterior margin of the posteromedial maxillary fenestra (foramen in maxillary pila *sensu* Choiniere et al., 2014) with both antra connected through a canal lateral to the strut. Posterodorsal to the suprantral strut is the epiantral recess excavating the interfenestral strut (the area between the maxillary and antorbital fenestrae) posteriorly (Fig. 4E, I, J) as in allosauroids and tyrannosauroids (Hendrickx and Mateus, 2014). The area anterior to the maxillary antrum is severely damaged, while the promaxillary recess is clearly present near the anterodorsal margin of the maxillary body (Fig. 4E).

Thirteen alveoli are discernible in the maxilla with four erupted teeth preserved in the second, fifth, eighth and 10th alveoli (Fig. 4E, F). Each of the 5th to 7th, 9th and 10th alveoli has an opening dorsally on the medial shelf. The CT images reveal one more alveolus *contra* to the original description (Azuma et al., 2016). Each of the 5th, 8th and 10th maxillary teeth is followed by an unerupted replacement tooth mediodorsally.

Jugal

The right jugal is partitioned into the anterior and posterior parts by the breakage along the midline of the ascending ramus (Fig. 5C, E). The anterior part lacks the anterior end, and the ascending ramus is shifted ventrally by the breakage, which is correctly positioned in Fig. 5 and Table 1. In lateral view, the jugal is triradiate with a nearly straight ventral margin as in other coelurosaurs, while bending anterodorsally below the junction of the ascending and anterior rami (Fig. 5E). The jugal is thinned ventrally to form a keen edge on the ventral margin, and the ventral part of the element below the ascending ramus is

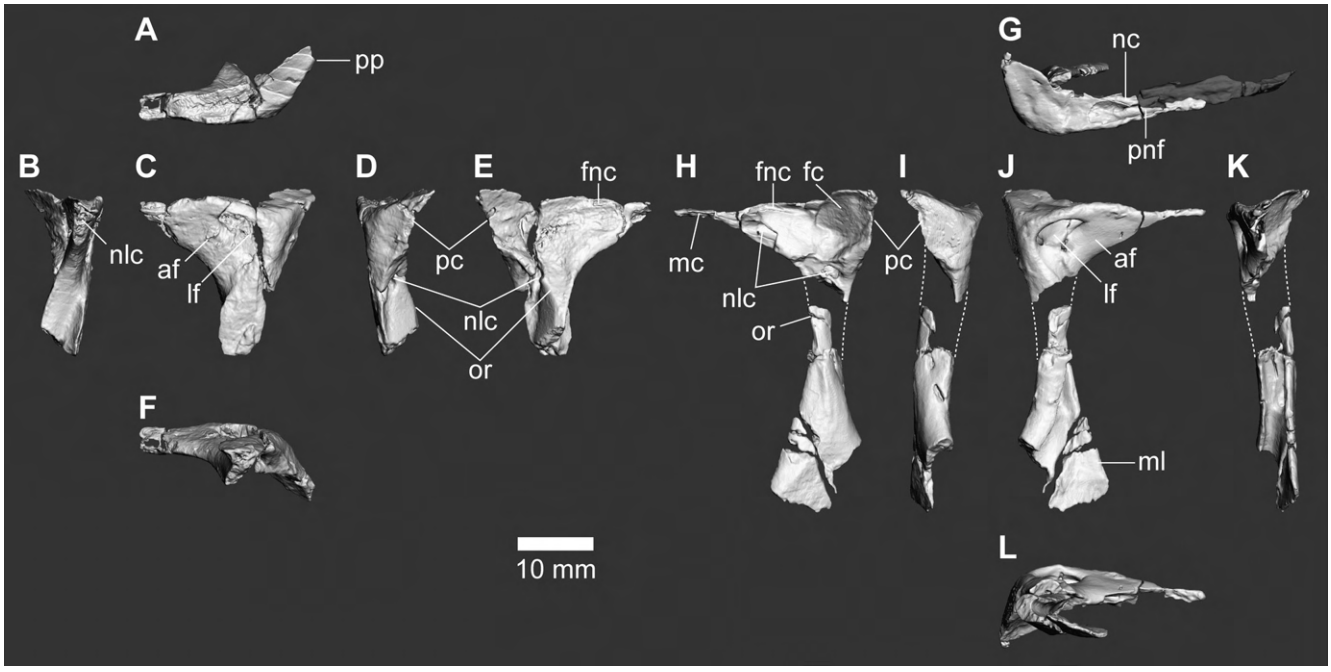

FIGURE 6. Lacrimals of FPDM-V-8461. Left lacrimal (**A**–**F**), right lacrimal incorporating the posterodorsal part of the right maxilla (shaded) as preserved (**G**), and right lacrimal (**H**–**L**) in dorsal (A, G), anterior (B, K), lateral (C, J), posterior (D, I), medial (E, H) and ventral (F, L) views. Abbreviations: af, antorbital fossa fc, frontal contact; fnc, frontal or nasal contact; lf, acrimal foramen; ml, medial lamina; nlc, nasolacrimal canal; or, orbitonasal ridge; pc, postorbital contact; pnf, pneumatic foramen; pp, posterodorsal process.

curved ventromedially to form a broad, concave medial surface (Fig. 5C).

The anterior ramus is inflated by a large pneumatic cavity within it so that the lateral surface is rounded and continuous with the dorsal surface forming an unusually thick dorsal margin to border the ventral rim of the orbit (Fig. 5A). Similarly, the medial surface of the anterior ramus is mostly convex (Fig. 5C). The breakage at the posterodorsal part of the ramus indicates the presence of the pneumatic cavity (Fig. 5B, C). In lateral view, at least two small foramina are present along the ventral margin of the anterior ramus (Fig. 5E). Both foramina continue to the internal pneumatic cavity.

The ascending ramus projects posterodorsally in lateral view. The contact surface for the postorbital is present as a shallow depression along the anterior margin of the dorsal two-thirds of the ascending ramus. The posterior ramus is slightly shorter than the ascending ramus as preserved and bears dorsal and ventral prongs projected posteriorly to contact with the quadratojugal. In medial view, the cleft between both prongs continues anteriorly as a groove on the medial surface of the jugal below the ascending ramus, probably for the quadratojugal contact (Fig. 5C).

Lacrimal

The elements originally identified as the right postorbital and the left lacrimal by Azuma et al. (2016) is re-identified as the left (Fig. 6A–F) and right (Fig. 6G–L) lacrimals, respectively. The right lacrimal is nearly complete and preserved in articulation with the distalmost part of the dorsal ramus of the right maxilla (Fig. 6G). The left lacrimal, on the other hand, lacks the anterior end and most of the ventral ramus. The anterior extent of the right lacrimal only slightly exceeds the preserved anterior margin of the frontal when in articulation, indicating that the contact between the lacrimal and the nasal was faint to absent in *Fukuivenator*.

In lateral view, the medial lamina is visible in the ventral half of the ventral ramus (Fig. 6J). In medial view, the orbitonasal ridge runs anteroventrally from the ventral margin of the posterodorsal process to meet the medial lamina just above the middle of the ventral ramus (Fig. 6D, E, H). The laterodorsal margin of the lacrimal forms a stout ridge which does not extend posteriorly to the level of the orbit (Fig. 6C, J). The anterior ramus is narrowed anteriorly, and its dorsal surface bears a depression (Fig. 6A, G). This depression deepens anteriorly to bear a dorsal opening at the anterior margin of the nasolacrimal canal perforating the lacrimal posteroventrally. This canal is anteriorly continuous with the one within the ascending ramus of the maxilla through the contact surface between the lacrimal and maxilla. The canal has another opening just posterior to the orbitonasal ridge on the medial surface. A deep anteroposterior groove is present on the mediodorsal margin of the anterior

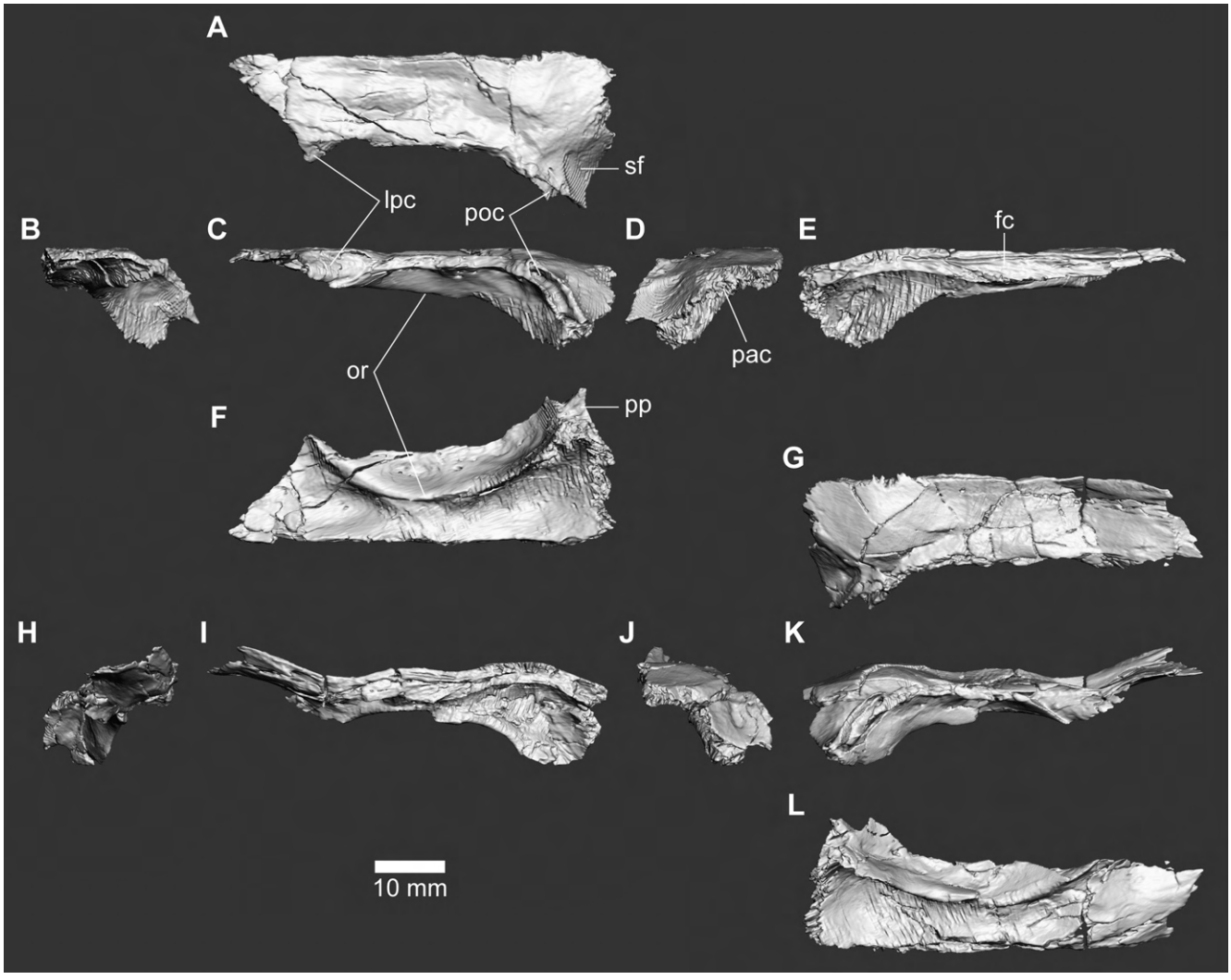

FIGURE 7. Frontals of FPDM-V-8461. Left (**A–F**) and right (**G–L**) frontals in dorsal (A, G), anterior (B, H), lateral (C, K), posterior (D, J), medial (E, I) and ventral (F, L) views. Abbreviations: lpc, lacrimal and prefrontal contact; or, orbitonasal ridge; pac, parietal contact; poc, postorbital contact: pp, postorbital process; sf, supratemporal fossa

ramus and probably represents a contact surface for the frontal or nasal (Fig. 6E, H).

The posterodorsal process forms a conical process set into a deep pit on the lateral surface of the frontal in lateral view (Fig. 6C, J). The medial surface of the process is slightly concave to fit with the swelling within a pit on the anterolateral margin of the frontal (Fig. 6E, H). The posteromedial margin of the process exhibits a narrow, rough surface probably for the contact with the prefrontal (Fig. 6D, I). The lacrimal body (in which the anterior and ventral rami meet) and a short posterodorsal process are excavated by a large lacrimal recess with a single, moderately sized foramen opening laterally (Fig. 6C, J). The lacrimal recess does not inflate the anterior ramus unlike those of some tyrannosaurines (Carr, 2005) and oviraptorosaurs (Gold et al., 2013). The subcutaneous surface anterior to the lacrimal foramen is not demarcated from the lateral surface of the antorbital fossa; they rather blend into each other as in some tyrannosaurines (Carr, 2005).

Frontal

Both frontals are preserved while the anterior margins are broken, hindering their conjoined morphology (Fig. 7). The posterior part of the element expands laterally, and its lateral margin exhibits a smooth transition from the orbital margin to the postorbital process (Fig. 7A, G). The dorsal surface of the posterior expansion is mostly occupied by the supratemporal fossa with strongly sinusoidal anterior margin that is medially formed by a blunt ridge and laterally by a sharp ridge along the postorbital contact. The posterior margin exhibits a nearly straight and somewhat indented suture for the parietal at the level slightly posterior to the apex of the postorbital process.

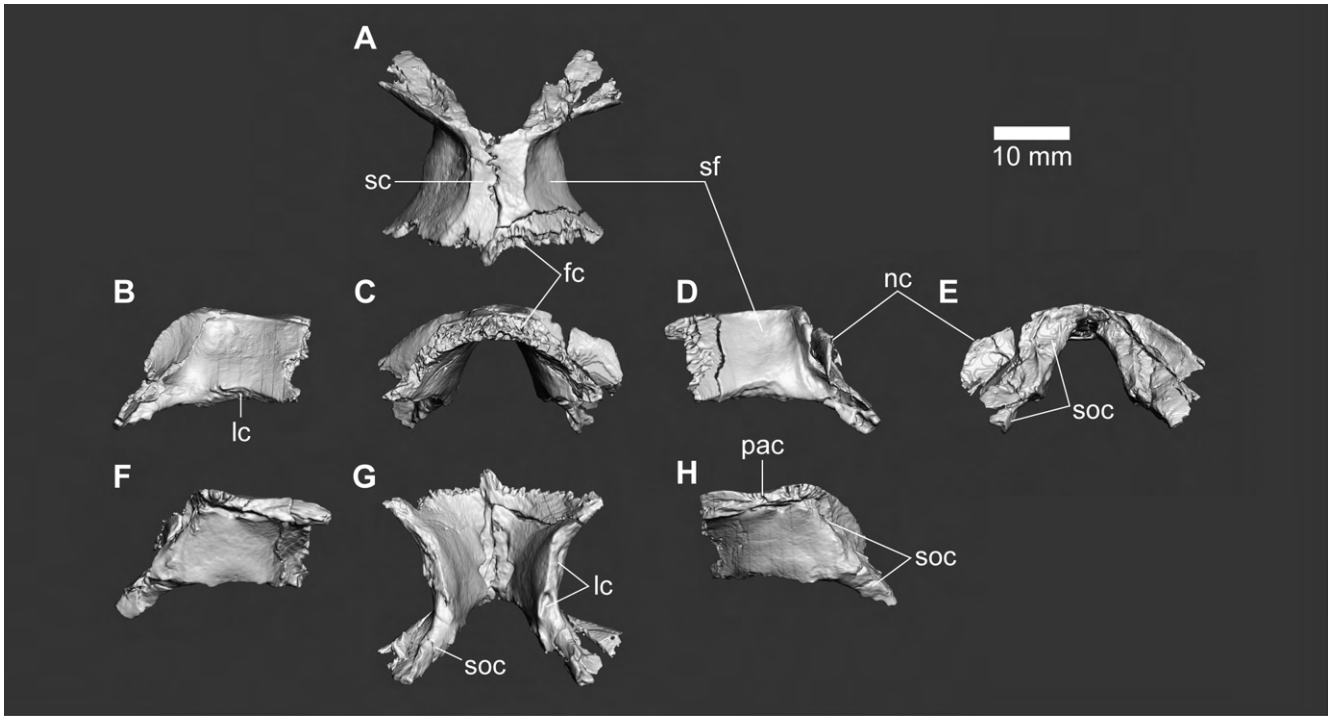

FIGURE 8. Parietals of FPDM-V-8461. Assembled (**A**, **C**, **E**, **G**), right (**B**, **H**) and left (**D**, **F**) parietals in dorsal (A), lateral (B, D), anterior (C), posterior (E), medial (F, H) and ventral (G) views. Abbreviations: fc, frontal contact; lc, laterosphenoid contact; nc, nuchal crest; pac, parietal contact; sc, sagittal crest; sf, supratemporal fossa; soc, supraoccipital contact.

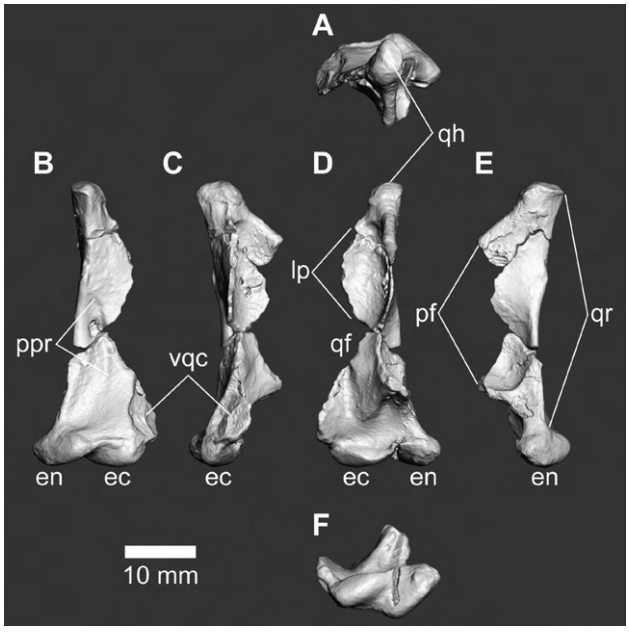

FIGURE 9. Quadrate of FPDM-V-8461. Right quadrate in dorsal (**A**), posterior (**B**), lateral (**C**), anterior (**D**), medial (**E**) and ventral (**F**) views. Abbreviations: ec, ectocondyle; en, entocondyle; lp, lateral process; pf, pterygoid flange; ppr, posterior pneumatic recess; qf, quadrate foramen; qh, quadrate head; vqc, ventral quadratojugal contact.

In lateral view, a discrete longitudinal notch for the contact with the lacrimal and prefrontal is observable anteriorly (Fig. 7C, K). This contact surface gradually projects laterally toward its anterior end so that it is also visible in dorsal view (Fig. 7A, G). The projection matches with the medial surface of the posterodorsal process of the lacrimal (Fig. 6E, H). Therefore, the remaining posterior part of the notch is likely for the contact with the prefrontal. Posteriorly, the lateral (orbital) margin between the prefrontal and postorbital contacts exhibits a narrow, slightly rough surface.

Posterior to the orbital margin, the postorbital contact forms a large, deep and posterolaterally-directed notch (Fig. 7C, K) as in some troodontids (Currie, 1985; Turner et al., 2012). In addition, this contact is partially visible in the dorsal view (Fig. 7A, G). Although such contacts are also visible in dorsal view in *Stenonychosaurus* (van der Reest and Currie, 2017) and *Latenivenatrix* (van der Reest and Currie, 2017:fig. 5), they are located posteriorly along the postorbital process, in contrast to the one in *Fukuivenator* in which it is situated anteriorly.

Parietal

Both parietals are completely preserved (Fig. 8). The parietal exhibits a square shape in dorsal view with a concave lateral margin demarcating the supratemporal fenestra (Fig. 8A). The anterior margin is somewhat indented to fit with the posterior margin of the frontal, while they are not fused with each other.

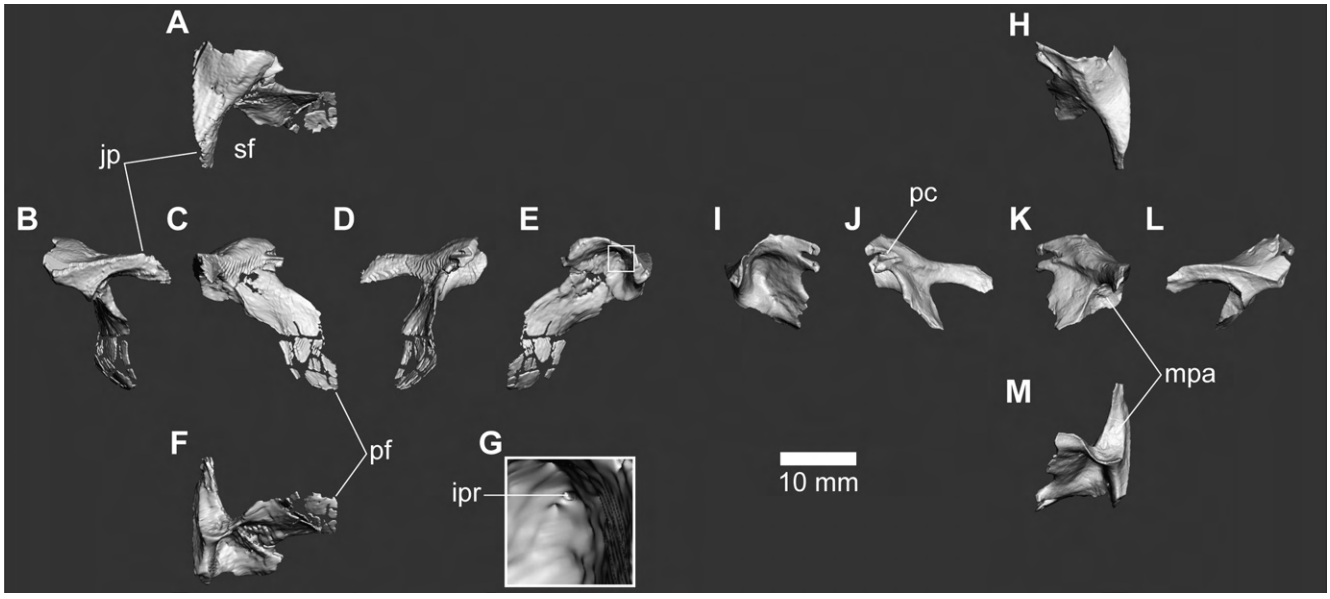

FIGURE 10. Ectopterygoids of FPDM-V-8461. Left (**A**–**G**) and right (**H**–**M**) ectopterygoids in dorsal (A, H), anterior (B, L), lateral (C, K), posterior (D, J), medial (E, G, I) and ventral (F, M) views. Open square within E indicates the area magnified in G. Abbreviations: jp, jugal process; pf, posterior flange; sf, subtemporal fenestra; ipr, opening of the internal pneumatic recess; mpa, m. pterygoideus attachment.

Similarly, the medial margin is nearly straight and somewhat indented in dorsal view, and the medial surface does not exhibit a trace for fusion with another parietal (Fig. 8F, H). The dorsal surface is occupied by a convex, laterodorsally-facing supratemporal fossa except for the sagittal and nuchal crests along the medial and posterior margins, respectively (Fig. 8A, B, D). The sagittal crest is represented by a flat, slightly elevated skull table occupying about the medial fourth of the dorsal surface. The nuchal crest emerges from the posteroventral margin of the skull table and is sloped lateroventrally in posterior view (Fig. 8E). Additionally, it forms a broad occipital surface facing posterodorsally with a slight concavity in its medial third for the contact with the supraoccipital. The supraoccipital also contacts the posteroventral part of the parietal, forming a narrow, medioventrally facing surface on the latter (Fig. 8F, H). In ventral view, a narrow concavity anterior to the supraoccipital contact is facing ventrally most likely to contact with the laterosphenoid (Fig. 8G). The remaining anterior half of the lateroventral margin bears a lateroventrally facing surface probably representing another contact for the laterosphenoid.

Quadrate

Only the right quadrate is preserved and lacks most of the pterygoid flange and lateral process (Fig. 9). The quadrate head has a single articular surface for the squamosal dorsally (Fig. 9A, D). From the posterior margin of the quadrate head, the quadrate ridge emerges and extends ventrally toward the middle of the posteromedial margin of the entocondyle (Fig. 9E). The ridge is bowed laterally and bears a slight depression in the proximal third in medial view. Just lateral to the quadrate ridge, an oval fossa is present in the midheight of the posterior surface (Fig. 9B), probably corresponding to the posterior pneumatic recess (Eddy and Clarke, 2011). Although the lateral margin is incomplete in the dorsal half, the medioventral margin of the quadrate foramen is preserved above the ventral quadratojugal contact (Fig. 9D). Above the ento- and ectocondyles, the base of the pterygoid flange projects anteriorly to bear a shallow fossa ventrally (Fig. 9E, F), while lacking the deep recess unlike *Falcarius* (Zanno, 2010) and pantyrannosaurs (Brusatte et al., 2014). The ventral quadratojugal contact faces posterolaterally to the quadratojugal process and only partially invades into the lateral surface of the ectocondyle (Fig. 9C). The medial margin of the ventral quadratojugal contact directs vertically in posterior view (Fig. 9B).

Ectopterygoid

Both ectopterygoids are preserved, with the left one being more complete (Fig. 10). The anterior part is stout and composed of the medially-hollowed main body and the lateral projection, namely the jugal process. The posterior part forms the lateromedially thin, dorsoventrally tall flange. In dorsal view, the jugal process and the posterior flange constitutes the anterior and lateral rims of the subtemporal fenestra (Fig. 10A, H). In medial view, the ectopterygoid body is concave, and its deepest portion bears a very small opening of the internal pneumatic recess (Fig. 10E, G), although the body is not inflated unlike those of tyrannosaurines (Holtz, 2001; Brusatte et al., 2010; Gold et al., 2013). The anterior surface of the jugal ramus is slightly concave to form a shallow groove directed laterally

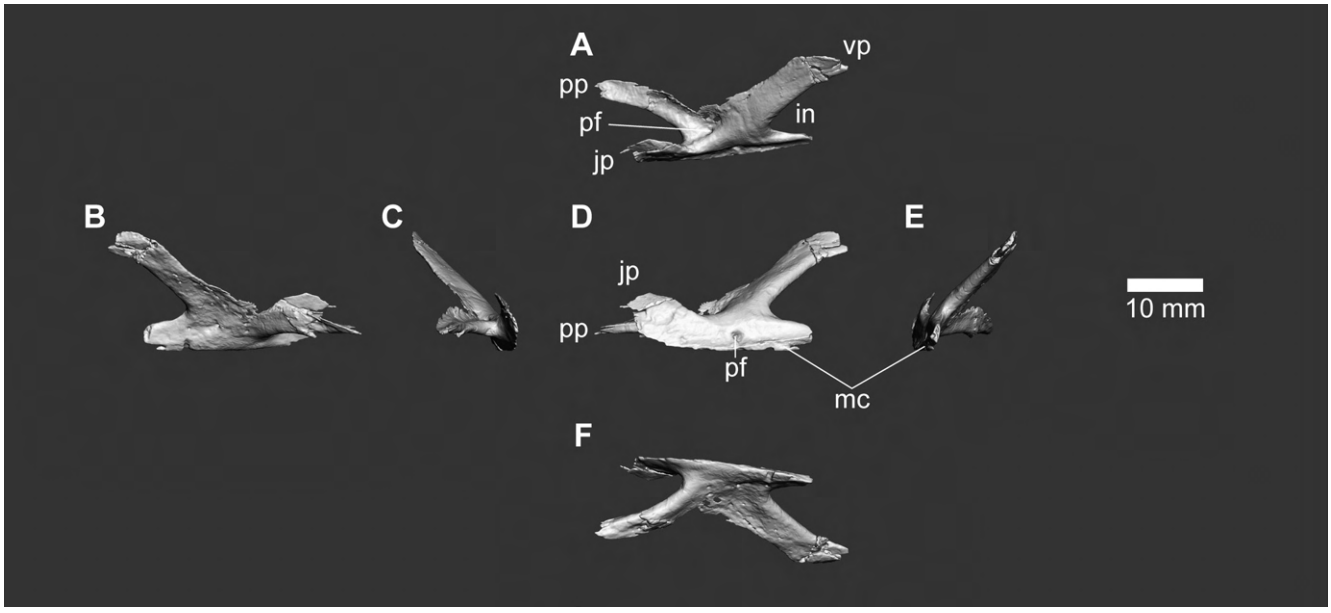

FIGURE 11. Palatine of FPDM-V-8461. Right palatine in dorsal (**A**), medial (**B**), posterior (**C**), lateral (**D**), anterior (**E**) and ventral (**F**) views. Abbreviations: in, internal naris; jp, jugal process; mc, maxilla contact; pf, pneumatic foramen; pp, pterygoid process; vp, vomeropterygoid process.

(Fig. 10B, L). Ventrally on the jugal ramus, another concave surface partially invades the anterolateral margin of the posterior flange (Fig. 10K, M). This concavity probably represents the attachment of m. pterygoideus as in *Deinonychus* (Ostrom, 1969). The contact for the jugal on the lateral end of the jugal process is ambiguous. The posterior margin of the main body is bifurcated by a notch in lateral view, possibly for the contact with the pterygoid (Fig. 10E, I).

Palatine

Right palatine is nearly complete (Fig. 11). In lateral view, the vomeropterygoid process is projected anterodorsally (Fig. 11D). The contact for the maxilla is present as a narrow longitudinal surface along the ventral border. Dorsally along the contact, a shallow longitudinal groove is present, extending to the anterior region of the jugal process. A pneumatic recess within the main body exhibits a primary opening at the central part of the laterodorsal surface and the secondary opening in the middle of the shallow longitudinal groove above the maxillary contact (Fig. 11A, D).

Braincase (supraoccipital, otoccipital, basioccipital, basisphenoid, prootic, orbitosphenoid and parasphenoid)

The braincase is preserved well except for the laterosphenoids (Fig. 12). Parietals are also present and not in contact with the braincase. The basisphenoid is partly disarticulated from the prootic and basioccipital.

Although the supraoccipital exhibits its dorsal margin flat in posterior view (Fig. 12D), it represents a postmortem artifact because it does not fill the contact surface on parietals. The occipital surface faces posterodorsally when the lateral semicircular canal is oriented horizontally (Fig. 12C). The occipital surface of the supraoccipital exhibits a triangular outline lacking its apex and a blunt medial swelling extending dorsoventrally in contrast to the prominent keel seen in *Incisivosaurus* (Xu et al., 2002a), *Linheraptor* (Xu et al., 2015) and *Zanabazar* (Turner et al., 2012). Lateral to the swelling, a pair of semi-circular depressions is present along the suture against the parietals (Fig. 12D). The dorsoventral margin of each depression is pierced as an exit of the caudal middle cerebral vein canal. The depression accompanying the caudal middle cerebral vein canal is also present in *Alioramus* (Bever et al., 2013:fig. 6) and *Linheraptor* (Xu et al., 2015:fig. 3), while not in *Falcarius* (Smith et al., 2011:figs. 1, 2).

The neck of the occipital condyle is not constricted in lateral width, whereas it is slightly constricted in dorsoventral height by a ventral excavation (Fig. 12A, C) as in *Falcarius* (Smith et al., 2011:fig. 1) and *Velociraptor* (Norell et al., 2004:fig. 5.1), in which the excavation is shallower than in *Dromaeosaurus* (Currie, 1995:fig. 4). The foramen magnum is sub-triangular, slightly wider (9.9 mm) than tall (9.3 mm) in posterior view (Fig. 12D), and is larger than the occipital condyle as in most maniraptorans except for troodontids (Maryańska et al., 2002; Zanno et al., 2009). The contribution of each bone to the foramen magnum is hardly discernable due to their complete fusion.

In posterior view, the paroccipital process formed by the otoccipital (coossified exoccipital and opisthotic) is straight,

mediolaterally long and dorsoventrally narrow unlike short and wide ones in pennaraptorans (Turner et al., 2012). Distally, the paroccipital process is widening slightly dorsoventrally to form a squared end (Fig. 12D) as in tyrannosauroids (Bever et al., 2013; Brochu, 2003:figs. 3–5), *Nqwebasaurus* (Choiniere et al., 2012:fig. 7) and dromaeosaurids (Colbert and Russell, 1969; Norell et al., 2004). Although the paroccipital process is also elongated in late-diverging ornithomimosaurs (Osmólska et al., 1972:fig. 3; Kobayashi and Barsbold, 2005a), *Haplocheirus* (Choiniere et al., 2014) and therizinosaurs (Smith et al., 2011; Lautenschlager et al., 2014), it is tapered distally to form a rounded end. The paroccipital process projects posterolaterally in dorsal view (Fig. 12A) and its distal end is twisted to face posterodorsally as in most dromaeosaurids (Colbert and Russell, 1969; Norell et al., 2004). On the posterior surface of the base of the paroccipital process, a mediolaterally elongate fossa excavates the process laterodorsally (Fig. 12D). The ventral margin of the paroccipital process is continuous with the metotic strut, which is short and robust as in most other theropods (Turner et al., 2012). Mediolateral width across opposing struts is extensive so that is greater than one half of the dorsoventral depth of the braincase.

In posterior view, three exits for cranial nerves (CNs) are located together within a shallow depression immediately lateral to the occipital condyle and medial to the metotic strut (Fig. 12D) as in some dromaeosaurids (Norell et al., 2004; Norell et al., 2006). The lateral one is for the glossopharyngeal, vagus and accessory nerves (CNs IX–XI), the dorso- and ventromedial ones are for the hypoglossal nerve (CN XII). The basal tubera are separated by a shallow concavity on the posteroventral margin of the basioccipital. The conjoined width of the basal tubera is slightly greater than that of the occipital condyle unlike the reduced ones of alvarezsaurs and most troodontids (Makovicky et al., 2003; Turner et al., 2012). On the other hand, the dorsoventral depth of the basal tubera does not exceed that of the occipital condyle.

The prootic and orbitosphenoid are completely fused to form the lateroventral wall of the brain and bear exits for the trigeminal and facial nerves (CNs V, VII) and the otic recess on the lateral surface (Fig. 12C, E). The exit for trigeminal nerve is incompletely divided into the dorsal and ventral foramina, which are completely separated in *Erlikosaurus* (Lautenschlager et al., 2014). The dorsal foramen probably corresponds to the exit for the maxillary branch (CN V2) and lacks the dorsal margin originally formed by the missing laterosphenoid. If this is the case, the ventral foramen should correspond to an exit for the mandibular branch (CN V3). Within the otic recess, two fossae are separated dorsoventrally by the crista interfenestralis, where the dorsal region forms the fenestra ovalis (or vestibularis) and the ventral region forms the fenestra pseudorotundum (or cochlearis). A stapedial groove is oriented posterolaterally from the fenestra pseudorotundum, as well as the posterior tympanic recess about the half the length of the groove as in *Falcarius* (Smith et al., 2011).

The basipterygoid process is well projected lateroventrally from the ventral margin of the basisphenoid. The lateral surface of the basisphenoid is excavated by a large fossa comprising three recesses (Fig. 12C, E). The basipterygoid recess is present immediately above the basipterygoid processes and followed posteriorly by the anterior tympanic recess, which is subdivided dorsoventrally by a thin lamina into the dorsal region corresponding to the prootic recess and the ventral region corresponding to the subotic recess. The presence of subotic recess is known in ornithomimosaurs (Osmólska et al., 1972:fig. 5A; Makovicky and Norell, 1998; Tahara and Larsson, 2011), therizinosaurs (Smith et al., 2011, 2018) and some troodontids (Currie and Zhao, 1993b; Norell et al., 2000, 2009; Yin et al., 2018) and also reported in an alvarezsaur *Xiyunykus* (Xu et al., 2018) and an oviraptorosaur *Conchoraptor* (Kundrát and Janáček, 2007). Among them, the subotic recess of *Fukuivenator* is especially similar to that of *Falcarius* due to its position anteroventral to the otic recess, anterior to the basal tuber and posteroventral to the prootic recess (Fig. 12C; Smith et al., 2011:fig. 2C). Left and right prootic recesses excavate the bone deeply to connect with each other. The anterodorsal margin of the prootic recess is demarcated by a distinct crest, namely the otosphenoidal crest. The dorsal surface of the basisphenoid is laterally narrow and is excavated by the pituitary (hypophyseal) fossa (Fig. 12A). The deepest part of the pituitary fossa bears a narrow canal for the internal carotid passage (Fig. 12B). Ventrally, this passage is bifurcated and directed lateroventrally to exit just below the anteroventral margins of otosphenoidal crests (Fig. 12C, E). The anterior surface of the basisphenoid also has a significant fossa continuous with the ventral groove of the cultriform process (Fig. 12B, F). Ventrally, the basisphenoid recess is present as a broad fossa facing posteroventrally as in early-diverging tyrannosauroids (Brusatte et al., 2010) and spanning the basisphenoid and basioccipital (Fig. 12F). In the basioccipital, the basisphenoid recess is deep and further divided into two by an anteroposteriorly-directed septum. The basicranium defined by positions of basal tubera and basipterygoid processes faces posteroventrally and is anteroposteriorly longer than mediolaterally wide.

The parasphenoids form an anteroposteriorly-elongated cultriform process (parasphenoid rostrum) with deep ventral concavity continuous with the fossa present anteriorly on the basisphenoids (Fig. 12F). Laterally, the base of the cultriform process is slightly pneumatized by a shallow fossa (Fig. 12C, E) and lacks apparent parasphenoid bulla unlike those of highly pneumatized taxa such as late-diverging troodontids (Barsbold, 1974; Currie, 1985) and ornithomimosaurs (Osmólska et al., 1972; Barsbold, 1981; Pérez-Moreno et al., 1994; Kobayashi and Lü, 2003; Tahara and Larsson, 2011).

Cranial Endocast

Computed tomography images of frontals, parietals, and partial braincase allow reconstruction of nearly complete cranial endocast (Fig. 13). However, the degree of development of the optic lobes and the positional relationship between the forebrain and midbrain are unknown because the cranial portion covering the midbrain area is missing (Fig. 12).

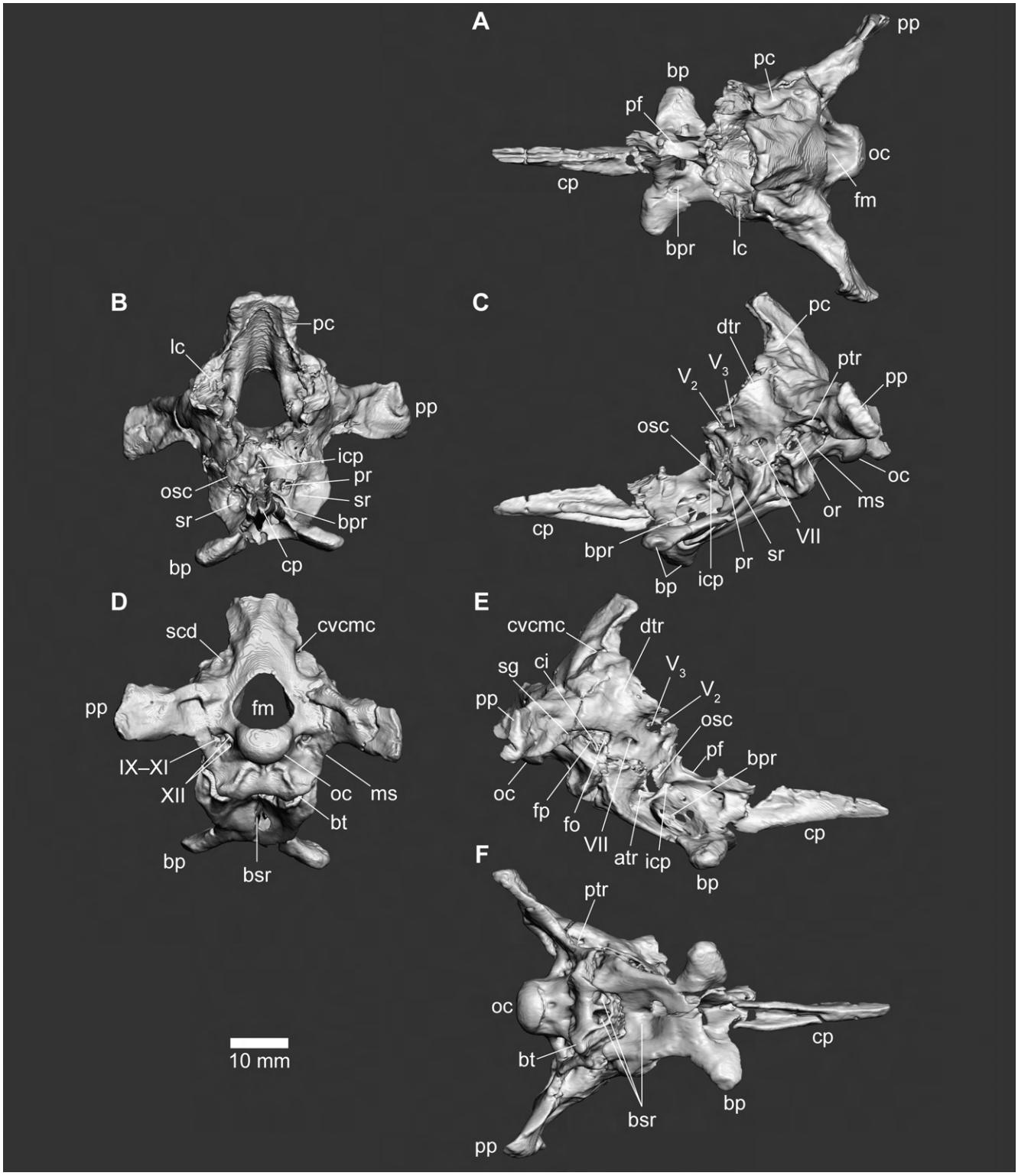

FIGURE 12. Braincase of FPDM-V-8461. Braincase in dorsal (**A**), anterior (**B**), left lateral (**C**), posterior (**D**), right lateral (**E**) and ventral (**F**) views. Abbreviations: atr, anterior tympanic recess; bp, basipterygoid process; bpr, basipterygoid recess; bsr, basisphenoid recess; bt, basal tuber; ci, crista interfenestralis; cp, cultriform process; cvcmc, caudal middle cerebral vein canal; dtr, dorsal tympanic recess; fm, foramen magnum; fo, fenestra ovalis; fp, fenestra pseudorotundum; icp, internal carotid passage; lc, laterosphenoid contact; ms, metotic strut; oc, occipital condyle; or, otic recess; osc, otosphenoidal crest; pc, parietal contact; pf, pituitary fossa; pp, paroccipital process; pr, prootic recess; ptr, posterior tympanic recess; scd, semi-circular depression; sg, stapedial groove; sr, subotic recess; V_2, exit for maxillary branch of trigeminal nerve ;V_3, exit for mandibular branch of trigeminal nerve; VII, exit for facial nerve; IX–XI, exit for glossopharyngeal, vagus and accessory nerves; XII; exit for hypoglossal nerve.

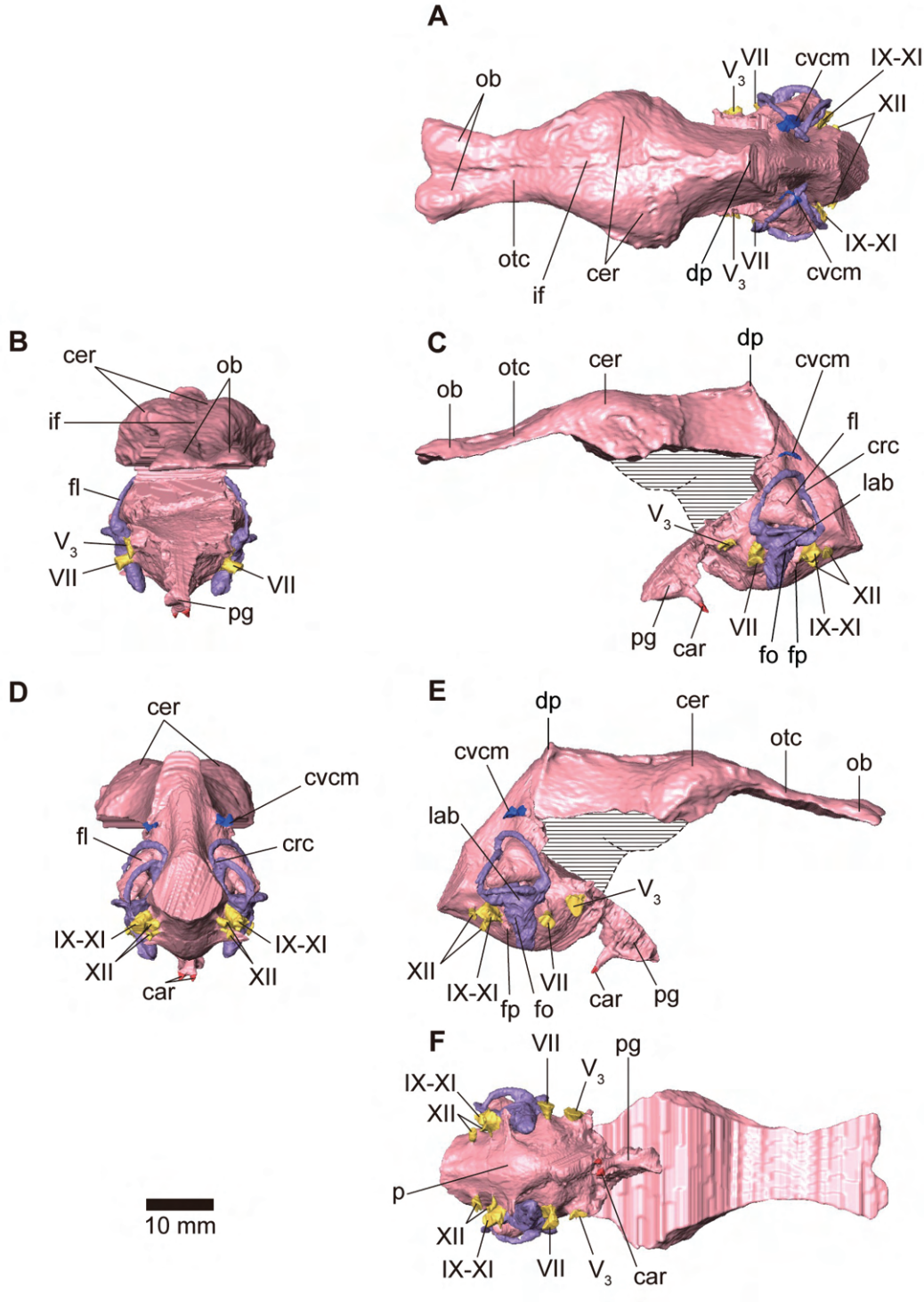

FIGURE 13. Cranial endocast of FPDM-V-8461. Cranial endocast in dorsal (**A**), anterior (**B**), left lateral (**C**), posterior (**D**), right lateral (**E**) and ventral (**F**) views. Midbrain area is reconstructed as the hatched area in lateral views. Abbreviations: car, cerebral carotid artery canal; cer, cerebral hemisphere; cvcm, caudal middle cerebral vein; crc, crus communis; fl, floccular lobe; fo, cast of fenestra ovalis; fp, cast of fenestra pseudorotundum; if, interhemispherical fissure; lab, endosseous labyrinth; p, pone; pg, pituitary gland; ob, olfactory bulb; otc, olfactory tract; V_2, canal for maxillary branch of trigeminal nerve; V_3, canal for mandibular branch of trigeminal nerve; VII, canal for facial nerve; IX–XI, shared canal for glossopharyngeal, vagus and spinal accessory nerve; XII, canal for hypoglossal nerve.

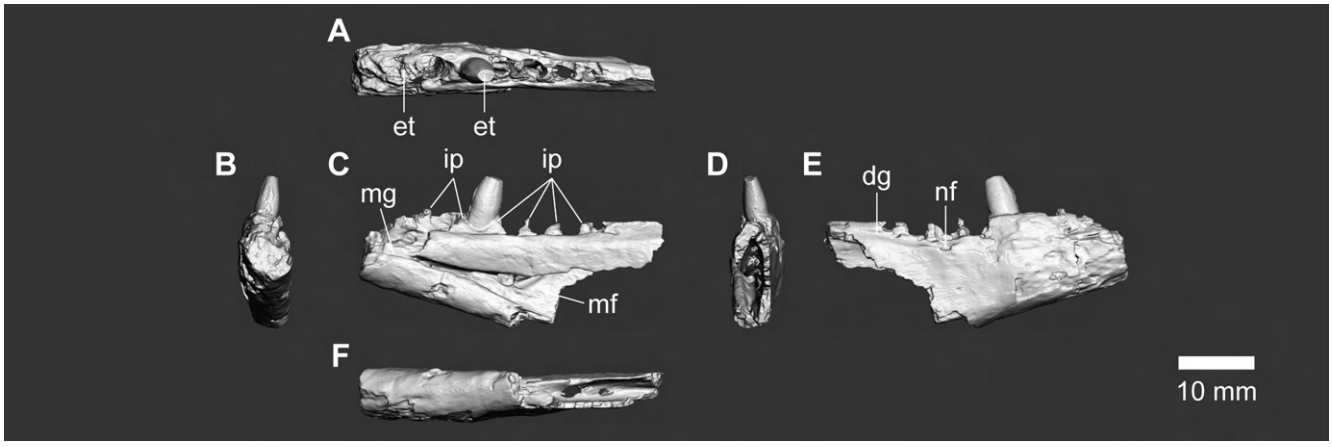

FIGURE 14. Dentary of FPDM-V-8461. Right dentary in dorsal (**A**), anterior (**B**), medial (**C**), posterior (**D**), lateral (**E**) and ventral (**F**) views. Abbreviations: dg, dentary groove; et, erupted tooth; ip, interdental plate; mf, meckelian fossa; mg, meckelian groove; nf, neurovascular foramen.

TABLE 1. Measurements on the skull of FPDM-V-8461.

Element	Anteroposterior length (mm)	Mediolateral width (mm)	Dorsoventral height (mm)
Maxilla (L)	92.0*	13.9	42.1*
Maxilla (R)	54.4*	8.7*	49.0
Jugal (R)	47.6*	6.7	29.4*
Lacrimal (L)	23.8*	9.3	22.0*
Lacrimal (R)	27.7	11.3	43.8*
Frontal (L)	51.7*	21.2	13.7
Frontal (R)	57.6*	19.6	17.2
Parietal (L)	28.8	19.1	17.3
Parietal (R)	26.2	16.0	16.3
Quadrate (R)	13.3*	17.6*	40.3
Ectopterygoid (L)	19.3	16.9	20.3
Ectopterygoid (R)	12.6*	17.0	12.7*
Palatine (R)	33.8*	14.3*	14.7
Braincase	67.0	49.9	48.3
Dentary (R)	40.4*	7.3	15.4*

*Specimen incomplete in measured dimension.

The olfactory bulbs appear relatively short, with the olfactory tracts being as long as the bulbs (Fig. 13A). Generally, long olfactory tracts are a primitive trait in theropods and they tend to be shorter in those closer to the crown Aves (Witmer and Ridgely, 2009). Therefore, the olfactory condition in *Fukuivenator* represents a late-diverging tetanuran feature. The cerebrum lacks its posteroventral part, whereas a partial pituitary gland and the carotid artery are present in its ventral part (Fig. 13C, E, F). The canal for CN V is observed on the posterodorsal side of the pituitary gland, and the route of the mandibular branch of CN V, in particular, is preserved. The canal for CN VII presents anteriorly to the cochlear duct, and the cast of the fenestra pseudorotundum and the canals for CNs IX–XI and XII are present posteriorly to the duct. While the ventral part is missing, the cerebrum region appears caudolaterally expanded (Fig. 13A), resembling that of *Erlikosaurus* (Lautenschlager et al., 2012). The cerebral hemispheres are partitioned dorsally by a deep interhemispheric fissure.

The cranial endocast of *Fukuivenator* bears well-marked cerebral and pontine flexures (Fig. 13C, E). The posterior part of the cerebellum slopes steeply toward the foramen magnum. This configuration is found in small theropods including *Archaeopteryx* (Domínguez Alonso et al., 2004; Kundrát, 2007; Kundrát et al., 2020). The midbrain to hindbrain morphology is relatively similar to that of *Falcarius* among therizinosaurs, while differing largely from that of *Nothronychus* and *Erlikosaurus* which exhibit an overall linear structure (Lautenschlager et al., 2012). A moderately developed dural peak is found in the cerebellar region, and the pone is elongated mediolaterally, resembling therizinosaurian endocasts (Lautenschlager et al., 2012). The cerebellar floccular lobes are expanded laterally toward the level of the lateral semicircular canals (Fig. 13B). They are much more developed than other maniraptoriforms (Balanoff et al., 2018) and fill most of the space formed by the rostral semicircular canal. Such

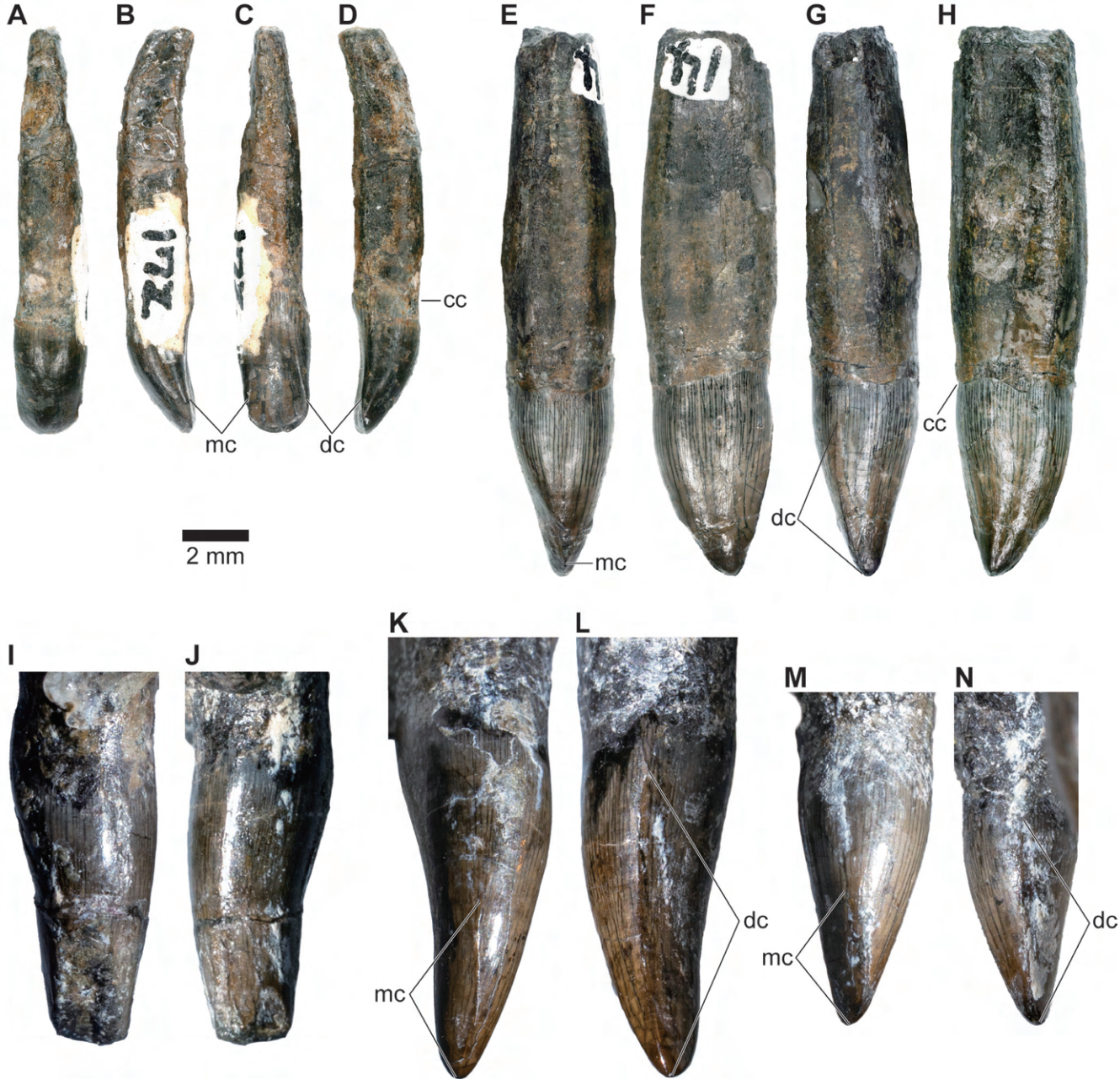

FIGURE 15. Teeth of FPDM-V-8461. Mesialmost tooth tentatively oriented as right premaxillary tooth (**A**–**D**), mesial tooth tentatively oriented as left premaxillary tooth (**E**–**H**), and second (**I**, **J**), fifth (**K**, **L**) and eighth (**M**, **N**) maxillary teeth in labial (A, F), mesial (B, E, I, K, M), lingual (C, H), distal (D, G, J, L, N) views. I–N are only roughly adapted to the scale. Abbreviations: cc, cervix constriction; dc, distal carina; mc, mesial carina.

well-developed cerebellar floccular lobes are shared with *Erlikosaurus* (Lautenschlager et al., 2012), *Nothronychus* (Smith et al., 2018) and *Falcarius* (Smith, 2014), and can be considered a unique feature of Therizinosauria shared with *Fukuivenator*.

Endosseous Labyrinth

The vestibular system including the semicircular canal and the ventral cochlear duct are preserved in the braincase (Fig. 13). The cochlear duct is relatively long, and its distal part is slightly medially oriented (Azuma et al., 2016; Fig. 13B). On the other hand, the cochlear duct is shorter than those of therizinosaurs *Erlikosaurus* and *Nothronychus*, while comparable to *Falcarius* (Lautenschlager et al., 2012). The vestibular system is well developed with the rostral semicircular canal being elongated dorsally (Azuma et al., 2016; Fig. 13C, E). Overall, the inner ear morphology is notably similar to that

of *Falcarius* (Lautenschlager et al., 2012). Additionally, the anterior canal extends slightly caudal to the crus commune, a feature seen in maniraptoriforms such as *Struthiomimus altus* (Witmer & Ridgely, 2009; Hanson et al., 2021; Bronzati et al., 2021).

Dentary

The posterior part of the right dentary bearing the last seven alveoli is preserved, and at least the posteroventral end is missing (Fig. 14). The preserved part appears subtriangular in shape tapering anteriorly with straight dorsal and ventral margins in lateral view (Fig. 14E), which indicates that the missing anterior part might be shallower dorsoventrally than the preserved anterior end (about 9 mm) when present. In dorsal view, the body is straight and mediolaterally narrow, on which the tooth row is approximately in line with the flat lateral surface (Fig. 14A).

The lateral surface is well preserved in the posterior half while it is somewhat damaged in the anterior half (Fig. 14E). A shallow dentary groove emerges near the posterodorsal end of the lateral surface and extends anteriorly toward a small neurovascular foramen just ventral to the third alveolus from the last. This foramen is anteroposteriorly elongated and discontinuous with anterior foramina unlike troodontids where several foramina form a deep groove (Currie, 1987; Brusatte et al., 2010; Turner et al., 2012). All alveoli are separated to each other by the interdental plates (Fig. 14C). Each interdental plate is smooth, subtriangular in medial view, and bordered from neighboring plates by small foramen for the apex of the replacement teeth situated mediodorsal to each alveolus. The meckelian fossa is dorsoventrally broad posteriorly and abruptly narrows anteriorly to be closed at the level of the sixth alveolus from the last. The four last alveoli partially perforate the dorsal wall of the meckelian fossa (Fig. 14F). In medial view, the pointed anterior end of the meckelian fossa is continuous with a shallow meckelian groove sitting approximately at midheight of the dentary in the preserved anterior end (Fig. 14C).

Dentition

Although the premaxilla and the anterior part of the dentary are not preserved, two isolated mesial teeth were found associated with the rest of the skeleton (Fig. 15). These teeth are substantially different in size from each other. The smaller one is potentially the mesialmost tooth exhibiting a characteristic spatulate shape with convex labial surface and slightly concave lingual surface (Fig. 15A–D). The apical margin of the crown is rounded in lingual view and is continuous with both the mesial and distal carinae, both of which are on the lingual surface to enclose the slight concavity (Fig. 15C). Around the cervix, a faint constriction is present (Fig. 15D). The root narrows apically by a slight inclination of the left lateral margin in lingual view and ends bluntly (Fig. 15C).

Another, much larger mesial tooth representing a left premaxillary or right dentary tooth exhibits a conical shape with subtle carinae along the convex mesial and straight distal margins (Fig. 15E–H). The mesial carina is present only in the apical third of the crown at most (Fig. 15E), whereas the distal carina runs along the labial margin of the distal aspect and ends slightly before reaching the cervix with curving slightly basolingually (Fig. 15G). In mesial view, the labial margin is convex whereas the lingual is almost straight with a slight convexity near the cervix (Fig. 15E). The cervix exhibits a weak constriction (Fig. 15H), which is more apparent than that of the anteriormost tooth (Fig. 15D). Although the crown shape of the larger mesial tooth is quite similar to those of lateral teeth, the former is smaller than the latter (Fig. 3). Additionally, the dorsoventral depths of the posterior parts of the maxilla and dentary, as well as the estimated depth in the anterior part of the latter, are unlikely to house such a long root. In both mesial teeth, there is no trace of any replacement teeth in the roots.

Among four erupted teeth in the left maxilla, the apicobasal heights are somewhat variable with the greatest in the 5th and the lowest in the 8th and 10th (Fig. 4B–F). As in the larger mesial and dentary teeth, all preserved maxillary teeth have suboval cross sections resulting in mediolaterally thicker maxillary teeth than the ziphodont teeth seen in most basal theropods, and do not bear denticles (Fig. 15I–N). In labial view, the second and fifth maxillary teeth are recurved apicodistally (Fig. 4C). In contrast, the 8th and 10th teeth are not recurved, exhibiting the convex mesial and straight distal margins in labial view and a faint constriction at each cervix. In mesial view, the second maxillary tooth bears an apex ending bluntly due to the wearing and/or postmortem damage mainly on the mesial and slightly on the distal margins (Fig. 15I, J), whereas apices of other maxillary teeth are well pointed (Fig. 15K–N). In addition, the crown in the second tooth lacks both mesial and distal carinae (Fig. 15I, J), whereas those of the fifth, eighth and 10th exhibit a short mesial carinae in the apical half and a longer distal carina that nearly extends to the base (Fig. 15K–N).

On the dentary, two intact teeth are preserved (Fig. 14A–E). The mesial tooth entirely lacks the crown whereas the lateral tooth preserves nearly whole crown except for the apex. The latter is quite similar to the 8th and 10th preserved teeth of maxilla by exhibiting unrecurved crown with a suboval cross section and short mesial and longer distal carinae while lacking any serrations. As in the maxilla, the size of the dentary teeth is relatively large for the dorsoventral depth of the dentary housing them.

Axial skeleton

Cervical vertebrae

Fukuivenator possessed at least 11 cervical vertebrae, including preserved 9 cervicals (1st to 3rd, 5th, 6th and 8th to 11th) and missing 4th and 7th (Figs. 16–20; Table 2). This number of cervical vertebrae is greater than those of most other theropods (10 or less), and such numerical increase indicates the elongation of the neck known in therizinosaurs and oviraptorosaurs (Zanno and Makovicky, 2011). Atlantal neurapophyses are added to the series originally described in Azuma et al. (2016) in which they are misidentified as axial ribs.

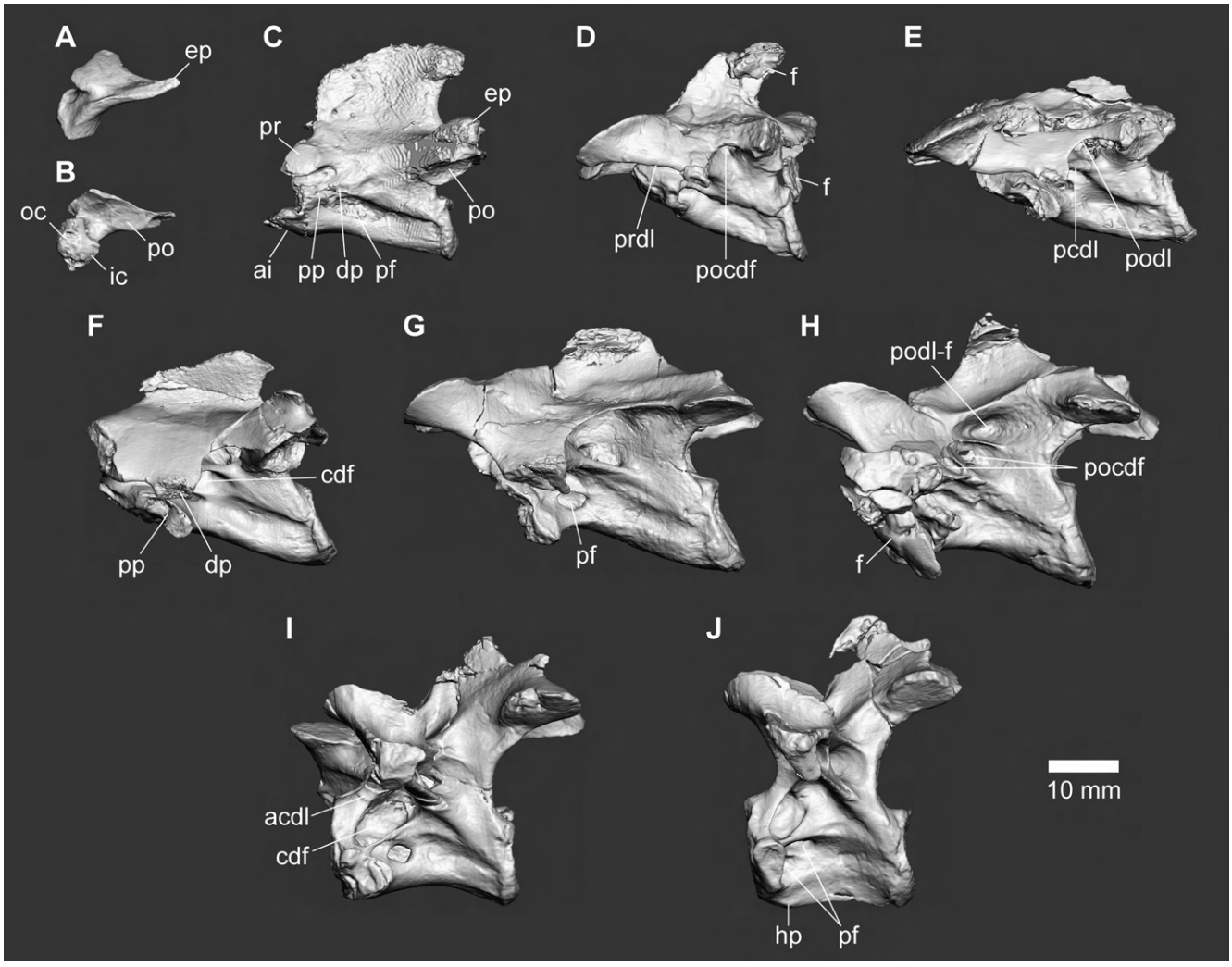

FIGURE 16. Cervical vertebrae of FPDM-V-8461. Left lateral views of left (**A**) and right (**B**) atlantal neurapophyses, axis (**C**) and 3rd (**D**), 5th (**E**), 6th (**F**), 8th (**G**), 9th (**H**), 10th (**I**) and 11th (**J**) cervical vertebrae. Abbreviations: acdl, anterior centrodiapophyseal lamina; ai, axis intercentrum; cdf, centrodiapophyseal fossa; dp, diapophysis; ep, epipophysis; f, bone fragment; hp, hypapophysis; ic, intercentrum contact; oc, occipital condyle contact; pcdl, posterior centrodiapophyseal lamina; pf, pneumatic foramen; po, postzygapophysis; pocdf, postzygocentrodiapophyseal fossa; podl, postzygodiapophyseal lamina; podl-f, intralaminar fossa of postzygodiapophyseal lamina; pp, parapophysis; pr, prezygapophysis; prdl, prezygodiapophyseal lamina.

The left postzygapophysis of the third cervical is missing.

Whereas all of eight well-preserved centra are anteroposteriorly long and dorsoventrally shallow in lateral view (Fig. 16), they are not in the "hyperelongate" condition, unlike those of ornithomimids and therizinosaurs (Zanno et al., 2009); for example, the third cervical centra is 10.1 mm in width at the narrowest (in the posterior end) and 27.7 mm in length. At the posterior articular surface in each centrum, the lateral width is subequal to the dorsoventral height (Fig. 18C–J). In the third to eighth cervical centra, the anterior articular surfaces are strongly inclined ventrally, and distinctly wider than high in anterior view (Fig. 17D–G) as in other maniraptoriforms (Xu et al., 2002b). In addition, the anterior surface of the ninth is inclined somewhat ventrally (Fig. 17H) and posterior surfaces of the third to the ninth are inclined somewhat dorsally (Fig. 16D–H). The cervical centra exhibit intermediate condition between amphiplatyan and platycoelous with flat-to-concave anterior surfaces and slightly more concave posterior surfaces (Figs. 17, 18) as in *Deinonychus* (Ostrom, 1969). The posterior extent of the centrum in anterior to middle cervical vertebrae terminates approximately at the level of the neural arch (Fig. 16C–F).

All the cervical centra possess at least one pneumatic foramen on each side (Fig. 16). In addition, the 8th and 11th exhibit two pneumatic foramina at least on each side, in which pneumatic foramina are dorsoventrally separated by horizontally oriented septa (Figs. 16J, 18K) as in *Sinovenator*, therizinosaurs and

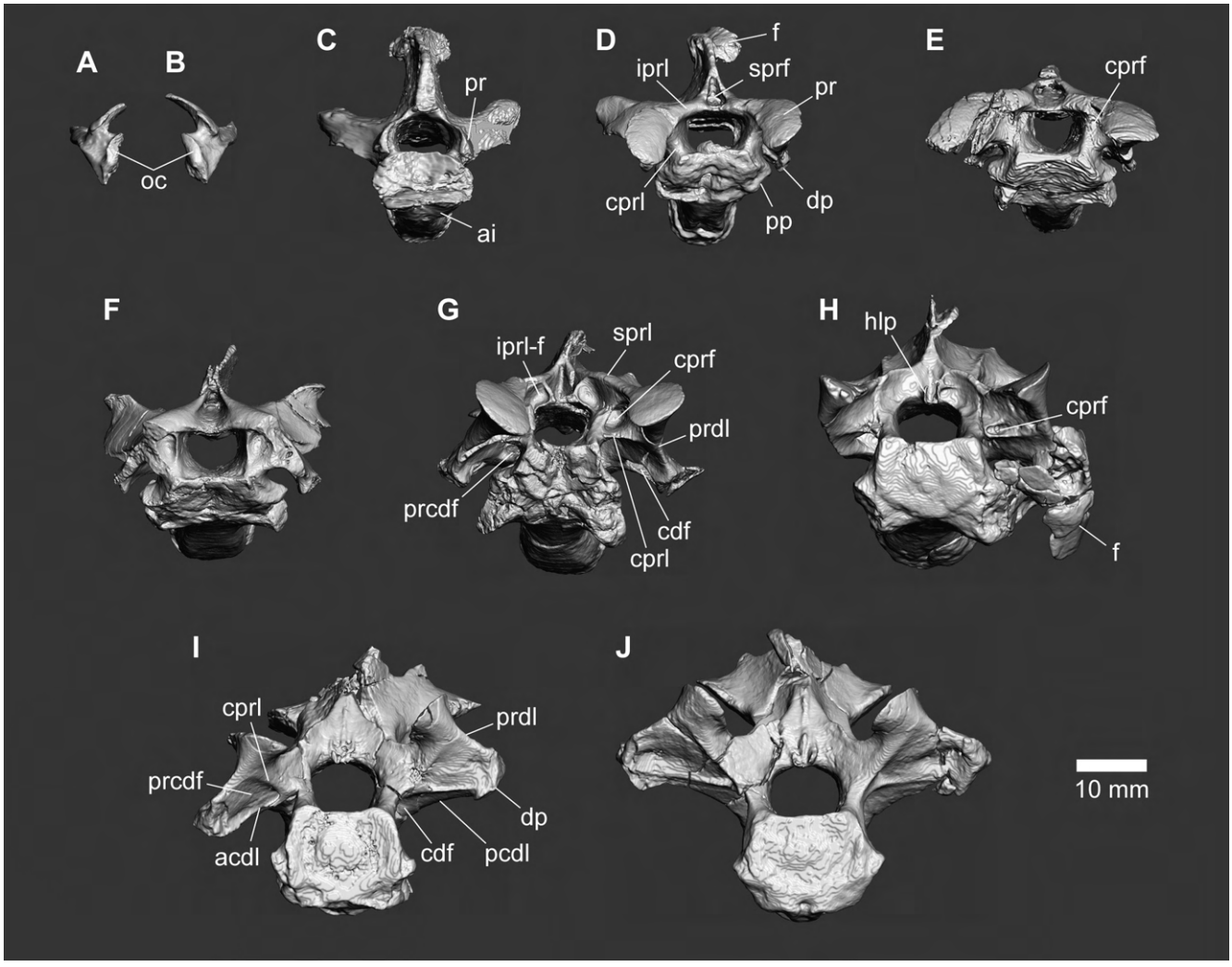

FIGURE 17. Cervical vertebrae of FPDM-V-8461. Anterior views of right (**A**) and left (**B**) atlantal neurapophyses, axis (**C**) and 3rd (**D**), 5th (**E**), 6th (**F**), 8th (**G**), 9th (**H**), 10th (**I**) and 11th (**J**) cervical vertebrae. Abbreviations: acdl, anterior centrodiapophyseal lamina; ai, axis intercentrum; cprf; centroprezygapophyseal fossa; cprl, centroprezygapophyseal lamina; dp, diapophysis; f, bone fragment; hlp, hypantrum-like projection; iprl, intraprezygapophyseal lamina; iprl-f, intralaminar fossa of intraprezygapophyseal lamina; oc, occipital condyle contact; pp, parapophysis; pr, prezygapophysis; prcdf, prezygocentrodiapophyseal fossa; prdl, prezygodiapophyseal lamina; sprf, spinoprezygapophyseal fossa; sprl, spinoprezygapophyseal lamina.

some oviraptorosaurs (Gauthier, 1986; Turner et al., 2012). Although the number of pneumatic foramina on the centra varies among cervicals in *Fukuivenator*, similar condition is known at least in *Falcarius* (Zanno, 2010) and *Jianchangosaurus* (Pu et al., 2013). The pneumatic foramina connect to the internal pneumatopore except in the axis and the 11th. Most of the lateral surface of the axial centrum is occupied by an anteroposteriorly-elongated fossa below the neurocentral suture, and the pneumatic foramen is present as the deepest part in its anterior half, just posterior to the parapophysis (Fig. 16C). The pneumatic foramen of the 11th is present as a fossa in the right side whereas it is separated into a dorsal deep pit and ventral shallow pit in the left side (Fig. 16J). In the axis, the parapophysis is indistinctly present as a small bulge, situated dorsally, and separated from the ventral margin of the centrum in lateral view (Fig. 16C). The parapophysis is present as a distinct lateral projection from the anteroventral margin of the centrum in the postaxial cervicals (Fig. 16D–J). In the sixth cervical vertebra, the parapophysis is best preserved among postaxial cervicals and has a distinct concavity on the middle part of the facet in lateral view (Fig. 16F).

Except for the 10th and 11th, ventral surfaces of the cervical centra are essentially flat even between both parapophyses, resulting in the lack of the carotid processes (Fig. 20C–G). The ventral surface of the ninth is somewhat concave anteriorly due to the enlargement of parapophyses (Fig. 20H). The ventral

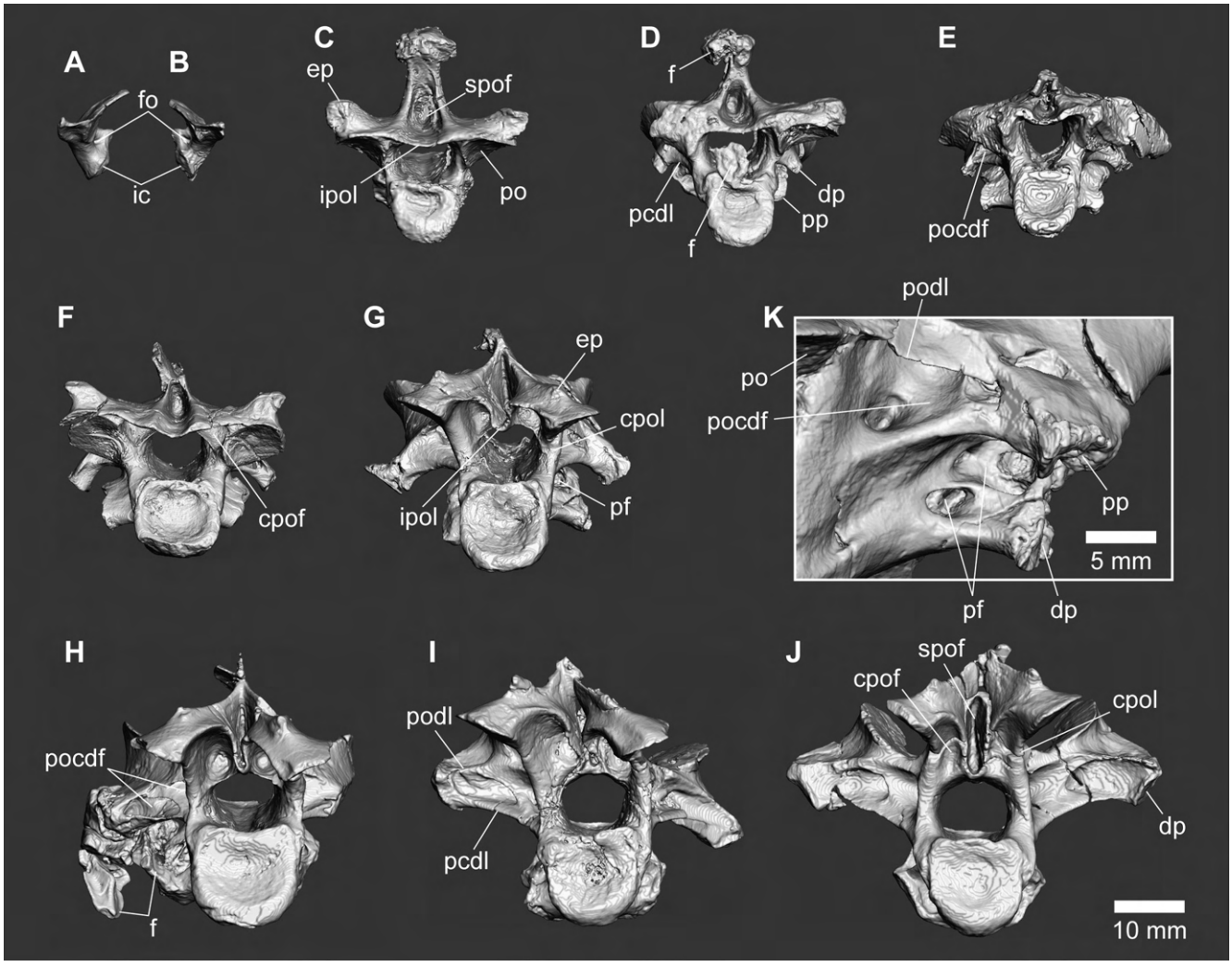

FIGURE 18. Cervical vertebrae of FPDM-V-8461. Posterior (**A**–**J**) and close-up right posterolateral (**K**) views of left (A) and right (B) atlantal neurapophyses, axis (C) and 3rd (D), 5th (E), 6th (F), 8th (G, K), 9th (H), 10th (I) and 11th (J) cervical vertebrae. Abbreviations: cpof, centropostzygapophyseal fossa; cpol, centropostzygapophyseal lamina; dp, diapophysis; ep, epipophysis; f, bone fragment; fo, foramen; ic, intercentrum contact; ipol, intrapostzygapophyseal lamina; pcdl, posterior centrodiapophyseal lamina; pf, pneumatic foramen; po, postzygapophysis; pocdf, postzygocentrodiapophyseal fossa; podl, postzygodiapophyseal lamina; pp, parapophysis; spof, spinopostzygapophyseal fossa.

surface of the 10th is flat anteriorly, while it becomes convex posteriorly (Fig. 20I). The 11th cervical centrum is ventrally pinched to form a distinct median ridge or hypapophysis (Fig. 20J), whereas it is not as projected ventrally as those of *Sinraptor* (Currie and Zhao, 1993a), *Avimimus* (Kurzanov, 1981), *Nothronychus* (Kirkland and Wolfe, 2001) and *Deinonychus* (Ostrom, 1969). In the anterior-middle cervicals, the lateroventral margins become angular posteriorly (Fig. 20C–F); however, they do not form "finlike" crests seen in therizinosauroids and some basal oviraptorosaurs (Zanno et al., 2009).

On the neural arch of the atlas, paired atlantal neurapophyses are well preserved. Each neurapophysis exhibits triradiate shape in lateral view represented by anterodorsal, anteroventral and posterior processes (Fig. 16A). In medial view, the main body bears a tabular zygapophyseal facet facing medioventrally (Fig. 16B). The anteroventral process projects somewhat medially to form a large contact surface composed of a convex anterodorsal part for the occipital condyle and a flatter posteroventral part for the intercentrum (Fig. 17A, B). In posterior view, a small foramen is present at the base of the anteroventral process, between the large contact surface and the postzygapophyseal facet (Fig. 18A, B). The anterodorsal process is formed by a thin, flange-like structure facing its broad surface laterodorsally, which medially forms the roof of the neural canal and laterally covers a part of the anteroventral process in dorsal view (Fig.

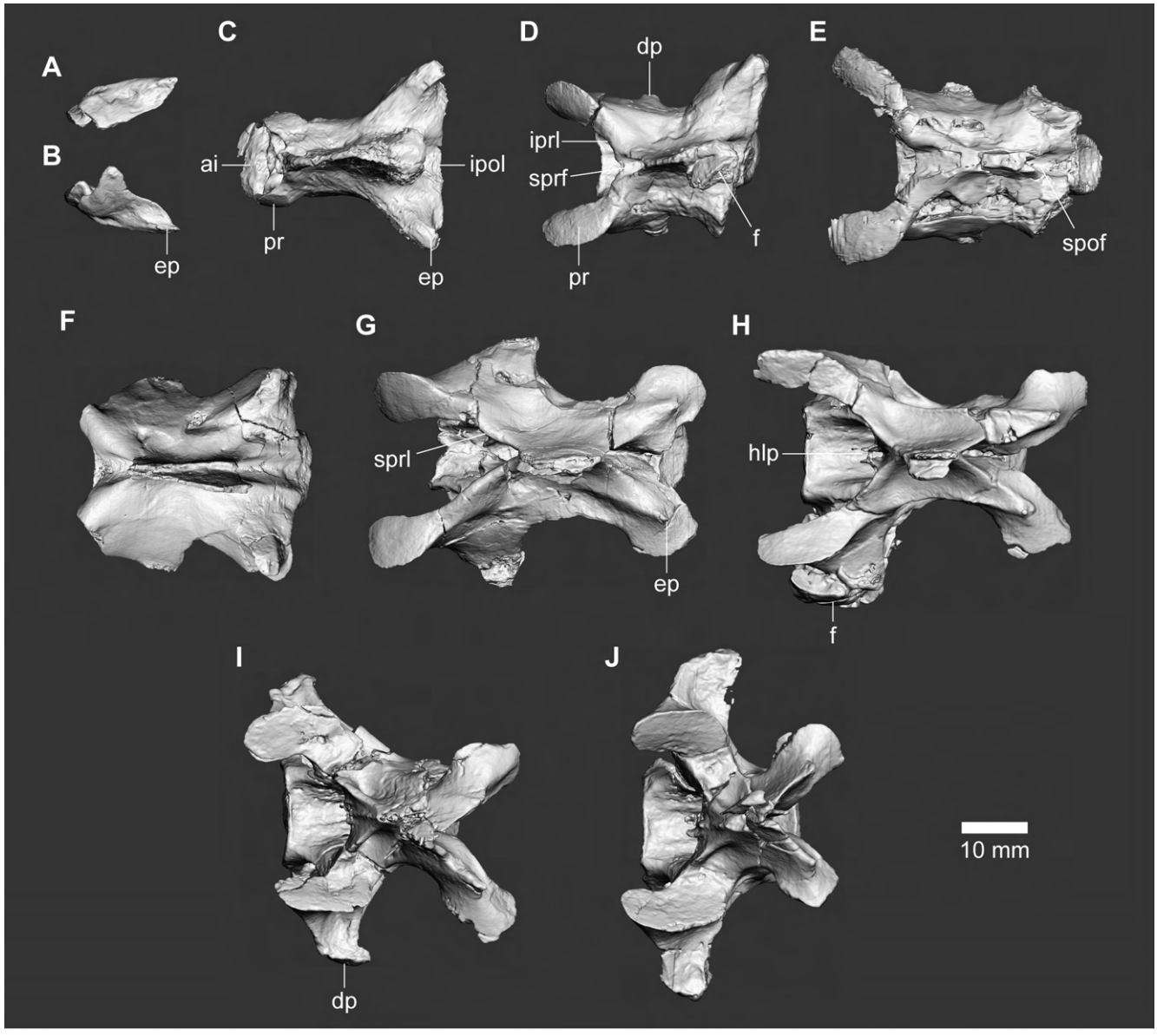

FIGURE 19. Cervical vertebrae of FPDM-V-8461. Dorsal views of right (**A**) and left (**B**) atlantal neurapophyses, axis (**C**) and 3rd (**D**), 5th (**E**), 6th (**F**), 8th (**G**), 9th (**H**), 10th (**I**) and 11th (**J**) cervical vertebrae. Abbreviations: acdl, anterior centrodiapophyseal lamina; ai, axis intercentrum; cdf, centrodiapophyseal fossa; cpof, centropostzygapophyseal fossa; cprl, centroprezygapophyseal lamina; dp, diapophysis; ep, epipophysis; f, bone fragment; hlp, hipantrum-like projection; ipol, intrapostzygapophyseal lamina; ipol, intrapostzygapophyseal lamina; iprl, intraprezygapophyseal lamina; pcdl, posterior centrodiapophyseal lamina; po, postzygapophysis; podl, postzygodiapophyseal lamina; pp, parapophysis; pr, prezygapophysis; prcdf, prezygocentrodiapophyseal fossa; prdl, prezygodiapophyseal lamina; spof, spinopostzygapophyseal fossa; sprf, spinoprezygapophyseal fossa; sprl, spinoprezygapophyseal lamina.

19A, B). The posterior process is dorsoventrally thin, while broad and triangular in dorsal view. The posterior end of the dorsal surface bears a short longitudinal ridge representing an epipophysis.

On the neural arch of the axis, the prezygapophyseal facet of the axis is situated dorsal to the anterior end of the centrum as in the posterior cervicals in lateral view (Fig. 16C) and dorsal to the lateral margin of the centrum in anterior view (Fig. 17C). The prezygapophyseal facets face laterally in the axis in contrast to those of postaxial cervicals facing dorsally or mediodorsally (Fig. 17C–J). The diapophysis of the axis is present as a low mound posteroventral to the fossa below the prezygapophysis, and posteriorly accompanied by a shallow depression (Fig. 16C). The axial epipophysis is well developed to form a large, posterolaterally-directed projection extending beyond the lateral margin of the postzygapophysis (Figs. 19C, 20C). The neural

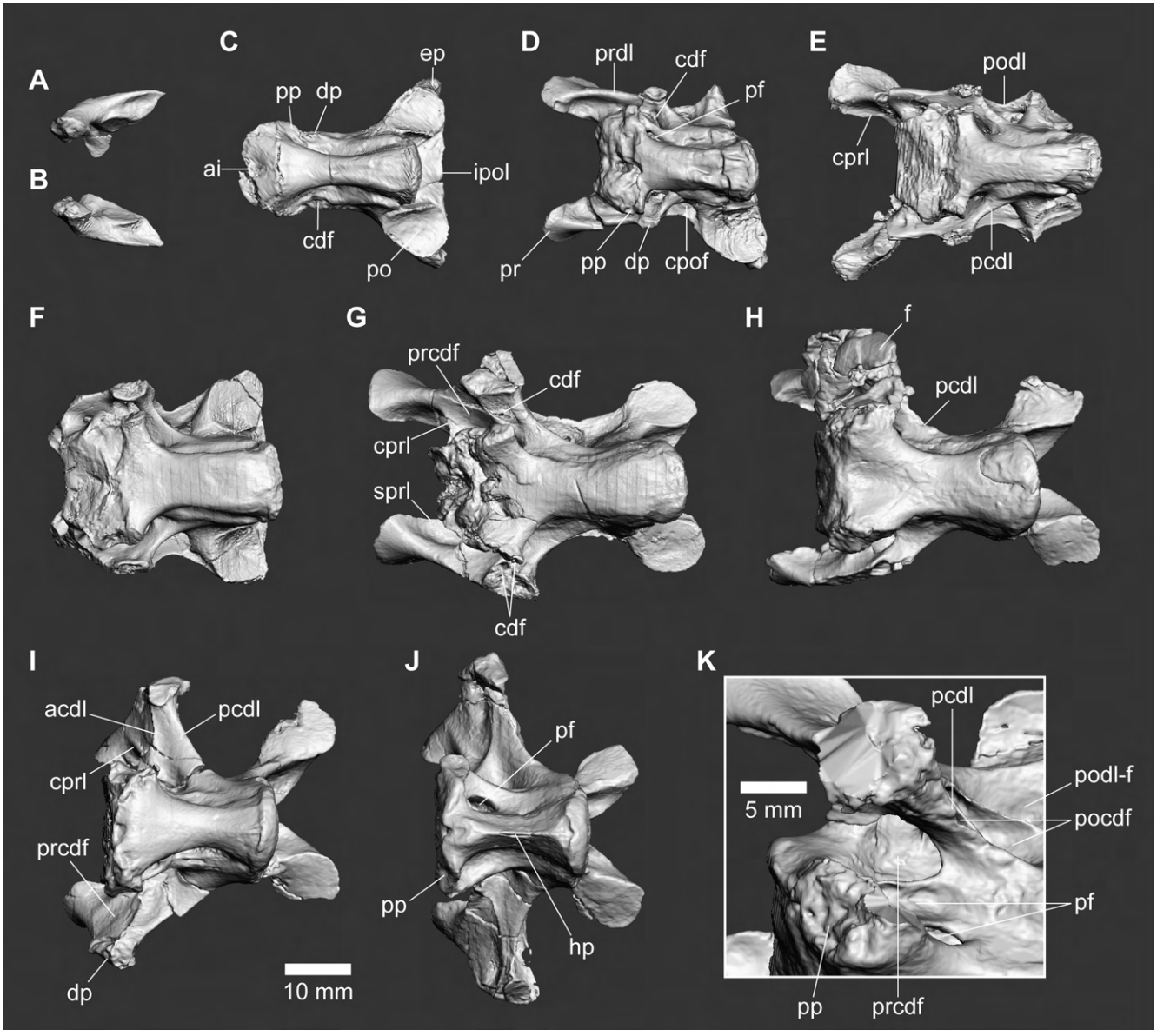

FIGURE 20. Cervical vertebrae of FPDM-V-8461. Ventral (**A**–**J**) and close-up left lateroventral (**K**) views of left (A) and right (B) atlantal neurapophyses, axis (C) and 3rd (D), 5th (E), 6th (F), 8th (G), 9th (H, K), 10th (I) and 11th (J) cervical vertebrae. Note that the bone fragment in the 9th is digitally removed in K. Abbreviations: acdl, anterior centrodiapophyseal lamina; ai, axis intercentrum; cdf, centrodiapophyseal fossa; cpof, centropostzygapophyseal fossa; cprl, centroprezygapophyseal lamina; dp, diapophysis; ep, epipophysis; f, bone fragment; hp, hypapophysis; pcdl, posterior centrodiapophyseal lamina; pf, pneumatic foramen; po, postzygapophysis; podl-f, intralaminar fossa of postzygodiapophyseal lamina; pp, parapophysis; pr, prezygapophysis; prcdf, prezygocentrodiapophyseal fossa; prdl, prezygodiapophyseal lamina.

spine of the axis is anteroposteriorly wide through its depth and expanded further posteriorly at its dorsal margin, so that its anteroposterior length reaches that of the centrum (Fig. 16C). The posterodorsal portion of the axial neural spine is flared laterally as in the third while being dissimilar to that in the middle to posterior cervicals (Fig. 19C).

Neural arches of the postaxial cervicals essentially resemble each other. In lateral view, the prezygapophysis is projected anteriorly and flexed slightly ventrally (Fig. 16D–J). The prezygapophyses project well anteriorly in the third 3rd to 8th cervicals to place the facets entirely anterior to the centrum (Fig. 16D–F), in contrast to the facets of the axis and 10th and 11th cervicals that are situated dorsal to the anterior part of the centrum (Fig. 16C, I, J), and the 9th cervical exhibit an intermediate condition (Fig. 16H). In anterior view, the prezygapophyses overhang the centrum to place

prezygapophyseal facets entirely lateral to the centrum in most cervicals (Fig. 17D–J). The prezygapophyseal facets face dorsally in the fifth cervical in contrast to those of other postaxial cervicals facing mediodorsally. In the third to sixth cervicals, the bases of both prezygapophyses connect to each other by a horizontal interprezygapophyseal lamina (Fig. 17D–F). In the eighth and ninth cervicals, the lateral parts of the intraprezygapophyseal lamina are divided dorsoventrally by a pair of intralaminar fossae (Fig. 17G, H). In the eighth and more posterior cervicals, the spinoprezygapophyseal laminae are well-developed accompanied with the presence of anterior projection of the lateroventral margin of the spinoprezygapophyseal fossa (Fig. 17G–J). Although this projection is originally described as the hypantrum (Azuma et al., 2016), it does not reach hyposphene-like projection of the preceding cervical. Ventrally, each prezygapophysis of the 3rd to 11th cervicals is supported by the centroprezygapophyseal and prezygodiapophyseal laminae (Fig. 20D–J). The centroprezygapophyseal fossae are present between the intraprezygapophyseal and centroprezygapophyseal laminae in the fifth to eighth cervicals and is reduced in the ninth to a remnant only present in the left side (Fig. 17E–H). In the axis and third to sixth cervicals, the intrapostzygapophyseal lamina is expanded posteriorly from the base of the neural spine to form a broad platform covering the neural canal in dorsal view (Fig. 19C–F). In the eighth and more posterior cervicals, the medial part of the intrapostzygapophyseal lamina bends ventrally to form a hyposphene-like projection just below the spinopostzygapophyseal lamina (Fig. 19G–J). A pair of deep centropostzygapophyseal fossae are situated below the intrapostzygapophyseal lamina in the sixth and more posterior cervicals (Fig. 18F–J). Such a complex lamina system surrounding the neural canal, resulting in deep and wide grooves for interspinous ligaments and additional deep sockets, represents a unique feature among theropods (Azuma et al., 2016).

In postaxial cervicals, the posterior centrodiapophyseal lamina is strongly developed as a thick, laterally-offset lamina that demarcates the centrodiapophyseal fossa dorsally (Fig. 20D–J). The anterior centrodiapophyseal lamina recedes posteriorly toward the posterior centrodiapophyseal lamina by the expansion of the prezygocentrodiapophyseal fossa in the eighth and ninth cervicals. In the eighth cervical, the centrodiapophyseal fossa is present as a small pneumatic foramen in the ventral aspect of the diapophysis and divided anteroposteriorly by a transverse lamina in the right side (Fig. 20G). In the ninth cervical, the centrodiapophyseal fossa is absent at least in the left side (Fig. 20K). In contrast, the centrodiapophyseal fossa is developed as a large pneumatic foramen invading the conjoined base of the prezygapophysis and diapophysis in the 10th and 11th cervicals (Fig. 16I, J). Dorsal to the posterior centrodiapophyseal lamina, the postzygocentrodiapophyseal fossa is well developed as a foramen in postaxial cervicals (Fig. 16D–J) and dorsally demarcated by a well-developed horizontal postzygodiapophyseal lamina in the third to eighth cervicals (Fig. 16D–G). In combination with the intraprezygapophyseal, prezygodiapophyseal and intrapostzygapophyseal laminae, the postzygodiapophyseal lamina contributes to form an extensive horizontal platform in the anterior cervicals (Fig. 19D–G) that is unique among theropods (Azuma et al., 2016). In the ninth and more posterior cervicals, the medial part of the postzygodiapophyseal lamina is divided dorsoventrally by a presence of large fossa (intralaminar fossa of postzygodiapophyseal lamina) so that the lamina does not extend to the postzygapophysis (Fig. 16H–J). The dorsal division of the postzygodiapophyseal lamina is posteriorly continuous with the epipophysis in the 9th and 10th cervicals, whereas with the postzygapophysis in the 11th cervicals. In addition, in the ninth and more posterior cervicals, the postzygocentrodiapophyseal fossa is divided into two foramina by a posteroventrallydirected lamina, and another fossa develops between the postzygodiapophyseal and spinoprezygapophyseal laminae. In postaxial cervicals, epipophyses are placed above postzygapophyseal facets.

In postaxial cervicals, the neural spines are generally thin and plate-like, with no pneumatic foramen nor fossa on each side (Fig. 19C–J). Among preserved middle-posterior cervicals, only the eighth bears a nearly complete spine, which is shallower than the posterior centrum height (Fig. 16H) as in other coelurosaurs except for tyrannosaurids (Holtz, 2001; Brusatte et al., 2010). The anteroposterior lengths of the neural spines are shorter than those of the centra unlike that of the axis (Fig. 16D–J), especially in the eighth and more posterior cervicals to give an X-shaped appearance in dorsal view (Fig. 19G–J) as in most other coelurosaurs (Makovicky and Sues, 1998; Brusatte et al., 2014). The dorsal end of the neural spine is bifurcated laterally at least in the eighth and ninth cervical to bear a narrow longitudinal sulcus dorsally (Fig. 17G, H) unlike other theropods and rather like some sauropods (Azuma et al., 2016). The pre- and postspinal fossae are present throughout the cervical series except for the prespinal fossa of the axis (Figs. 17C–J, 18C–J). The rugosity of the ligament attachment scars is absent or only weakly developed within each fossa as in other coelurosaurs except for tyrannosaurids (Brusatte et al., 2010).

Dorsal vertebrae

The separately preserved 11 dorsals probably constitute a complete series (Figs. 21–25). Such number of dorsal vertebrae represents an intermediate condition between the plesiomorphic state (12 or more) seen in early-diverging maniraptorans and the derived state (10 or fewer) seen in some therizinosaurids such as *Suzhousaurus* (Dong, 1979) and *Nanshiungosaurus* (Daqing et al., 2007), and some oviraptorosaurs (Turner et al., 2012). The first centrum is severely damaged and the second dorsal lacks its neural arch.

The first dorsal is a cervicodorsal vertebra that appears very similar in morphology to the posteriormost cervical vertebrae (Figs. 16J, 21A). Although the parapophysis is not preserved, the preserved anterodorsal margin of the centrum indicates that the parapophysis does not reach the dorsal margin of the

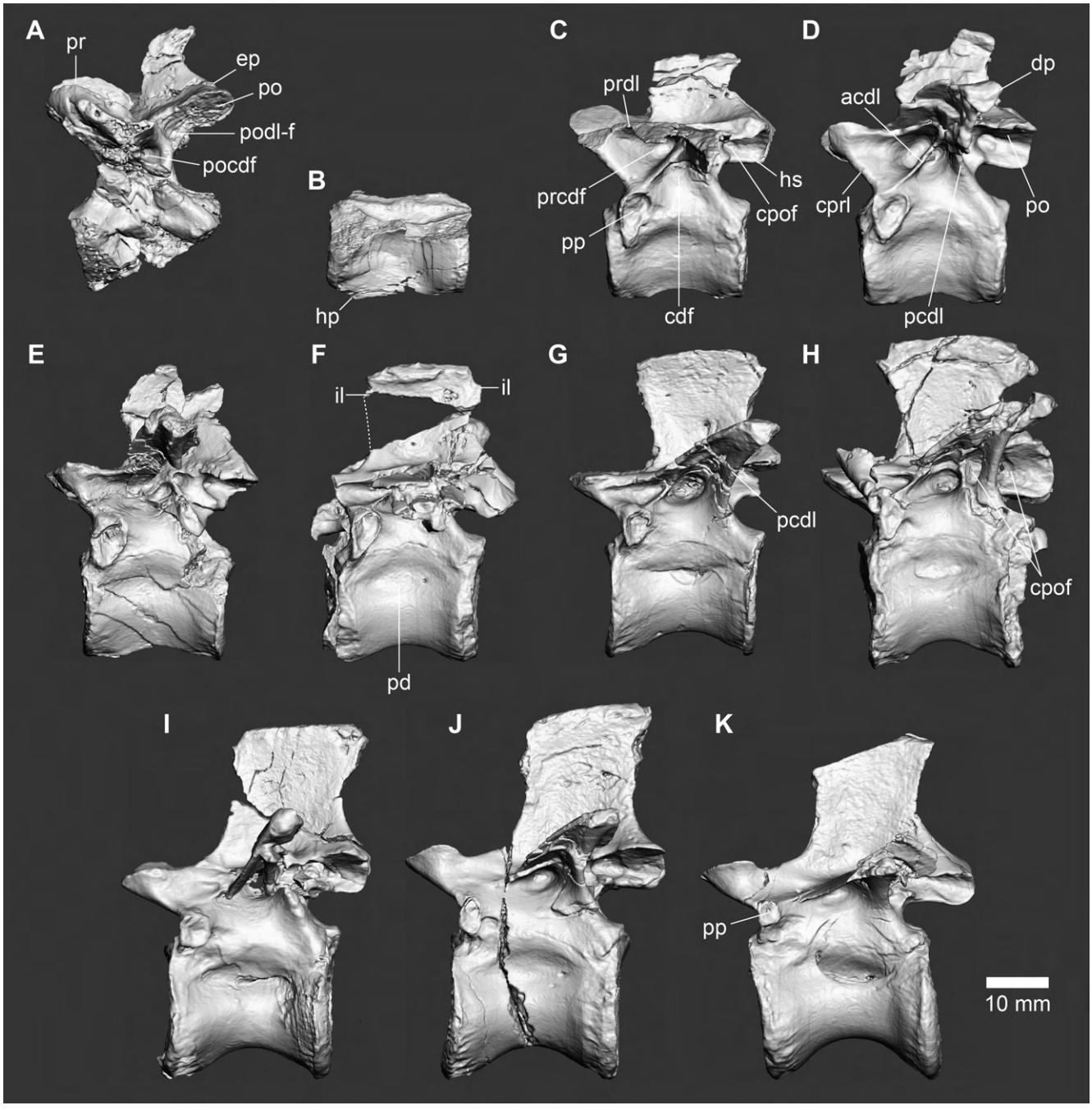

FIGURE 21. Dorsal vertebrae of FPDM-V-8461. Left lateral views of 1st (**A**), 2nd (**B**), 3rd (**C**), 4th (**D**), 5th (**E**), 6th (**F**), 7th (**G**), 8th (**H**), 9th (**I**), 10th (**J**) and 11th (**K**) dorsal vertebrae. Abbreviations: acdl, anterior centrodiapophyseal lamina; cdf, centrodiapophyseal fossa; cpof, centropostzygapophyseal fossa; cprl, centroprezygapophyseal lamina; dp, diapophysis; ep, epipophysis; hp, hypapophysis; hs, hyposphene; il, interspinous ligament scar; pcdl, posterior centrodiapophyseal lamina; pd, pleurocentral depression; po, postzygapophysis; pocdf, postzygocentrodiapophyseal fossa; podl-f, intralaminar fossa of postzygodiapophyseal lamina; pp, parapophysis; pr, prezygapophysis; prcdf, prezygocentrodiapophyseal fossa; prdl, prezygodiapophyseal lamina.

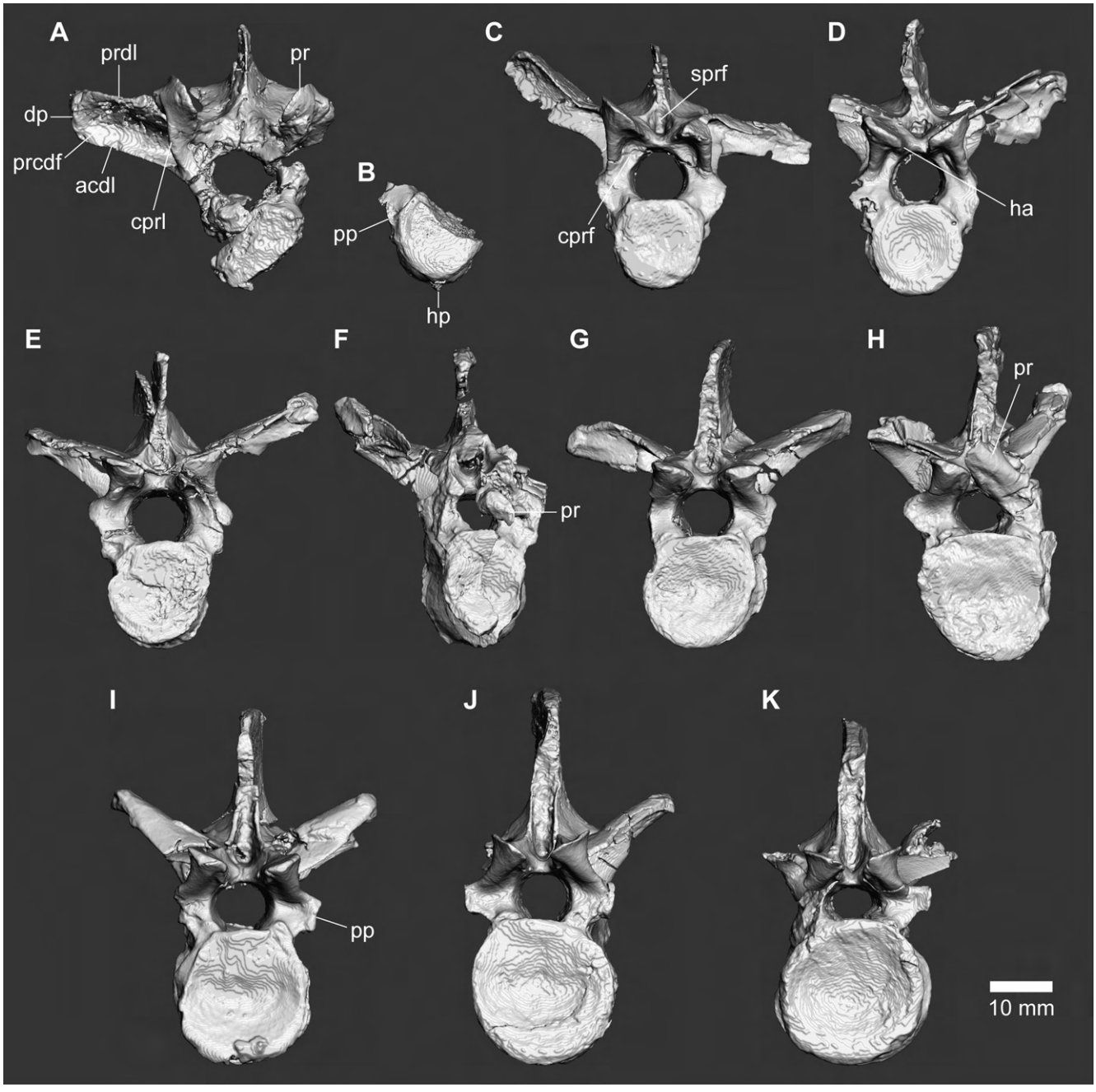

FIGURE 22. Dorsal vertebrae of FPDM-V-8461. Anterior views of 1st (**A**), 2nd (**B**), 3rd (**C**), 4th (**D**), 5th (**E**), 6th (**F**), 7th (**G**), 8th (**H**), 9th (**I**), 10th (**J**) and 11th (**K**) dorsal vertebrae. Abbreviations: acdl, anterior centrodiapophyseal lamina; cprf, centroprezygapophyseal fossa; cprl, centroprezygapophyseal lamina; dp, diapophysis; ha, hypantrum; pp, parapophysis; pr, prezygapophysis; prcdf, prezygocentrodiapophyseal fossa; prdl, prezygodiapophyseal lamina; sprf, spinoprezygapophyseal fossa.

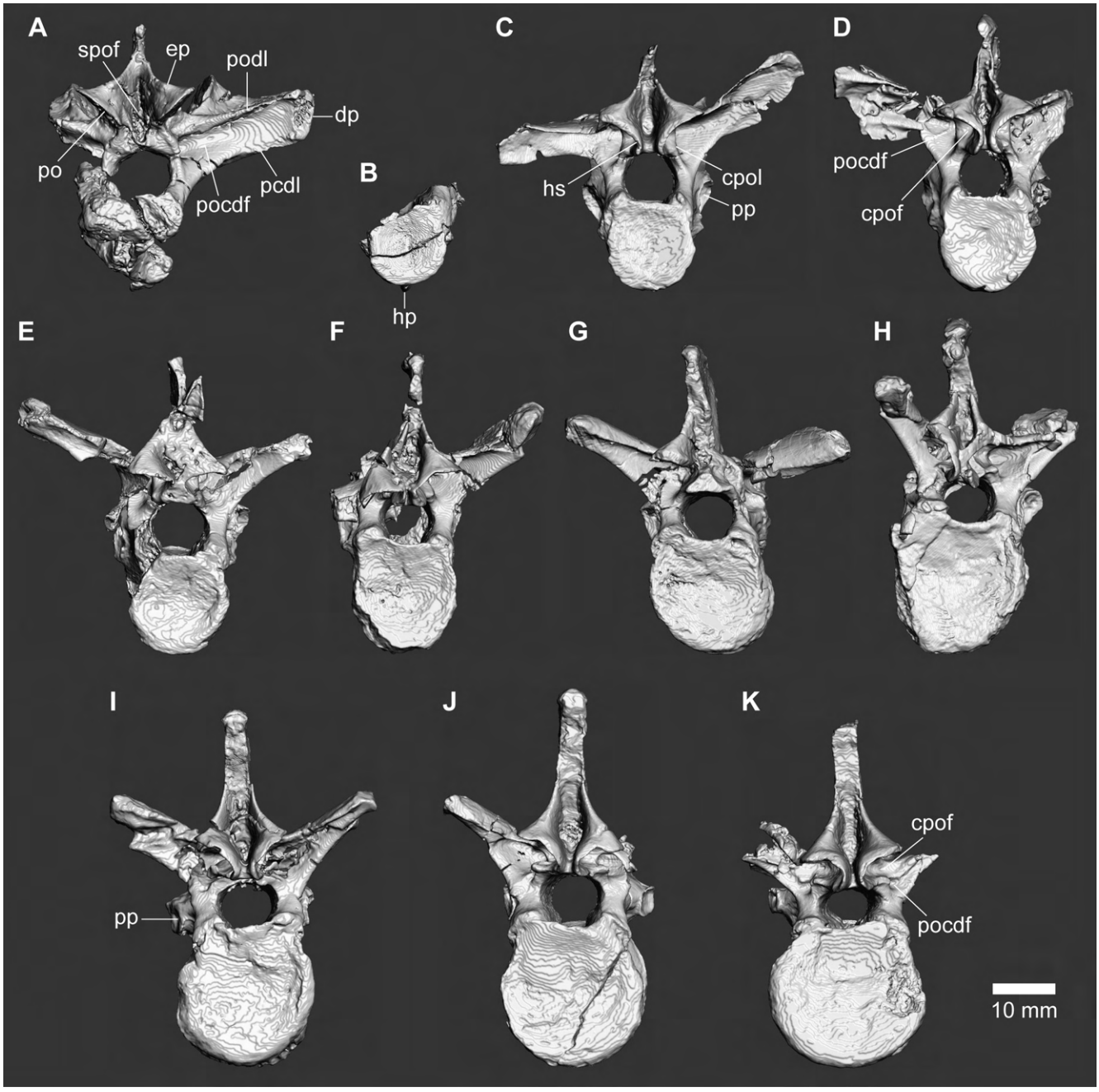

FIGURE 23. Dorsal vertebrae of FPDM-V-8461. Posterior views of 1st (**A**), 2nd (**B**), 3rd (**C**), 4th (**D**), 5th (**E**), 6h (**F**), 7th (**G**), 8th (**H**), 9th (**I**), 10th (**J**) and 11th (**K**) dorsal vertebrae. Abbreviations: cpof, centropostzygapophyseal fossa; cpol, centropostzygapophyseal lamina; dp, diapophysis; ep, epipophysis; hp, hypapophysis; hs, hyposphene; pcdl, posterior centrodiapophyseal lamina; po, postzygapophysis; pocdf, postzygocentrodiapophyseal fossa; podl, postzygodiapophyseal lamina; pp, parapophysis; spof, spinopostzygapophyseal fossa.

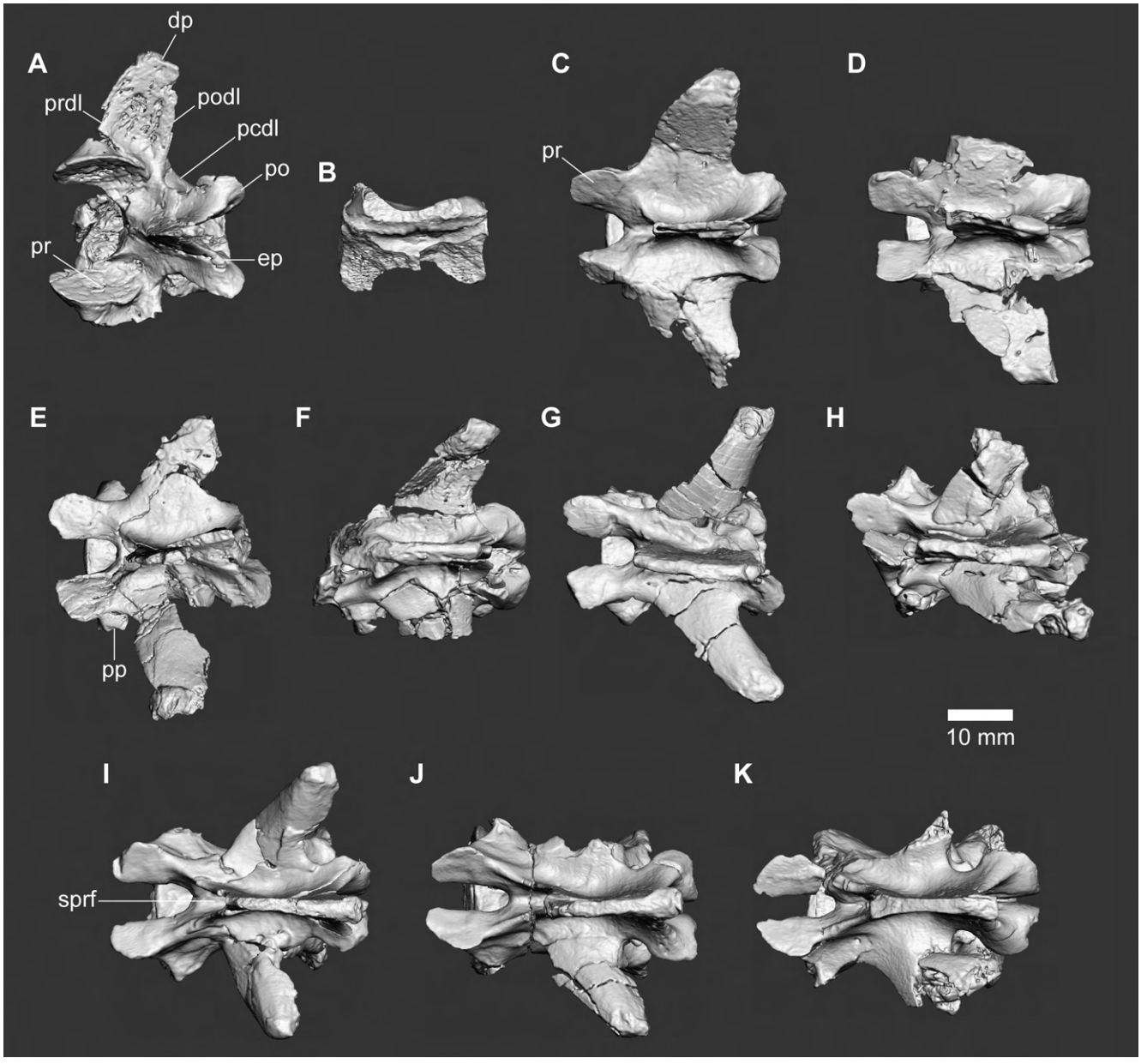

FIGURE 24. Dorsal vertebrae of FPDM-V-8461. Dorsal views of 1st (**A**), 2nd (**B**), 3rd (**C**), 4th (**D**), 5th (**E**), 6th (**F**), 7th (**G**), 8th (**H**), 9th (**I**), 10th (**J**) and 11th (**K**) dorsal vertebrae. Abbreviations: dp, diapophysis; ep, epipophysis; pcdl, posterior centrodiapophyseal lamina; po, postzygapophysis; podl, postzygodiapophyseal lamina; pp, parapophysis; pr, prezygapophysis; prdl, prezygodiapophyseal lamina; sprf, spinoprezygapophyseal fossa.

centrum in lateral view as in cervical vertebrae. The intralaminar fossa of postzygodiapophyseal lamina divides the postzygodiapophyseal lamina dorsoventrally (Fig. 21A) as in posterior cervicals (Fig. 16H–J). The transverse processes bearing the diapophyses are displaced anteriorly to conjoin with the prezygapophyses and widely separated from the postzygapophyses in dorsal view (Fig. 24A) as in posterior cervical vertebrae (Fig. 19H–J). The epipophysis is present above the postzygapophyseal facet (Fig. 21A) and much smaller than those of postaxial cervicals (Fig. 16C–J). The neural spine is anteroposteriorly narrow in lateral view (Fig. 21A) as in posterior cervicals (Fig. 16H–J). The transverse process emerges from the lateral margin of the prezygapophysis in dorsal view (Fig. 24A) as in the 10th and 11th cervicals (Fig. 19I, J). However, in anterior view, the transverse process is long and directed laterodorsally as in other dorsals (Fig. 22) while the one

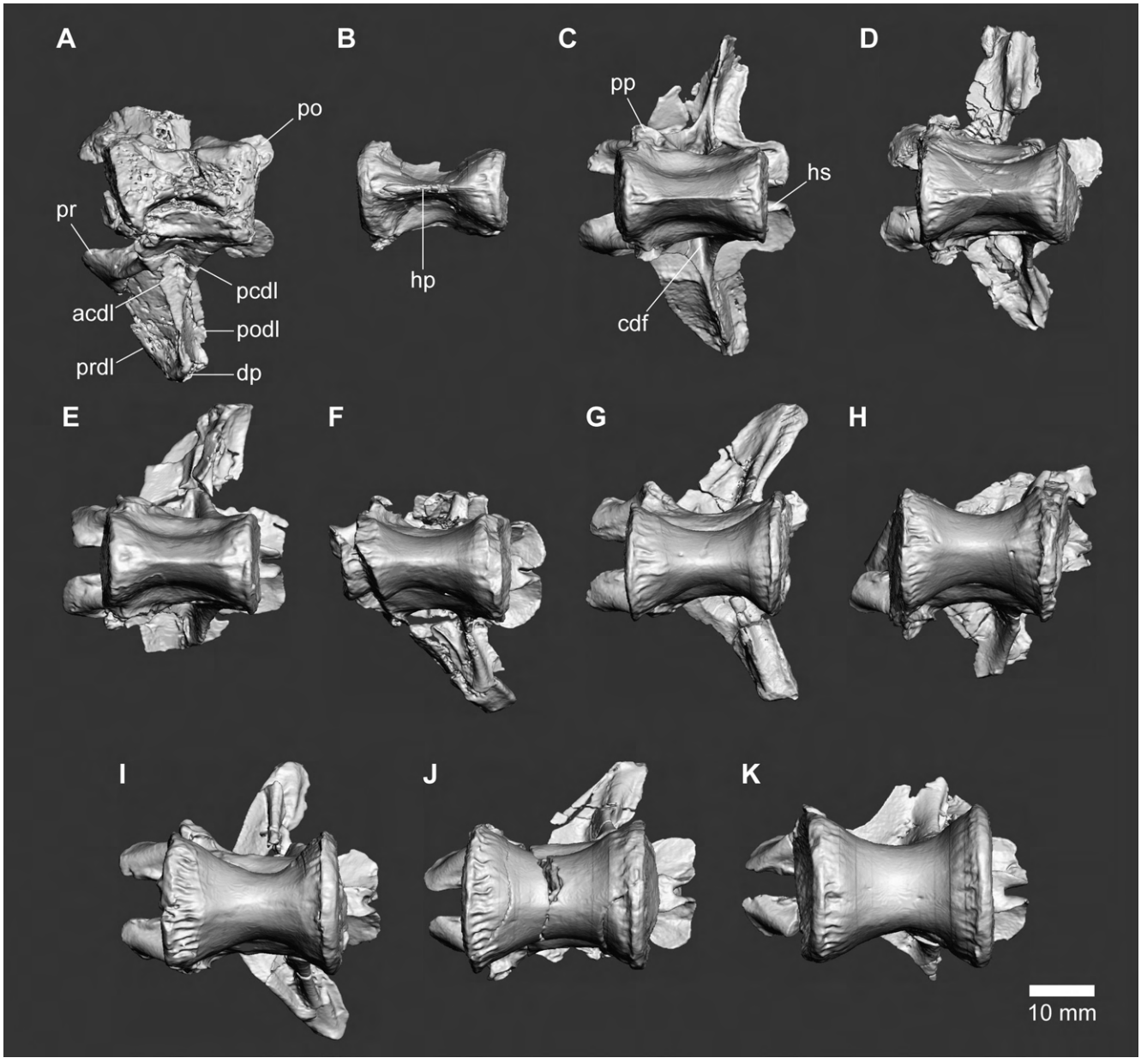

FIGURE 25. Dorsal vertebrae of FPDM-V-8461. Ventral views of 1st (**A**), 2nd (**B**), 3rd (**C**), 4th (**D**), 5th (**E**), 6th (**F**), 7th (**G**), 8th (**H**), 9th (**I**), 10th (**J**) and 11th (**K**) dorsal vertebrae. Abbreviations: acdl, anterior centrodiapophyseal lamina; cdf, centrodiapophyseal fossa; dp, diapophysis; ep, epipophysis; hp, hypapophysis; hs, hyposphene; pcdl, posterior centrodiapophyseal lamina; po, postzygapophysis; podl, postzygodiapophyseal lamina; pp, parapophysis; pr, prezygapophysis; prdl, prezygodiapophyseal lamina.

in posterior cervicals is short and directed lateroventrally (Fig. 17I, J). This condition makes the diapophysis more distant from the parapophysis to bear a dorsal rib with the capitulum further away from the tuberculum, as in other dorsal vertebrae.

All dorsal centra are amphicoelous, while the anteroposterior length is greater than the lateral width and the dorsoventral height in each centrum (Figs. 21–23). The first to third dorsal centra are ventrally pinched to form small hypapophyses (Fig. 25A–C) as in the posteriormost cervical (Fig. 20J), whereas the ventral margin of the first centrum is incompletely preserved. The depth of each preserved hypapophysis is greater than those of *Harpymimus* (ventral keel *sensu* Kobayashi and Barsbold, 2005b), while slightly less than those of *Nqwebasaurus* (Choiniere et al., 2012), *Mononykus* (ventral process *sensu* Perle et al., 1994) and *Falcarius* (Zanno, 2010). In addition, the ventrally pinched centrum is present in more posterior dorsals to

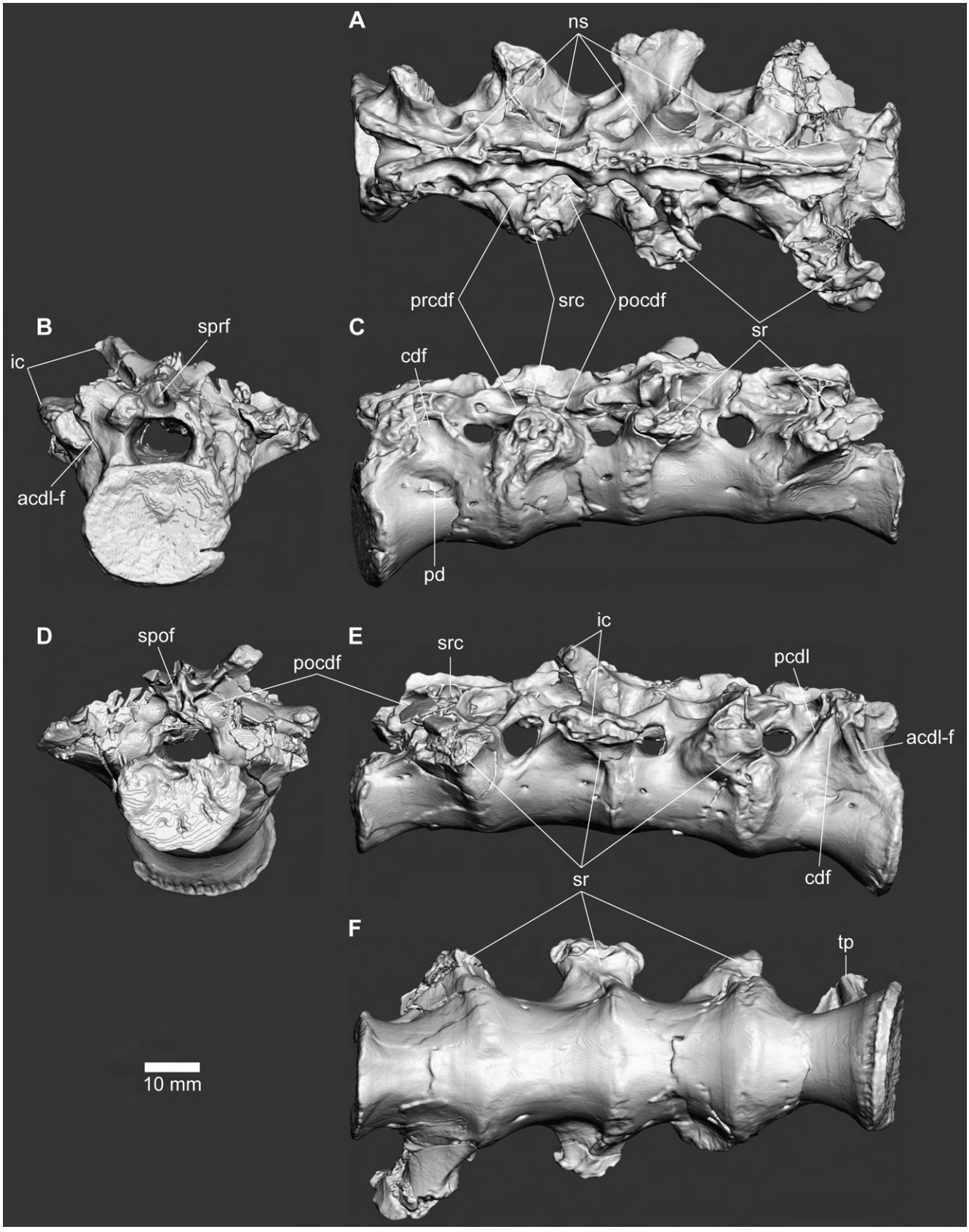

FIGURE 26. Fused sacral vertebrae with ribs of FPDM-V-8461. First through fourth sacral vertebrae with ribs in dorsal (**A**), anterior (**B**), left lateral (**C**), posterior (**D**), right lateral (**E**) and ventral (**F**) views. Abbreviations: acdl-f, intralaminar fossa of anterior centrodiapophyseal lamina; cdf, centrodiapophyseal fossa; hs, hyposphene; ic, ilium contact; ns, neural spine; pcdl, posterior centrodiapophyseal lamina; pd, pleurocentral depression; po, postzygapophysis; pocdf, postzygocentrodiapophyseal fossa; prcdf, prezygocentrodiapophyseal fossa; spof, spinopostzygapophyseal fossa; sprf, spinoprezygapophyseal fossa; sr, sacral rib; src, sacral rib contact; tp, transverse process.

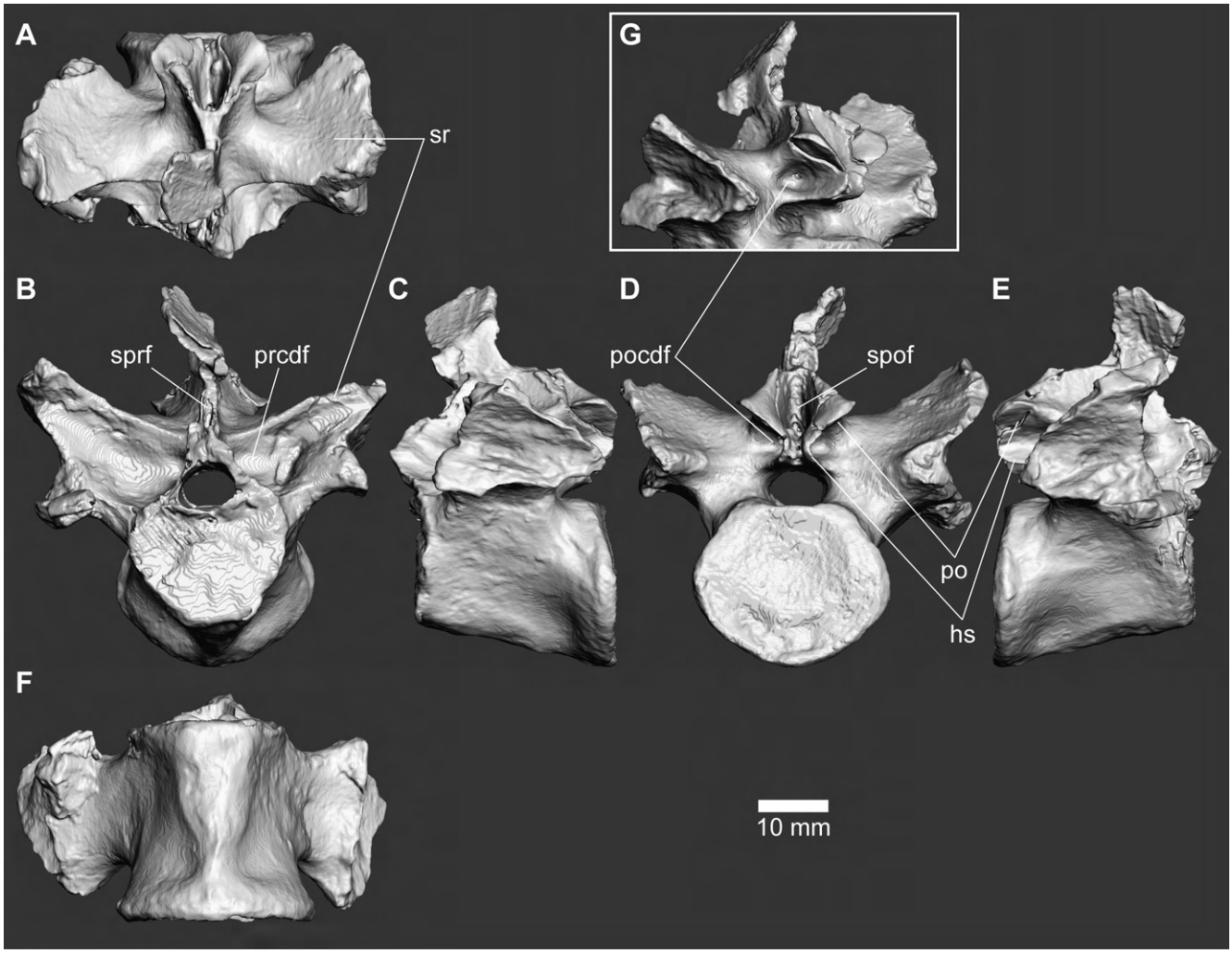

FIGURE 27. Isolated sacral vertebra with fused ribs of FPDM-V-8461. Fifth sacral vertebra with fused ribs in dorsal (**A**), anterior (**B**), left lateral (**C**), posterior (**D**), right lateral (**E**) and ventral (**F**) views, and its dorsal part in left posterolateral view (**G**). Abbreviations: hs, hyposphene; po, postzygapophysis; pocdf, postzygocentrodiapophyseal fossa; prcdf, prezygocentrodiapophyseal fossa; spof, spinopostzygapophyseal fossa; sprf, spinoprezygapophyseal fossa; sr, sacral rib.

the sixth, gradually becoming less prominent (Fig. 25D–F). In lateral view the parapophyses are situated entirely ventral to the transverse processes (Fig. 21C–J) unlike those of alvarezsaurs (Choiniere et al., 2010a), while it approaches to the level with the ventral margin of the transverse processes in the 11th cervical (Fig. 21K). In anterior view, the parapophysis are distinctly projected laterally below the base of the prezygapophyses (Fig. 22). In dorsal view, the parapophyses are partially obscured by the transverse process in the third and fourth dorsals (Fig. 24C, D), whereas they are situated entirely anteriorly in more posterior dorsals (Fig. 24E–K). At least in the third dorsal, the parapophysis is hypertrophied, with the dorsoventral depth of the parapophyseal facet greater than the half of that of the anterior articular surface (Fig. 21C) as in the anterior dorsals of *Avimimus*, therizinosaurids and some tyrannosauroids (Zanno et al., 2009; Brusatte et al., 2014). The parapophysis is the largest in the third among dorsal vertebrae and become gradually smaller in more posterior dorsal vertebrae (Fig. 21C–K). In the 9th and more posterior dorsals, the parapophysis is projected well laterally (Fig. 22I–K) like the stalked condition seen in alvarezsaurs and dromaeosaurids (Norell and Makovicky, 1999; Hwang et al., 2004). Instead of the pneumatic foramen, an indistinct pleurocentral depression is present on each lateral side of dorsal vertebra, which is less distinct in anterior five centra due to their ventrally pinched condition (Fig. 21).

The neural arch is dorsoventrally deep, with the depth between its base and the prezygodiapophyseal lamina greater

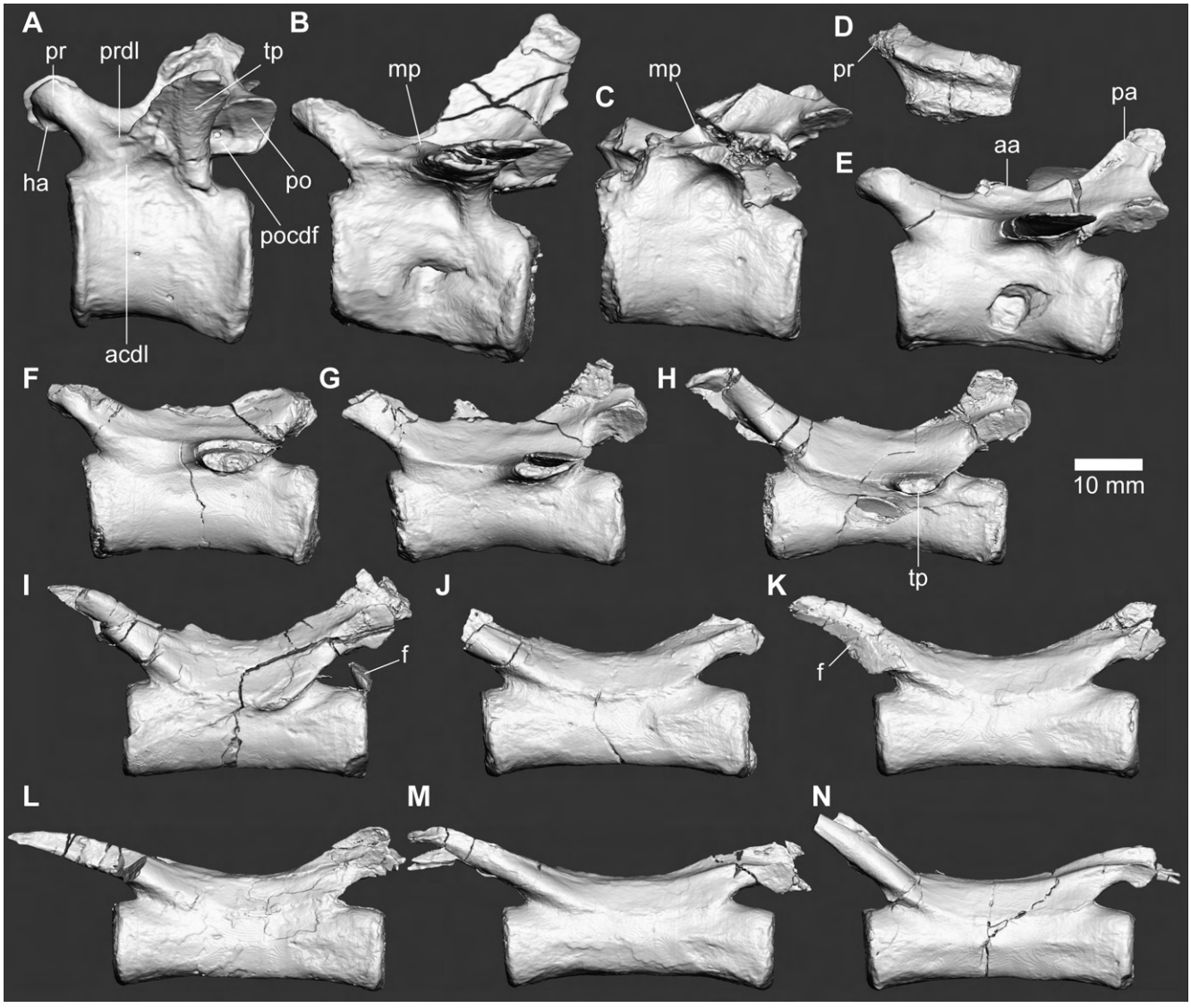

FIGURE 28. Anterior to middle caudal vertebrae of FPDM-V-8461. Left lateral views of 1st (**A**), 2nd (**B**), 3rd (**C**), 4th (**D**), 5th (**E**), 6th (**F**), 7th (**G**), 9th (**H**), 10th (**I**), 11th (**J**), 12th (**K**), 13th (**L**), 14th (**M**) and 15th (**N**) caudal vertebrae. Abbreviations: aa, anterior ala of neural spine; acdl, anterior centrodiapophyseal lamina; fm, bone fragment; ha, hypantrum; mp, mound-like dorsal projection; pa, posterior ala of neural spine; po, postzygapophysis; pocdf, postzygocentrodiapophyseal fossa; pr, prezygapophysis; prdl, prezygodiapophyseal lamina; tp, transverse process.

than that of the centrum at least in the third dorsal (Fig. 22) as in the anterior dorsals of therizinosaurs (Zanno et al., 2009). In lateral view, the prezygapophyses are at the same level with the postzygapophyses (Fig. 21) unlike those of ornithomimids and late-diverging tyrannosauroids in which the former located below the level of the latter (Brusatte et al., 2010). Just below the prezygapophysis, the centroprezygapophyseal fossa is present in the anterior dorsals, whereas it is absent in the fifth and more posterior dorsals (Fig. 22). The hypantrum is absent in the third, while present in more posterior dorsals, and its facet is relatively broad, dorsoventrally narrow and anteroposteriorly elongated.

The transverse processes of the anterior dorsal vertebrae are mediolaterally long and dorsoventrally thin (Fig. 22). The prezygodiapophyseal lamina forms the anterior margin of the transverse process in the first to eighth dorsals (Figs. 21C–H, 22A, C–H). Similarly, the prezygocentrodiapophyseal fossa is present in the first to eighth dorsals, with the remnant in the ninth (Fig. 21I). The anterior and posterior centrodiapophyseal laminae exist throughout the dorsal series and contact with each other on the ventral surface of transverse process, demarcating a triangular centrodiapophyseal fossa (Fig. 21). The anterior

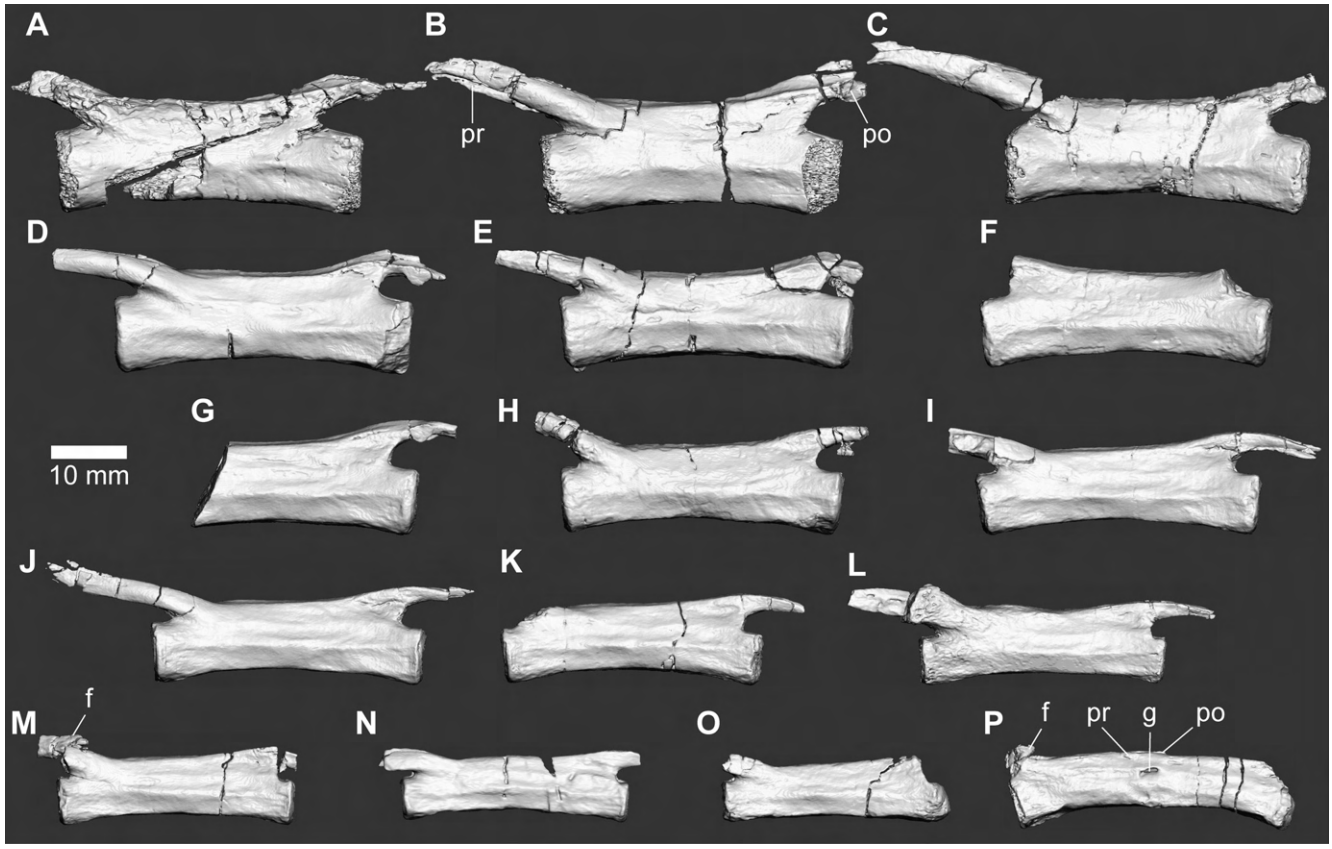

FIGURE 29. Middle to posterior caudal vertebrae of FPDM-V-8461. Left lateral views of 16th (**A**), 17th (**B**),18th (**C**), 19th (**D**), 20th (**E**), 21st (**F**), 22nd (**G**), 23rd (**H**), 24th (**I**), 25h (**J**), 26th (**K**), 27th (**L**), 28th (**M**), 29th (**N**), 30th (**O**) and 31st–32nd (**P**) caudal vertebrae. Abbreviations: f, bone fragment; g, gap between fused centra and fused zygapophyses; po, postzygapophysis; pr, prezygapophysis.

centrodiapophyseal lamina forms the anterior margin of the transverse process in the 9th to 11th dorsals instead of the disappearing prezygodiapophyseal lamina (Fig. 21I–K).

The hyposphene lamina is flared lateroventrally in the third and more posterior dorsal vertebrae (Fig. 23C–K). In addition, the hyposphene lamina is strongly curved lateroventrally in the middle and posterior dorsals to form a semi-canal (i.e., open-half-cylinder in shape) in posterior view with the postzygapophyseal facet (Azuma et al., 2016). Such feature is also present in the sacral and anteriormost caudal vertebrae (Figs. 26D, 27D, 31A). The opposite hyposphenes are separated as two laminae and ventrally conjoined by an inset web of bone comprising dorsal margin of the neural canal (Figs. 24C–K, 25C–K) as in ornithomimosaurs and some tyrannosauroids (Turner et al., 2012; Brusatte et al., 2014).

The dorsal neural spines are essentially rectangular in the third and more posterior dorsal vertebrae, and its dorsal ends are flared only slightly anteroposteriorly in lateral view (Fig. 21C–K) to form the spine table in anterior view (Fig. 22) unlike some theropods (Makovicky and Sues, 1998). The neural spine ends at nearly the same level as the posterior centrum face in the third and more posterior dorsals (Fig. 21C–K). In well-preserved dorsal neural spines of the sixth, seventh and eighth dorsals, the interspinous ligament scars are visible in the anterior and posterior aspects and ends slightly below the apex of the neural spine (Fig. 21F–H) as in deinonychosaurs (Turner et al., 2012). In the posterior dorsals, the neural spines are slightly greater in height than the anteroposterior width (Fig. 21I–K).

Sacral vertebrae

The sacral series consists of four fused and one isolated sacral vertebrae (Figs. 26, 27; Table 2), with most of neural spines missing in the first four. In contrast to Azuma et al. (2016) which regards the isolated one as the sixth or more posterior sacral, CT analyses performed in the present study identify it as the fifth with its anterior surface of the centrum matching the posterior surface of the fused sacrals. In addition, the posterior surface of the fifth is mostly flat and does not exhibit any traces for fusion (Fig. 27D), suggesting that it articulates with the unfused first caudal vertebra. The ventral margin of the fifth sacral is inclined posteroventrally in lateral view, forming the

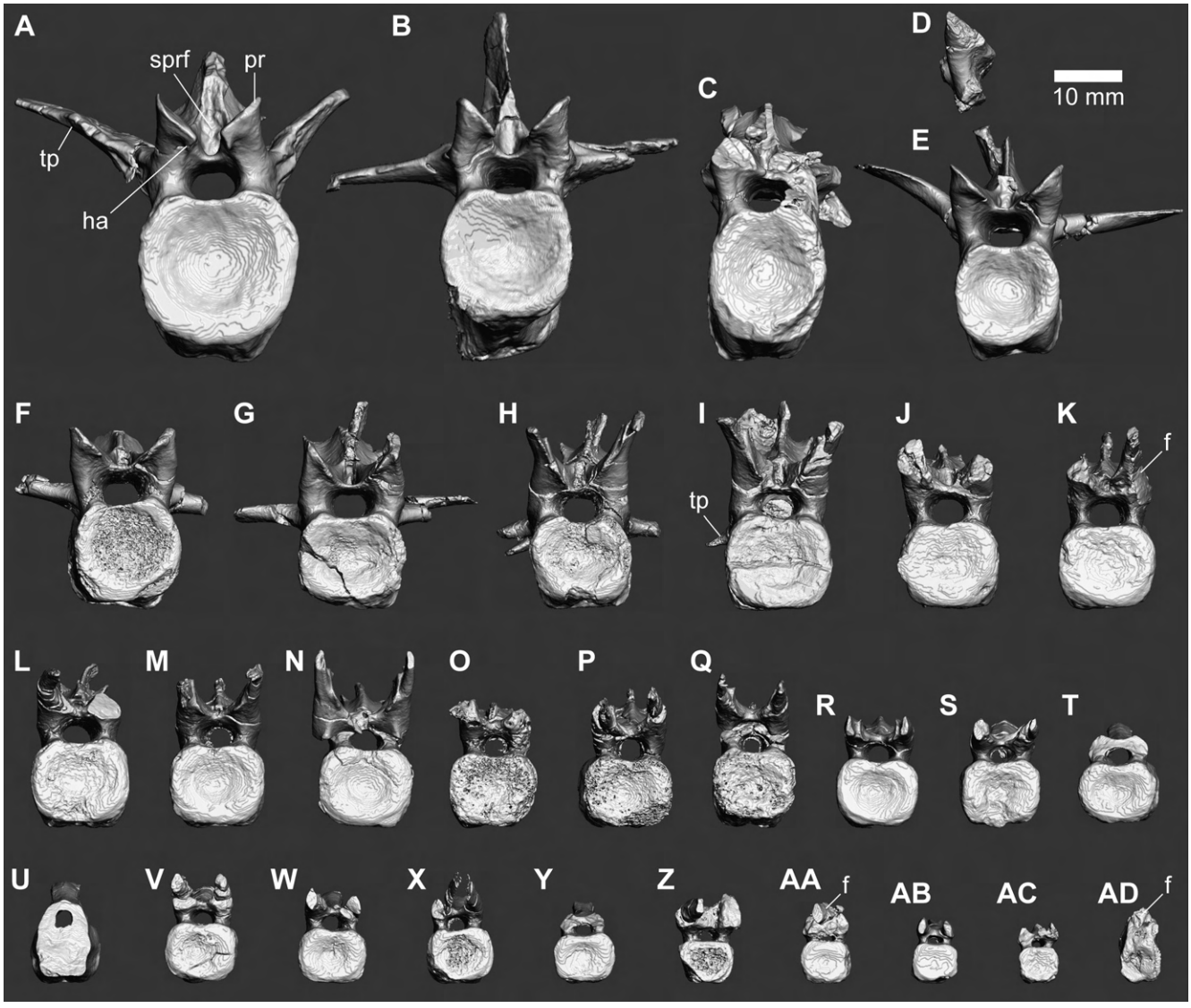

FIGURE 30. Caudal vertebrae of FPDM-V-8461. Anterior views of 1st (**A**), 2nd (**B**), 3rd (**C**), 4th (**D**), 5th (**E**), 6th (**F**), 7th (**G**), 9th (**H**), 10th (**I**), 11th (**J**), 12th (**K**), 13th (**L**), 14th (**ML**), 15th (**N**), 16th (**O**), 17th (**P**),18th (**Q**), 19th (**R**), 20th (**S**), 21st (**T**), 22nd (**U**), 23rd (**V**), 24th (**W**), 25th (**X**), 26th (**Y**), 27th (**Z**), 28th (**AA**), 29th (**AB**), 30th (**AC**) and 31st–32nd (**AD**) caudal vertebrae. Abbreviations: f, bone fragment; ha, hypantrum; pr, prezygapophysis; sprf, spinoprezygapophyseal fossa; tp, transverse process.

arched ventral margin of the sacrum (Figs. 26C, 27C). In ventral view, the second to fifth sacrals exhibit ventrally-flattened centra with extremely shallow sulcus at least in a portion of each (Figs. 26F, 27F). Only the posterior half of the isolated sacral vertebra shows a keeled ventral surface (Fig. 27F), less prominent than those in alvarezsaurids (Perle et al., 1994; Novas, 1997). Pneumatic foramina are absent on lateral surfaces of sacral vertebrae, whereas a pleurocentral depression is present on each lateral side of the first centrum (Fig. 26C, E).

Parapophyses are clearly absent in the first sacral vertebra (Fig. 26E). Instead, the anterior centrodiapophyseal lamina is divided into two to bear an intralaminar fossa as a narrow sulcus between them. In the second to fourth sacrals, sutures against the sacral ribs are expanded anteriorly from the diapophyseal region to invade the anterodorsal margin including the parapophyseal region of each vertebra to reach the border against the preceding sacral (Fig. 26C, E). The anterior margin of this suture never or only slightly invades the posterior margin of each preceding sacral centrum. The right rib of the third sacral is nearly complete and is bifurcated dorsoventrally (Fig. 26E). The dorsal part of the rib is pointed laterodorsally to form a narrow facet for the ilium, whereas the ventral part projects

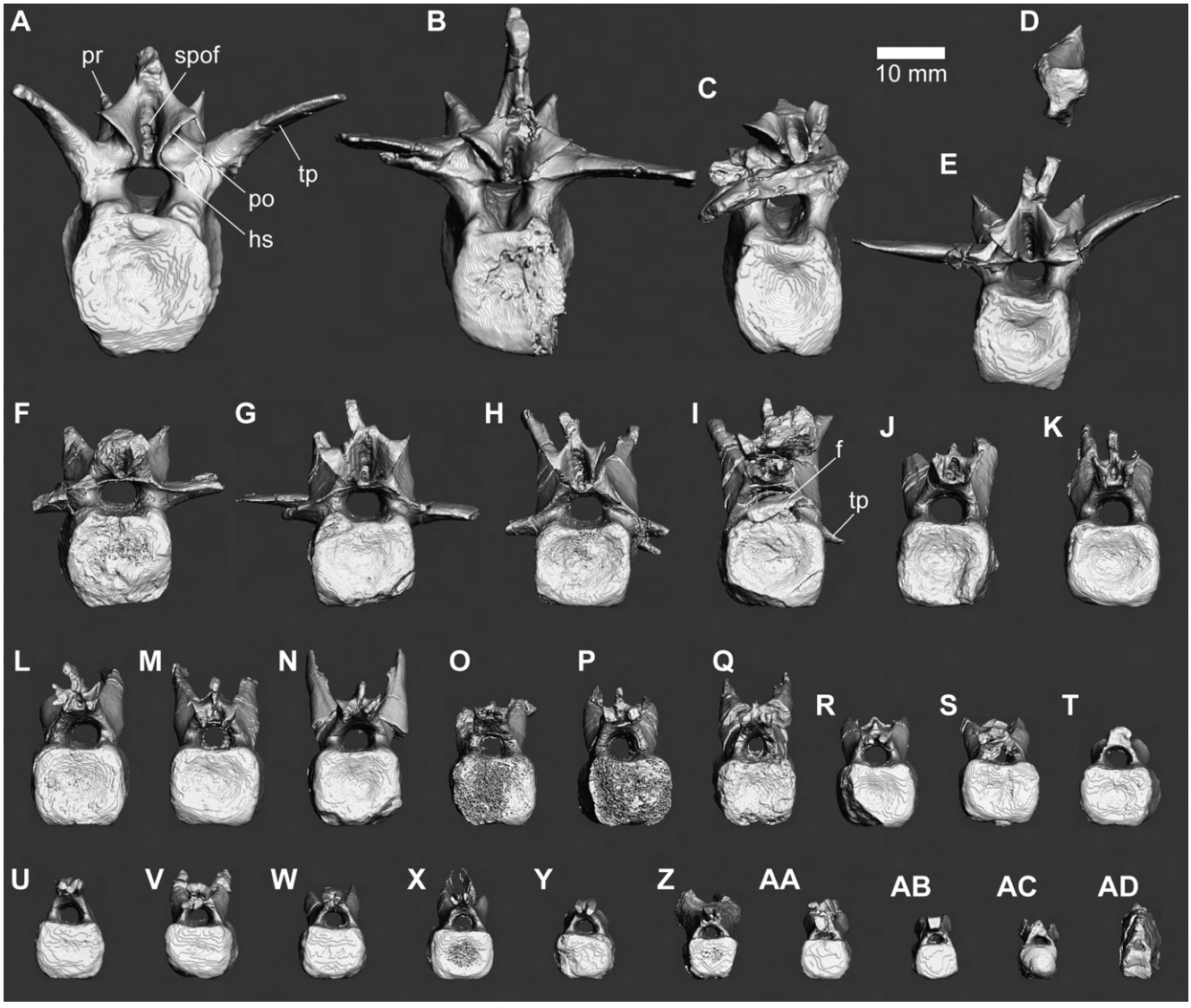

FIGURE 31. Caudal vertebrae of FPDM-V-8461. Posterior views of 1st (**A**), 2nd (**B**), 3rd (**C**), 4th (D), 5th (**E**), 6th (**F**), 7th (**G**), 9th (**H**), 10th (**I**), 11th (**J**), 12th (**K**), 13th (**L**), 14th (**M**), 15th (**N**), 16th (**O**), 17th (**P**),18th (**Q**), 19th (**R**), 20th (**S**), 21st (**T**), 22nd (**U**), 23rd (**V**), 24th (**W**), 25th (**X**), 26th (**Y**), 27th (**Z**), 28th (**AA**), 29th (**AB**), 30th (**AC**) and 31st–32nd (**AD**) caudal vertebrae. Abbreviations: f, bone fragment; hs, hyposphene; po, postzygapophysis; pr, prezygapophysis; spof, spinopostzygapophyseal fossa; tp, transverse process.

horizontally and expands anteroposteriorly to form a long iliac facet. The fifth sacral ribs are completely fused to the fifth sacral vertebra, where the suture between them appear indistinct and do not invade the posterior margin of the preceding sacral (Fig. 27C, E). Additionally, the fifth sacral rib is bifurcated dorsoventrally as in the third, although the dorsal part of the former is well expanded to form a long facet for the ilium as in the ventral part. The zygapophyses are fused to each other at least in the first to fourth sacrals to form a platform lateral to the neural spines (Fig. 26A) as in dromaeosaurids (Norell and Makovicky, 2004). The hyposphene preserved in the fifth sacral is small and not sheet-like (Fig. 27D) as in most coelurosaurs (Brusatte et al., 2010). The pre- and postzygocentrodiapophyseal fossae are well excavated besides the lacking prezygocentrodiapophyseal fossa in the first (Fig. 26A, C). The postzygocentrodiapophyseal fossa in the fifth sacral exhibits a small pneumatic foramen within it on the left side (Fig. 27G) as in the first caudal vertebra (Fig. 28A).

Caudal vertebrae

Preserved 31 caudal vertebrae represent most part of a complete set of 32 caudals, lacking the 8th and the majority of the 4th (Figs. 28–33). The anterior caudals include nine

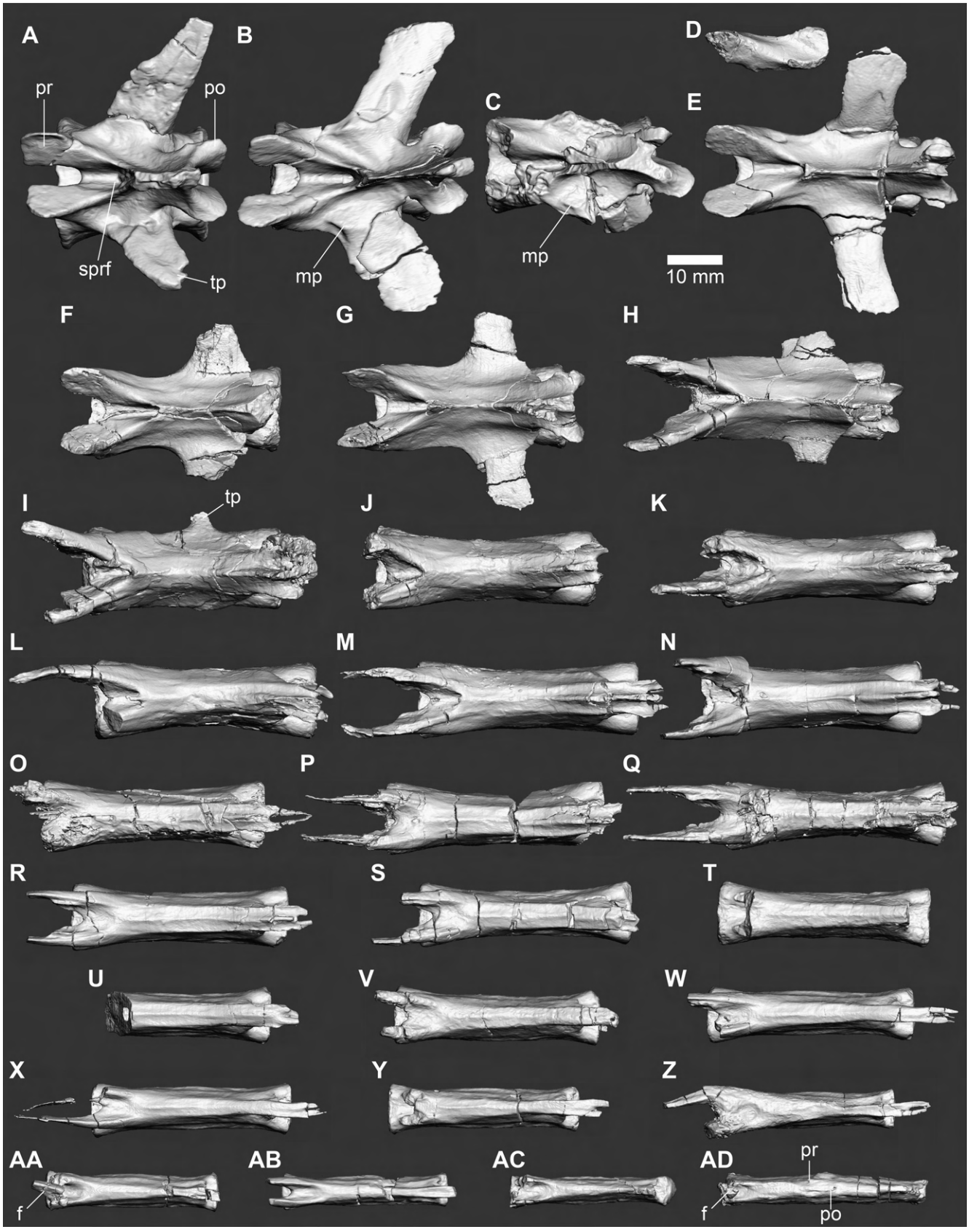

FIGURE 32. Caudal vertebrae of FPDM-V-8461. Dorsal views of 1st (**A**), 2nd (**B**), 3rd (**C**), 4th (**D**), 5th (**E**), 6th (**F**), 7th (**G**), 9th (**H**), 10th (**I**), 11th (**J**), 12th (**K**), 13th (**L**), 14th (**M**), 15th (**N**), 16th (**O**), 17th (**P**),18th (**Q**), 19th (**R**), 20th (**S**), 21st (**T**), 22nd (**U**), 23rd (**V**), 24th (**W**), 25th (**X**), 26th (**Y**), 27th (**Z**), 28th (**AA**), 29th (**AB**), 30th (**AC**) and 31st-32nd (**AD**) caudal vertebrae. Abbreviations: f, bone fragment; mp, mound-like dorsal projection; po, postzygapophysis; pr, prezygapophysis; sprf, spinoprezygapophyseal fossa; tp, transverse process.

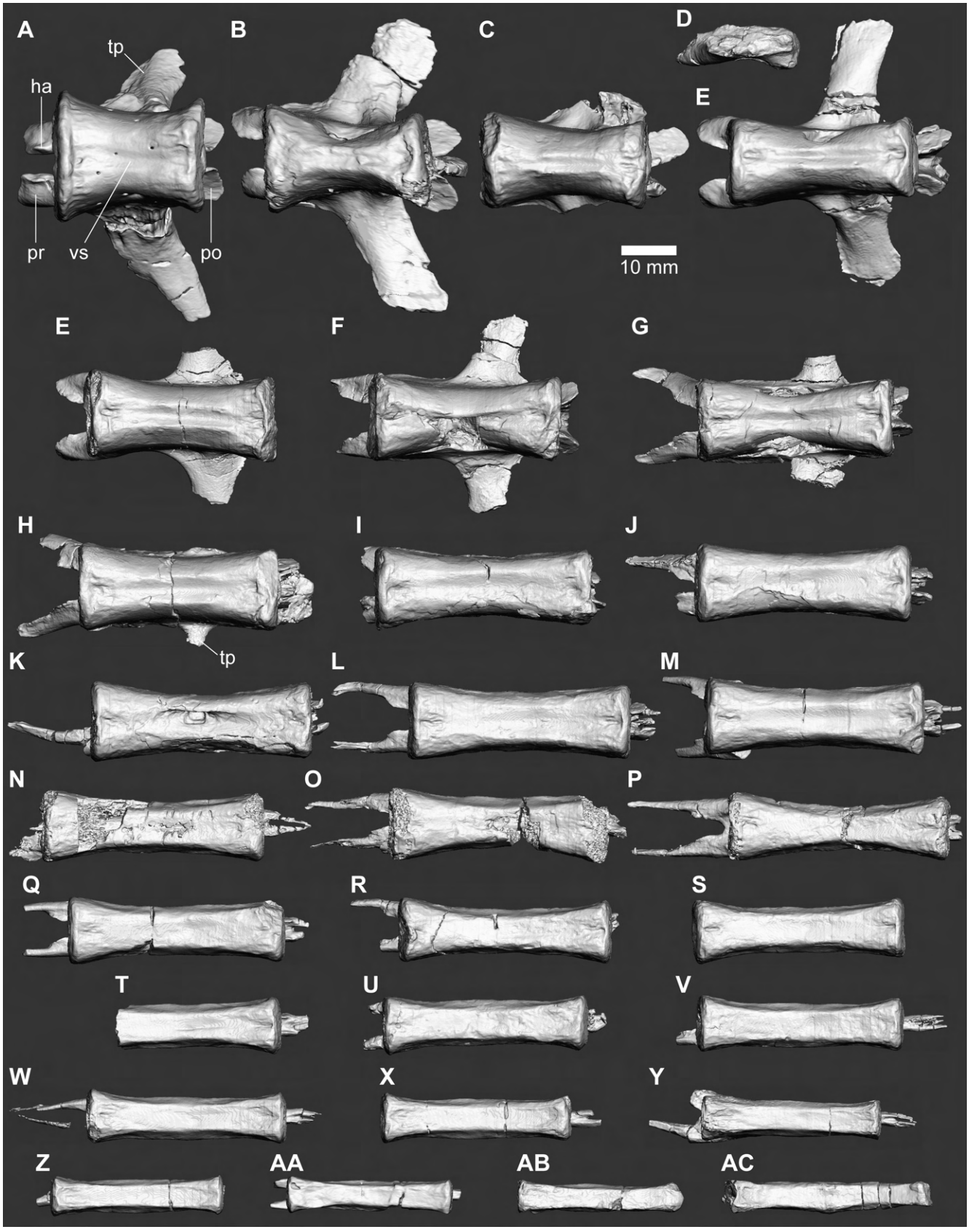

FIGURE 33. Caudal vertebrae of FPDM-V-8461. Ventral views of 1st (**A**), 2nd (**B**), 3rd (**C**), 4th (**D**), 5th (**E**), 6th (**F**), 7th (**G**), 9th (**H**), 10th (**I**), 11th (**J**), 12th (**K**), 13th (**L**), 14th (**M**), 15th (**N**), 16th (**O**), 17th (**P**),18th (**Q**), 19th (**R**), 20th (**S**), 21st (**T**), 22nd (**U**), 23rd (**V**), 24th (**W**), 25th (**X**), 26th (**Y**), 27th (**Z**), 28th (**AA**), 29th (**AB**), 30th (**AC**) and 31st-32nd (**AD**) caudal vertebrae. Abbreviations: ha, hypantrum; po, postzygapophysis; pr, prezygapophysis; tp, transverse process; vs, ventral sulcus.

TABLE 2. Measurements on the vertebrae of FPDM-V-8461.

Element	Anteroposterior length (mm)	Mediolateral width (mm)	Dorsoventral height (mm)
Atlas neural arch (L)	15.6	8.8	14.7
Atlas neural arch (R)	15.7	6.8*	13.3*
Axis	31.2	29.2	32.3
Cervical 3	34.6	29.6*	31.4
Cervical 5	41.8*	33.3*	24.0*
Cervical 6	35.8*	32.5*	30.8*
Cervical 8	51.4	38.1	34.9*
Cervical 9	51.0	36.7*	39.4
Cervical 10	42.2*	44.7*	38.5*
Cervical 11	34.1	53.7	41.9*
Dorsal 1	30.5	42.8*	42.9*
Dorsal 2	23.7*	16.9*	17.6*
Dorsal 3	33.5	49.6*	39.8*
Dorsal 4	34.6	47.3*	47.9*
Dorsal 5	35.1	38.7*	44.7*
Dorsal 6	33.7*	34.3*	48.3
Dorsal 7	34.5	46.1	49.9
Dorsal 8	38.4	33.1*	53.9
Dorsal 9	40.1	42.7	57.1
Dorsal 10	42.1	33.9*	60.7
Dorsal 11	44.5	31.7*	55.9*
Sacrals 1–4 with fused ribs	101.0	51.6*	45.9*
Sacral 5 with fused ribs	32.7	52.9	54.5*
Caudal 1	37.4	49.5*	45.9*
Caudal 2	42.8	53.0*	51.3
Caudal 3	38.1*	22.3*	38.2*
Caudal 4	22.6*	8.3*	15.1*
Caudal 5	46.4	48.6*	34.8
Caudal 6	40.3*	28.6*	26.9*
Caudal 7	45.3	36.2*	30.8
Caudal 9	51.2	24.3*	29.3
Caudal 10	54.0	20.6*	31.0
Caudal 11	44.9*	15.3	26.4*
Caudal 12	56.0	14.4	27.1
Caudal 13	58.4	14.6	24.3
Caudal 14	59.8	14.1	24.2
Caudal 15	54.5*	15.2	26.3*
Caudal 16	55.0*	13.1	19.1*
Caudal 17	58.6*	14.1	20.9
Caudal 18	60.9*	12.4	23.0
Caudal 19	52.1*	12.2	16.6
Caudal 20	48.9*	12.0	16.2
Caudal 21	38.9*	12.1	14.8*
Caudal 22	35.3*	10.4	15.2*
Caudal 23	44.4*	10.9	16.3*
Caudal 24	49.3*	10.2	14.1*
Caudal 25	56.7	10.0	16.6
Caudal 26	40.2*	9.2	12.2*
Caudal 27	48.7*	9.8	13.4
Caudal 28	34.4*	7.5	12.0*
Caudal 29	34.7*	6.9	9.9
Caudal 30	30.3*	6.2	9.0*
Caudals 31–32	38.4*	6.3	11.3*

*Specimen incomplete in measured dimension.

TABLE 3. Measurements on the chevrons of FPDM-V-8461.

Element	Dorsoventral height (mm)	Mediolateral width (mm)	Anteroposterior width (mm)
Chevron 9	37.2*	13.2	23.6*
Chevron 11	35.9*	12.8	24.6*
Chevron 14	19.3	12.0	19.3
Chevron 15	11.8*	12.1	13.4*
Chevron 16	15.0	10.9	21.2
Chevron 17	10.8*	12.2	9.9*

*Specimen incomplete in measured dimension.

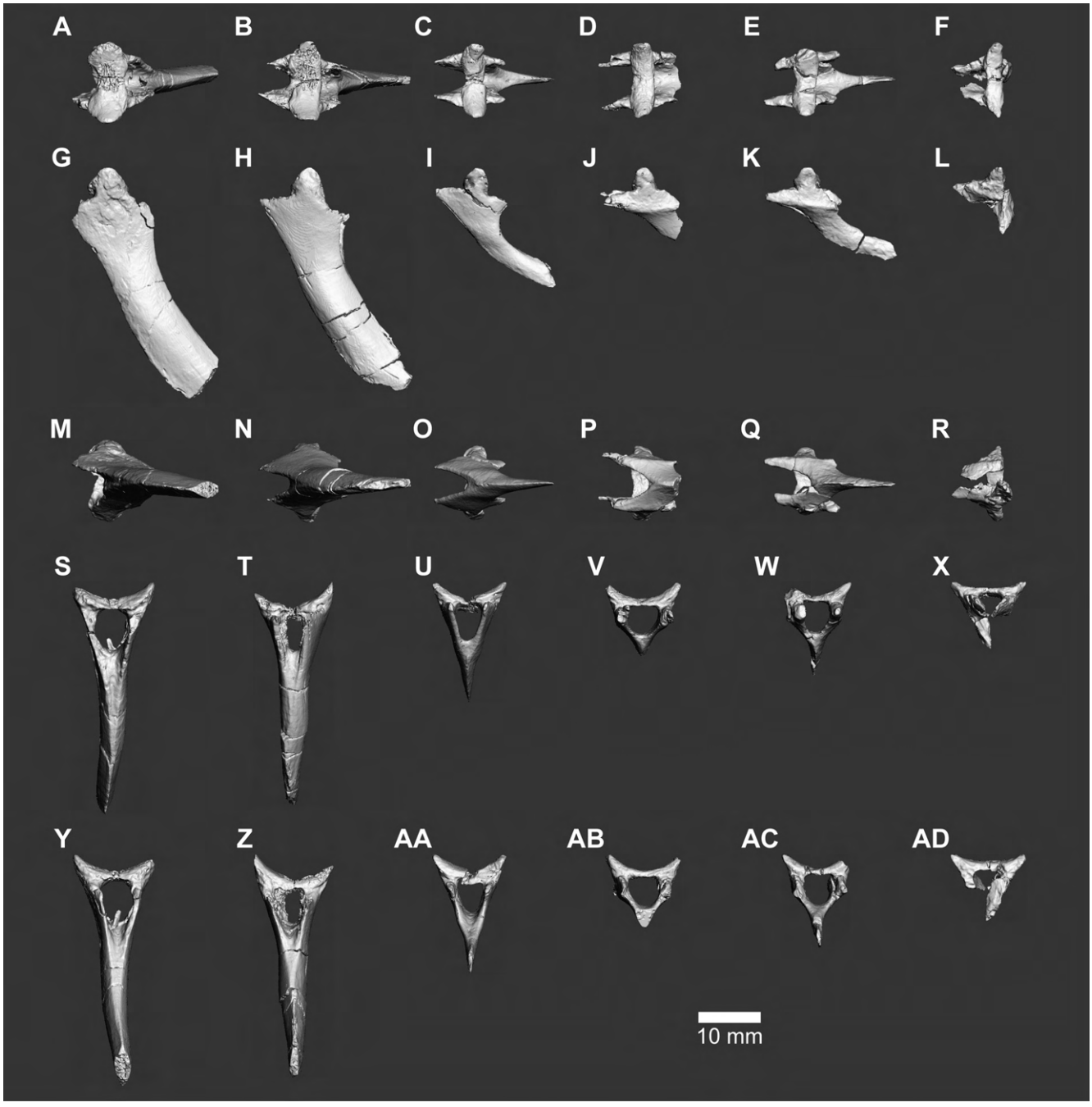

FIGURE 34. Chevrons of FPDM-V-8461. Dorsal (**A**–**F**), left lateral (**G**–**L**), ventral (**M**–**R**), anterior (**S**–**X**) and posterior (**Y**–**AD**) views of 9th (A, G, M, S, Y), 11th, (B, H, N, T, Z), 14th (C, I, O, U, AA), 15th (D, J, P, V, AB), 16th (E, K, Q, W, AC) and 17th (F, L, R, X, AD) chevrons.

preserved caudals with distinct transverse processes (Fig. 30A–I) which are absent in the posterior ones represented by the 11th and more posterior caudals (Fig. 30J–AD). The loss of the transverse processes represents a transitional point between the anterior and posterior caudals, which occurs more anteriorly in alvarezsaurs and paravians (Makovicky et al., 2005; Turner et al., 2012) or absent in oviraptorosaurs (Osmólska et al., 2004). Notably, the posteriormost two caudals are fused with each other (Fig. 29P), and only about 1.5 times longer than the preceding caudal vertebrae. The fragments between prezygapophyses in the 28th and fused posteriormost caudals are probably derived from the postzygapophyses of the

preceding caudals.

The caudal centra lack any pneumatic foramina and are all amphiplatyan except for the posterior caudals (Figs. 28, 29). The anteroposterior length of each caudal vertebra including pre- and postzygapophyses becomes greater posteriorly at least to the 18th caudal, which is nearly 50% longer anteroventrally than the longest dorsal vertebra (11th; Table 2). Similarly, the centrum length of each caudal becomes greater to the 16th, whereas its mediolateral width and dorsoventral height are reduced sequentially (Figs. 30, 31). In the first three caudals, each centrum is box-like in lateral view and its transverse section is nearly rectangular (Fig. 28A–C). The ventral surface of each 1st to 14th caudal centra exhibits a longitudinal sulcus, which becomes shallower posteriorly into nearly completely flat in the 16th and more posterior caudals (Fig. 33). In the fifth and more posterior caudal centra, the anteroposterior length is greater than twice the mediolateral width and dorsoventral height (Fig. 31).

In lateral view, each neural spine of the first two caudals exhibits beam-like shape and its posteroventral margin is situated slightly anterior to the posterior surface of the centrum (Fig. 28A, B). In the third and subsequent caudals, the dorsoventral height of each neural spine is low anteriorly and tall posteriorly, expressing L-shaped condition in lateral view (Fig. 28C–I). In the 5th to 10th caudals, the neural spine becomes lower and separated into the anterior and posterior alae (Fig. 28E–I), with the former absent in the 11th to 18th caudals (Figs. 28J–N, 29A–C). In more posterior caudals, the remnant of neural spine is present as a low ridge (Fig. 29D–P) as in some tyrannosauroids, ornithomimosaurs, therizinosaurs, oviraptorosaurs and avialans (Russell and Dong, 1993; Turner et al., 2012).

The transverse processes of the anterior caudals appear sub-rectangular and slightly narrow distally in dorsal view (Fig. 32). In the anterior caudals, the mediolateral length of each transverse process is subequal to the mediolateral width of the centrum (Fig. 30A–G), whereas such feature is obscure in the 9th and apparently reduced in the 10th (Fig. 30H, I). Although the diapophysis is absent in all caudals, the remnant of anterior centrodiapophyseal lamina is visible in the left lateral view of the first caudal (Fig. 28A). In the first caudal, a slight pneumaticity is present within the postzygodiapophyseal fossa in lateral view, as in the fifth sacral (Fig. 27G). In the second and third caudals, a low, mound-like dorsal projection is observable just above the proximoanterior margin of the transverse process (Figs. 28B, 32B).

In the posterior caudals, the prezygapophyses are elongated well anteriorly (Fig. 29). In the well-preserved posterior caudals, the prezygapophyses overlap about the posterior third or more of the preceding caudal centra, whereas the postzygapophyses overlap only the anterior fifth or less of the following caudal centra (Figs. 28K–M, 29B, C, J). The distal end of the prezygapophysis is preserved in both sides of the 14th caudal and bifurcated (Figs. 28M, 32M, 33M) unlike other known dinosaurs (Azuma et al., 2016). In 14–16th, 19th and 22nd caudals, a narrow spine-like process is preserved posterior to the postzygapophyseal facet (Figs. 28M, N, 29A, D, G). The postzygapophyseal facet is indistinct in the 22nd and more posterior caudals (Fig. 29H–N).

As mentioned, the posteriormost two caudals (31st and 32nd) are fused with each other. The suture between these two centra is marked by a slight eminence (Fig. 32AD) unlike the prominent line or tubercle seen in *Beipiaosaurus* (Liao et al., 2021). The suture is also visible between the neural arches due to the remnants of zygapophyses (Figs. 29P, 32AD). In addition, a narrow gap between the fused centra and fused zygapophyses is visible in lateral view (Fig. 29P), which are unreported in other theropods with fused posteriormost caudals. The dorsal margin of the posteriormost caudals bears a narrow, nearly flat dorsal surface (Fig. 32AD), whereas the ventral margin forms a broader, flat or slightly concave ventral surface (Fig. 33AD) as in the preceding caudals (Fig. 33O–AC) and the pygostyle of *Fukuipteryx* (Imai et al., 2019), in contrast to other fused posteriormost caudals in non-pygostylian theropods (Lee et al., 2014; Barsbold et al., 2000a:fig. 1). The anterior and posterior ends of the ventral margin projects ventrally to form an arch in lateral view (Fig. 29P). The anterior surface of the fused centra is concave to fit with the bulbous posterior surface of the 30th caudal (Fig. 29O, P).

Chevrons

Preserved six chevrons comprise two anterior and four posterior ones (Fig. 34). Each of them engages with the posteroventral margin of the 9th, 11th, 14–17th caudals (Fig. 2). Because it is unknown whether every caudal vertebra is equipped with a chevron, these chevrons are numbered here according with the corresponding caudal vertebra. As preserved, both the anterior and posterior chevrons are relatively long, slender, and recurved posteriorly in distal portions (Fig. 34G–K; Table 3). In dorsal view, the middle part of the haemal canal is covered by a narrow bridge bearing an articular facet for the caudal vertebrae (Fig. 34A–F). The articular facet is laterally concave and anteroposteriorly convex.

The proximal margins of the lateral walls of the haemal canal are anteroposteriorly expanded to form paired processes directed both anteriorly and posteriorly (Fig. 34B–F), which are missing in the 9th chevron (Fig. 34A). Posterior three chevrons bear horizontal ridges on lateral sides at the level of the anteroposterior expansion (Fig. 34J–L). The lateral walls distally become restricted anteroposteriorly and meet at the sagittal plane to form a distal blade (Fig. 34S–AD). The blade is more prominently restricted and recurved posteriorly in the posterior chevrons than the anterior ones (Fig. 34G–K). The distal ends of the posterior chevrons are not expanded anteroposteriorly as in the anterior chevrons (Fig. 34I, K).

Cervical ribs

Preserved nine cervical ribs represent left 5th and 7th to 11th and right 6th, 9th and 11th (Figs. 35, 36). Although possible another cervical rib is adhered to the anterolateral part of the ninth cervical centrum (Fig. 17H), its identification is problematic due to the severe damage causing unmatched articulation to any cervical diapophyses or parapophyses.

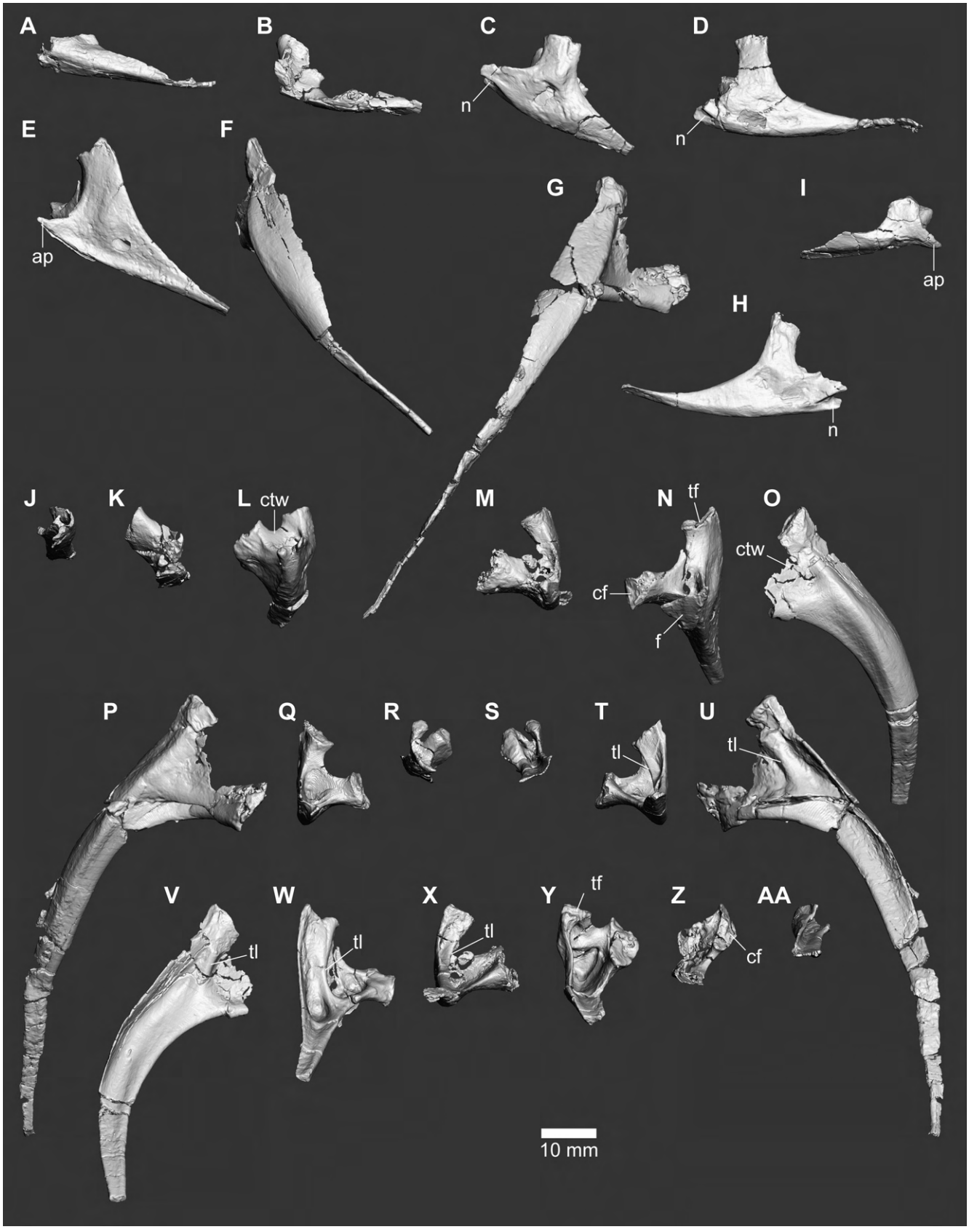

FIGURE 35. Cervical ribs of FPDM-V-8461. Lateral (**A**–**I**), anterior (**J**–**R**) and posterior (**S**–**AA**) views of left 5th (A, J, AA), 7th (B, K, Z), 8th (C, L, Y), 9th (D, M, X), 10th (E, N, W) and 11th (F, O, V) and right 6th (I, R, S), 9th (H, Q, T) and 11th (G, P, U) cervical ribs. Abbreviations: ap, anterior process; cf, capitular facet; ctw, capitular-tubercular web; f, bone fragment; n, notch for probable contact with preceding rib; tf, tubercular facet; tl, tubercular lamina.

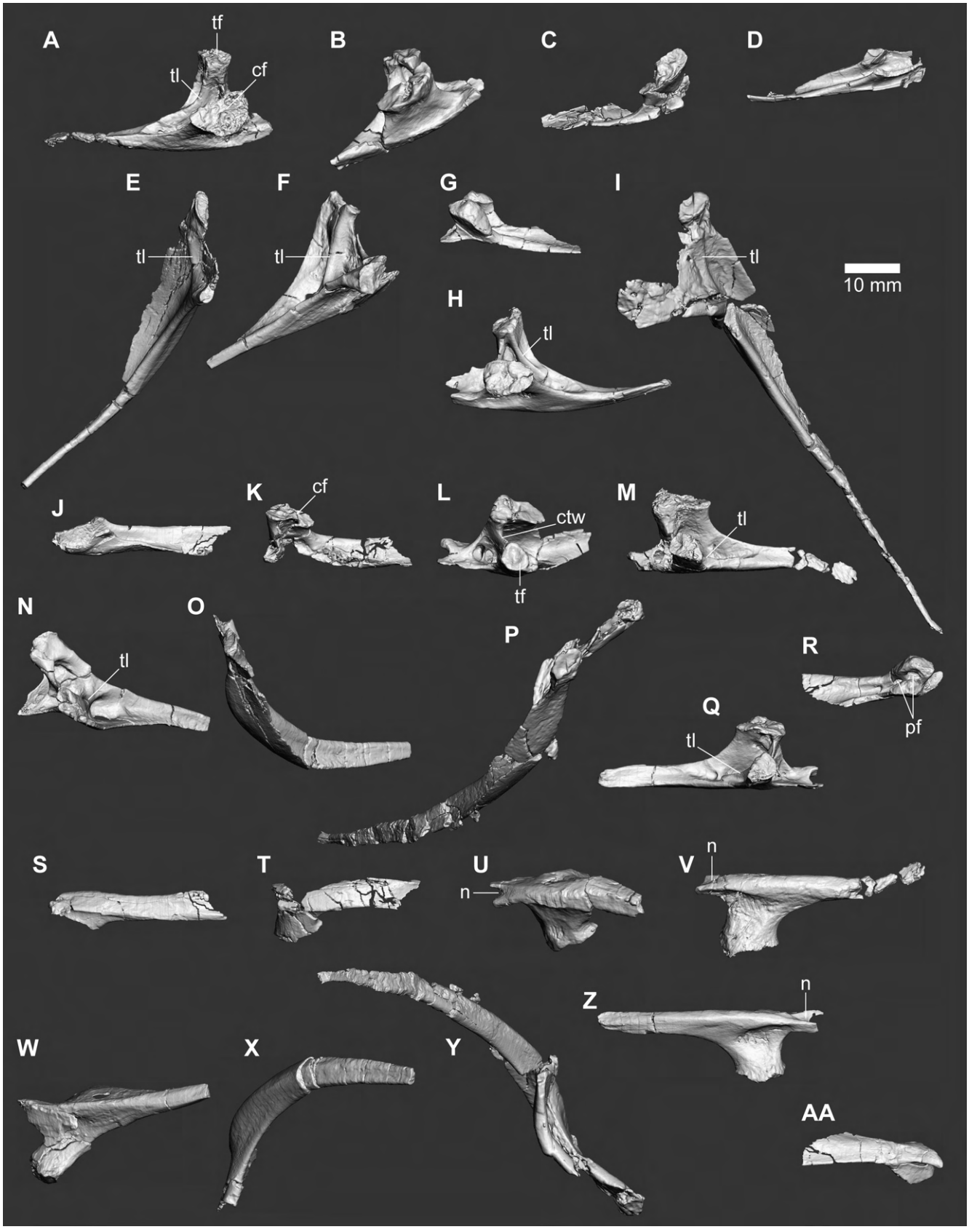

FIGURE 36. Cervical ribs of FPDM-V-8461. Medial (**A**–**I**), dorsal (**J**–**R**) and ventral (**S**–**AA**) views of left 5th (D, J, S), 7th (C, K, T), 8th (B, L, U), 9th (A, M, V), 10th (F, N, W) and 11th (E, O, X) and right 6th (G, R, AA), 9th (H, Q, Z) and 11th (I, P, Y) cervical ribs. Abbreviations: cf, capitular facet; ctw, capitular-tubercular web; n, notch for probable contact with preceding rib; pf, pneumatic foramen; tf, tubercular facet; tl, tubercular lamina.

TABLE 4. Measurements on the cervical ribs of FPDM-V-8461.

Element	Proximodistal length (mm)	Mediolateral width (mm)	Dorsoventral height (mm)
Cervical rib 5 (L)	33.0*	7.4	7.5*
Cervical rib 6 (R)	25.8*	9.5*	10.1
Cervical rib 7 (L)	29.0*	11.3	10.6*
Cervical rib 8 (L)	31.6*	14.9	16.6
Cervical rib 9 (L)	41.7	17.5	18.7
Cervical rib 9 (R)	41.2	13.5	19.2
Cervical rib 10 (L)	38.7*	17.5	20.8
Cervical rib 11 (L)	65.8*	21.5*	14.0
Cervical rib 11 (R)	96.8*	32.7*	19.8

*Specimen incomplete in measured dimension.

TABLE 5. Measurements on the dorsal ribs of FPDM-V-8461.

Element	Proximodistal length (mm)	Mediolateral width (mm)	Anteroposterior depth (mm)
Dorsal rib 1 (R)	70.3*	37.9	8.8
Dorsal rib 2 (L)	37.7*	18.2*	8.6*
Dorsal rib 3 (L)	29.5*	20.1*	7.0*
Dorsal rib 3 (R)	120.4*	45.7*	16.0*
Dorsal rib 4 (R)	53.8*	9.9*	8.9*
Dorsal rib 5 (L)	98.4*	14.1*	9.1
Dorsal rib 6 (R)	81.8*	43.1*	9.8*
Dorsal rib 6 (L)	16.5*	29.3*	5.1*
Dorsal rib 7 (L)	63.0*	9.3*	7.6*
Dorsal rib 7 (R)	113.7*	40.0	10.8
Dorsal rib 8 (L)	29.0*	14.6*	10.7*
Dorsal rib 8 (R)	116.2*	47.1	24.9
Dorsal rib 9 (R)	10.8*	25.0*	4.9*
Dorsal rib 10 (R)	107.4*	27.7	24.4
Dorsal rib 11 (R)	63.9*	29.2	7.8

*Specimen incomplete in measured dimension.

When in articulation with the corresponding cervical vertebra, each cervical rib is triangular in lateral view by a tuberculum directed dorsally and the shaft directed posteriorly or posteroventrally, the latter being much shorter than those of dorsal ribs (Figs. 35A–I; Tables 4, 5). The capitulum is directed medially or mediodorsally and not visible in lateral view. In addition, a short anterior process is present at the anteroventral corner except in the posteriormost cervical rib. The anterior process bears a longitudinal ridge projected ventrally that continues toward the distal end of the shaft (Fig. 36S–AA). This ridge forms the lateral margin of the concave ventral surface of the capitulum. In the eighth and ninth ribs, a sharp longitudinal notch is present on the lateroventral side of the anterior end of the longitudinal ridge for a possible contact with the distal end of the preceding ribs and makes the anterior process bifurcated (Figs. 35C, D, H, 36U, V, Z). The size of tubercular facet is about one-half of that of capitular facet, which is elongated anteroposteriorly (Fig. 36J–R). The incomplete shafts of the fifth and sixth cervical ribs are distally expanded mediolaterally, whereas those of the eighth and more posterior ribs are tapered (Fig. 36S–AA).

In dorsal view, a deep pneumatic cavity excavates the main body between the tubercular and capitular facets and continues posteriorly to form a concave dorsal surface of the shaft (Fig. 36J–R). The cavity is surrounded and divided by thin laminae best developed in the anterior margin corresponding to the capitular-tubercular web (*sensu* Currie and Zhao, 1993a) seen in the dorsal ribs. In the 9th and 10th ribs, another lamina extends posteroventrally from the medial margin of the tubercular facet (Figs. 35T, U, Z, 36A, F, I), and the remnant of this lamina is present in the 11th rib (Figs. 35S, AA, 36G, H). The cavity posterior to the capitular-tubercular web is further excavated by several foramina in the right sixth, in which the capitulum and tuberculum bear two and one foramina, respectively. In dorsal view, another small cavity excavates the anterior process and divided by thin, laterally-oriented laminae (Fig. 36L–N, Q).

Dorsal ribs

While most dorsal ribs are fragmented, right ones are better preserved than the left ones, including some nearly complete series lacking the second and fifth ribs (Figs. 37–41; Table 5). The distal end is not completely preserved in any dorsal ribs. No trace of ossified uncinate process is recognizable. When in articulation with a corresponding dorsal vertebra, the longitudinal axis of the capitulum is oriented anteromedially (Fig. 41A–H) and the shaft and the tuberculum exhibit a continuous flat surface facing laterally (Fig. 39A–H).

In the first dorsal rib, the capitulum is widely separated from the tuberculum by a notch in anterior view (Fig. 37D). In the third and more posterior dorsal ribs with the proximal part preserved, the notch is occupied by the capitular-tubercular web, which is much less developed in the first rib. The capitular facet is preserved in the 1st, 3rd, 6th, 7th, 8th and 11th. Among them, the area of the facet is largest in the third rib and successively reduced in more posterior ribs (Fig. 40).

Proximally, the lateral margin of the shaft is expanded

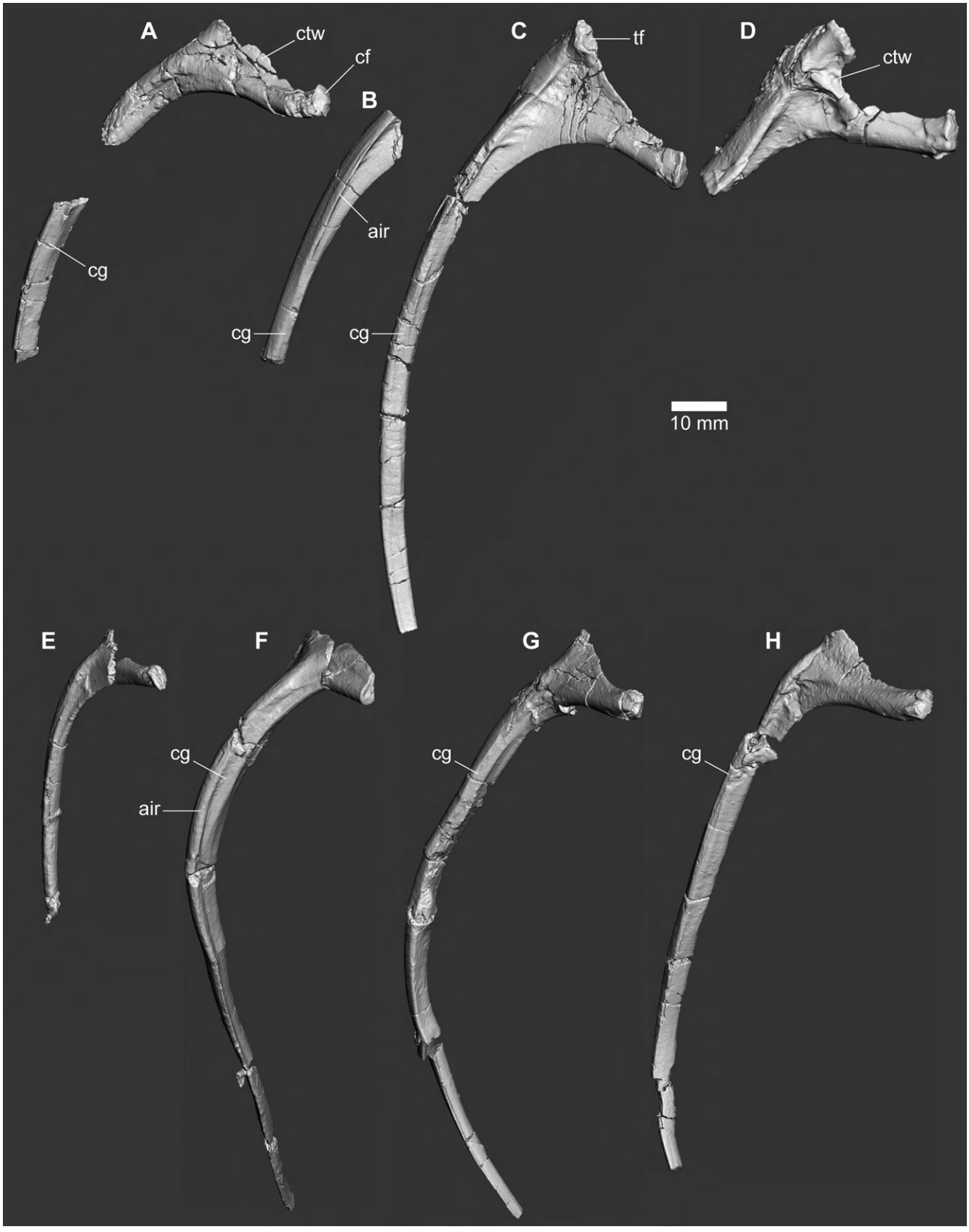

FIGURE 37. Dorsal ribs of FPDM-V-8461. Anterior views of right 1st (**D**), 3rd (**C**), 4th (**B**), 6th (**A**), 7th (**H**), 8th (**G**), 10th (**F**) and 11th (**E**) dorsal ribs. Abbreviations: air, anterior intercostal ridge; cf, capitular facet; cg, costal groove; ctw, capitular-tubercular web; tf, tubercular facet.

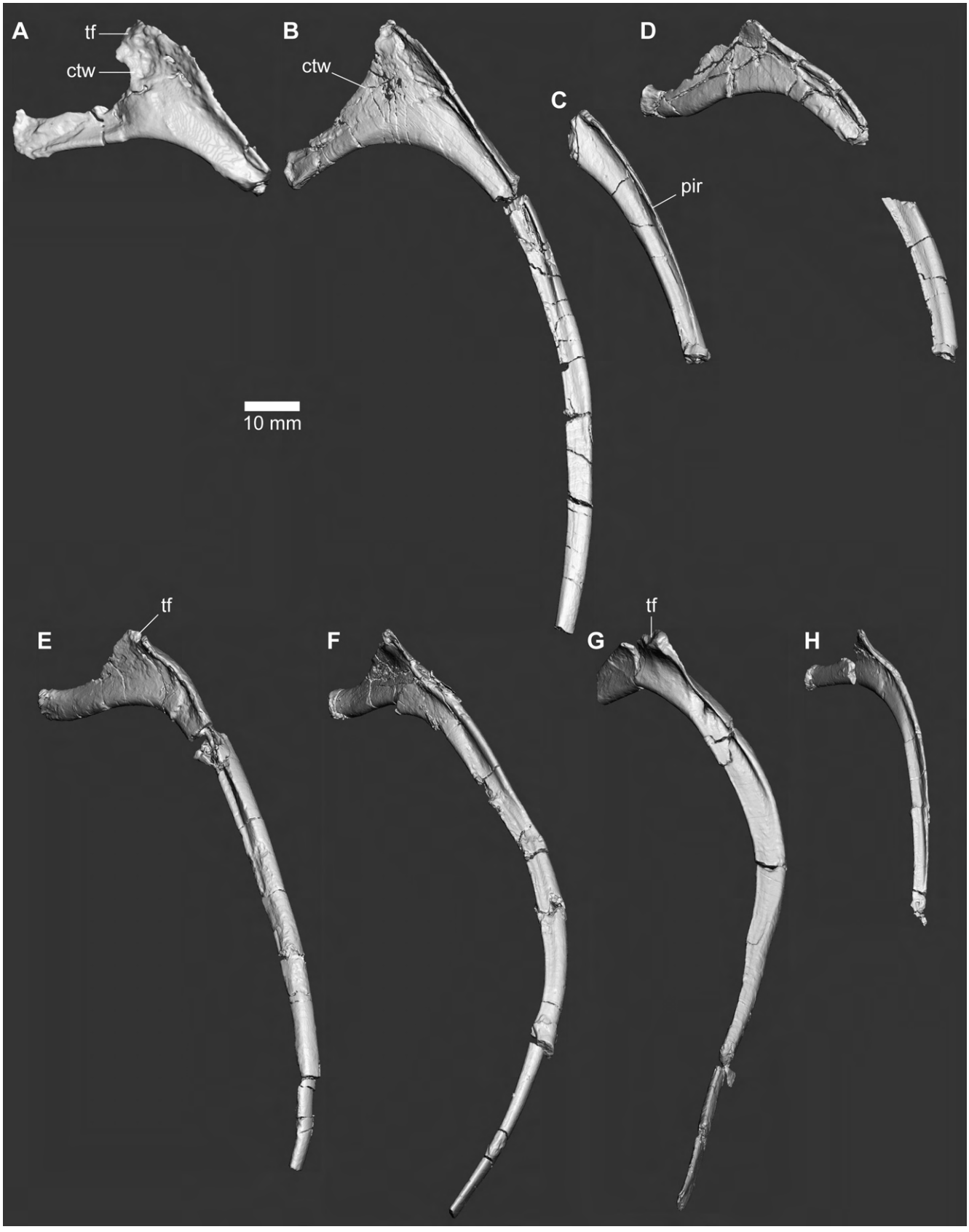

FIGURE 38. Dorsal ribs of FPDM-V-8461. Posterior views of right 1st (**A**), 2nd (**B**), 4th (**C**), 6th (**D**), 7th (**E**), 8th (**F**), 10th (**G**) and 11th (**H**) dorsal ribs. Abbreviations: ctw, capitular-tubercular web; pir, posterior intercostal ridge; tf, tubercular facet.

FIGURE 39. Dorsal ribs of FPDM-V-8461. Lateral views of right 1st (**E**), 2nd (**D**), 4th (**C**), 6th (**B**), 7th (**A**), 8th (**H**), 10th (**G**) and 11th (**F**) dorsal ribs. Abbreviations: cg, costal groove; ctw, capitular-tubercular web.

FIGURE 40. Dorsal ribs of FPDM-V-8461. Medial views of right 1st (**A**), 2nd (**B**), 4th (**C**), 6th (**D**), 7th (**E**), 8th (**F**), 10th (**G**) and 11th (**H**) dorsal ribs. Abbreviations: air, anterior intercostal ridge; cf, capitular facet; cg, costal groove; pir, posterior intercostal ridge; tf, tubercular facet.

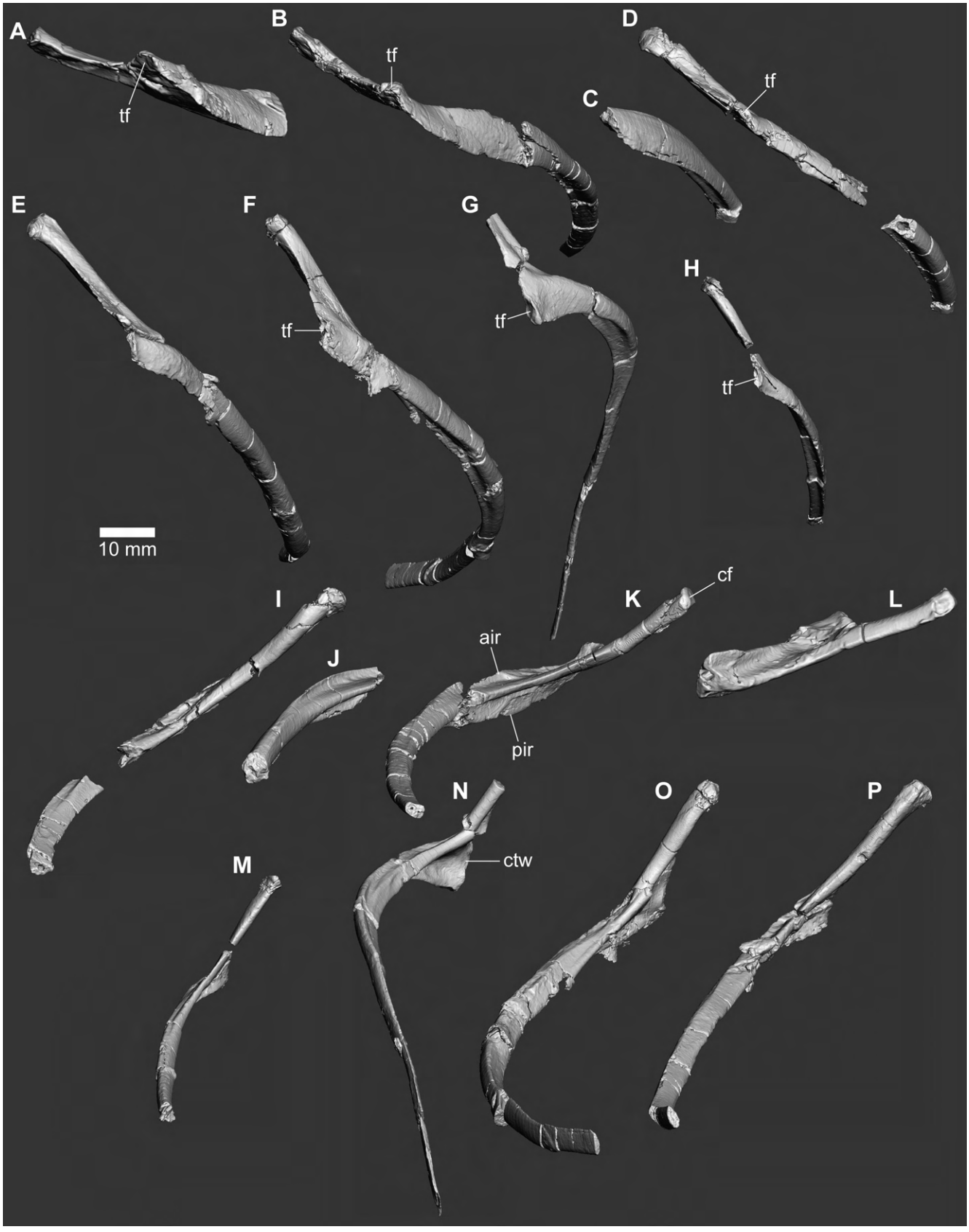

FIGURE 41. Dorsal ribs of FPDM-V-8461. Dorsal (**A**–**H**) and ventral (**I**–**P**) views of right 1st (A, L), 2nd (B, K), 4th (C, J), 6th (D, I), 7th (E, P), 8th (F, O), 10th (G, N) and 11th (H, M) dorsal ribs. Abbreviations: air, anterior intercostal ridge; cf, capitular facet; ctw, capitular-tubercular web; pir, posterior intercostal ridge; tf, tubercular facet.

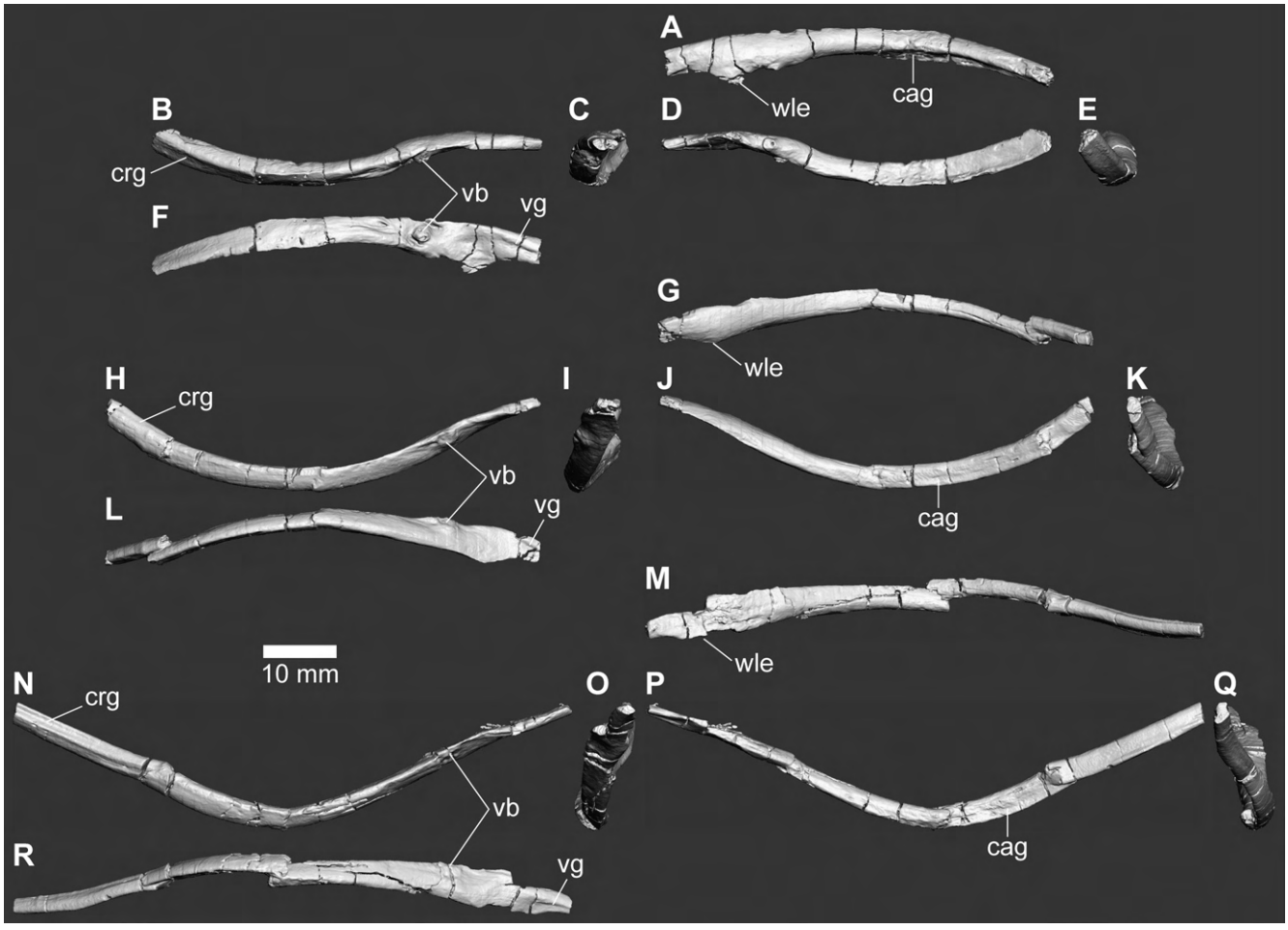

FIGURE 42. Gastralia of FPDM-V-8461. Right medial gastralia in dorsal (**A**, **G**, **M**), anterior (**B**, **H**, **N**), medial (**C**, **I**, **O**), posterior (**D**, **J**, **P**), lateral (**E**, **K**, **Q**) and ventral (**F**, **L**, **R**) views. Abbreviations: cag, caudal lateral groove; crg, cranial lateral groove; vb, ventral boss; vg, ventral groove; wle, wing-like expansion.

anteroposteriorly to form a flat lateral surface. Such lateral expansion is extensive in the first four among the thoracic series, probably for bearing the pectoral girdle (Fig. 39C–E). In contrast, the medial margin is narrow anteroposteriorly (Fig. 40), which makes a T-shaped cross section of the proximal shaft. The anterior and posterior margins of the lateral expansion represent intercostal ridges that define lateral margins of the concave anterior and posterior surfaces. The anterior ridge is deeper than the posterior ridge in the first rib, whereas, in the third and more posterior ribs, the anterior ridge is shallower and diminishes more proximally than the posterior ridge. In addition, the anterior ridge is medially invaded by the costal groove, which is particularly elongated in the 8th and 10th ribs (Fig. 37). In anterior ribs, the intercostal ridges diminish before reaching lateral vertex of the shaft, so that only the flange-like medial margin remains in the distal part to form a mediolaterally-elongated elliptical cross section of the rib (Fig. 41K). However, the medial margin is twisted posteriorly in the posterior ribs to form an anteroposteriorly-elongated elliptical cross section of the distal part (Fig. 41M–P). The tuberculum is present as a proximal protrusion of the shaft so that it also bears the intercostal ridge (Figs. 37, 38). The anterior concave surface of the capitular-tubercular web is distinguished from the one in the shaft by a stout ridge at the base of the tuberculum in the first rib (Fig. 37D). The tubercular facet faces proximomedially with an elliptical outline (Figs. 40, 41A–H), somewhat anteriorly in the third rib (Fig. 37C), and posteriorly in the 1st, 7th and 10th ribs (Fig. 38A, E, G).

Gastralia

Although several possible fragments of gastralia are collected, three of them are identified and described here (Fig. 42). Each of the three is the right medial gastralium preserving its medial ends. In anterior view, the shaft is curved laterodorsally and becomes thinner toward the medial end (Fig. 42B, H, N). The lateral part of the shaft bears longitudinal grooves on both the anterior (craniolateral groove *sensu*

FIGURE 43. Scapula of FPDM-V-8461. Left scapula in dorsal (**A**), anterior (**B**), lateral (**C**), posterior (**D**), medial (**E**) and ventral (**F**) views. Abbreviations: ap, acromion process; cc, coracoid contact; gf, glenoid fossa; nf, nutrient foramen; pgf, paraglenoid fossa.

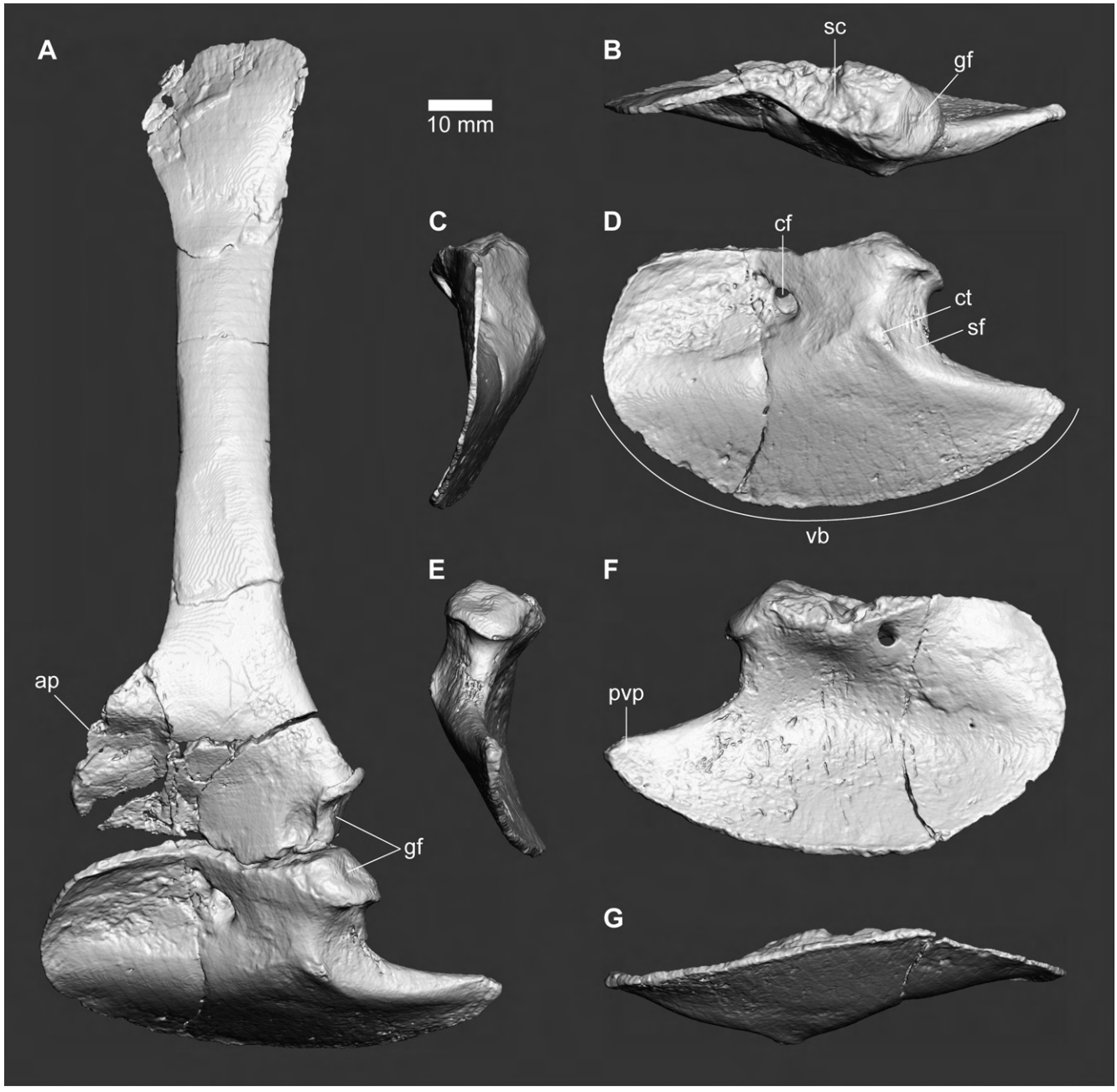

FIGURE 44. Pectoral girdle of FPDM-V-8461. Left pectoral girdle (**A**) and coracoid (**B**–**G**) in lateral (A, D), dorsal (B), anterior (C), posterior (E), medial (F) and ventral (G) views. Abbreviations: ap, acromion process; cf, coracoid foramen; ct, coracoid tuber; gf, glenoid fossa; pvp, posteroventral process; sc, scapula contact; sf, subglenoid fossa; vb, ventral blade.

Claessens, 2004) and posterior aspects, with the latter continuing more medially than the former (Fig. 42D, J, P). Medially, the shaft is expanded posteriorly in dorsal view (wing-like expansion *sensu* Claessens, 2004) to form relatively broad dorsal surface, while its width is constricted near the medial end by the depression of the posterior margin (Fig. 42A, G, M). The restricted part bears a short longitudinal groove which faces ventrally and continues to the concave ventral surface of the neighboring expanded part (Fig. 42F, L, R). Slightly lateral to the expanded part, the ventral surface bears a blunt to prominent boss near the anterior margin.

TABLE 6. Measurements on the pectoral girdles of FPDM-V-8461.

Element	Dorsoventral height (mm)	Mediolateral width (mm)	Anteroposterior depth (mm)
Scapula (L)	132.9*	24.1*	46.5
Scapula (R)	104.7*	28.4*	35.0*
Coracoid (L)	43.7	18.5	72.9
Coracoid (R)	48.5	18.0	73.1*

*Specimen incomplete in measured dimension.

Appendicular skeleton

Scapula

Both scapulae are preserved well. The left is nearly complete (Fig. 43) whereas the distal end and the acromion margin of the right scapula are damaged. The scapula is dorsoventrally elongated and approximately straight in lateral view (Fig. 43C). The dorsoventral height of the scapula is about nine times greater than the minimum anteroposterior width (14.5 mm), being approximately equal to the proximodistal length of the humerus (Table 7). Both the anterior and posterior margins of the scapular blade are slightly arched to constrict the anteroposterior width at its midlength. The ventrally facing contact surface for the coracoid is rugose and bears a longitudinal depression at its midline (Fig. 43F). In lateral view, the coracoid contact is almost straight and slightly swelled ventrally in its posterior half (Figs. 43C, 44A).

In the ventral fourth of the scapula, the acromion process projects anteriorly from the anterior margin of the blade (Fig. 43C). The ventral half of the lateral surface of the acromion region is concave to compose a broad fossa with the dorsal half of the coracoid (Fig. 44A). At the level of the acromion process, the posterior margin of the scapula curves posteroventrally to offset the glenoid well from the blade. The glenoid fossa of the scapula faces posteroventrally and its contribution to the glenoid is greater than the one of coracoid as in other maniraptorans except for alvarezsaurs and late-diverging dromaeosaurids (Brusatte et al., 2014). In lateral view, the angle between the scapula and coracoid within the glenoid is approximately 110 degrees, much greater than the approximate right angle seen in tyrannosauroids and alvarezsaurs (Brusatte et al., 2010), while the glenoid is rather like a continuous arc. On the lateral surface immediately anterior to the glenoid, a deep, circular fossa is present as in *Coelurus* and *Tanycolagreus* (Brusatte et al., 2014), termed here as the paraglenoid fossa (Fig. 43C).

Coracoid

The left coracoid is complete (Fig. 44), whereas the right lacks the anteroventral part. The coracoid is anteroposteriorly longer than dorsoventrally high (Table 6). The ventral blade is shallow and the posteroventral process is elongated (Fig. 44D, F) as in alvarezsaurs (Choiniere et al., 2010b) and ornithomimosaurs (Makovicky et al., 2004). The anterodorsal part of the lateral surface is concave to form a broad fossa with the anteroventral part of the scapula (Fig. 44A). The coracoid foramen penetrates mediodorsally from the posterior part of the concavity (Fig. 44D). The ventral half of the coracoid forms the ventral blade by a thin bony plate with gently curved ventral edge. The ventral blade and the anterodorsal concavity are separated by a blunt, anteroposteriorly oriented ridge that posteriorly meets a mound-like coracoid tuber (or biceps tubercle). The posterior third of the ventral blade forms a pointed posteroventral process (or postglenoid process), which is well separated from the glenoid by a deep notch in lateral view. The glenoid occupies the posterodorsal corner of the coracoid and faces mainly posterodorsally. A short ridge connects the coracoid tuber and the glenoid. Another ridge emerges from the coracoid tuber toward the posteroventral process of the coracoid. These two ridges are relatively blunt and only slightly project laterally to form the anteroventral rim of a shallow subglenoid fossa, which contrasts with the deep subglenoid fossa in paravians (Norell and Makovicky, 1999; Hwang et al., 2002; Turner et al., 2012) and most ornithomimosaurs (Sereno, 2017).

The medial surface is flat ventrally, concave at the middle and convex dorsally, so that the coracoid foramen exits on the convex surface (Fig. 44F) as in some alvarezsaurids and *Microvenator* (Brusatte et al., 2014). The dorsal surface is rugose and mediolaterally thin and thickens posteriorly to meet the thickness of the glenoid (Fig. 44B). In lateral view, the dorsal margin is nearly straight with a shallow concavity in the posterior part to fit with the ventral margin of the scapula (Fig. 44A, D).

Humerus

The left humerus is well preserved with only missing proximalmost part (Fig. 45). The right humerus preserves only the distal end. The length of the humerus is approximately the same with the scapula and about 70% of the femur (Table 7). The overall shape is slightly sigmoidal in lateral view with curving posteriorly in proximal whilst anteriorly in distal parts.

A large, distinct deltopectoral crest projects anteriorly from the proximal third of the humerus to make it quadrangular in lateral view (Fig.43C). The crest has approximately the same anteroposterior thickness with the shaft in medial view (Fig. 45E). The anterior extremity of the crest has a slight medial expansion to bear a shallowly concave surface facing anterolaterally (Fig. 45A, B), possibly for the insertion of the m. deltoideus clavicularis (Burch, 2014). This surface is demarcated laterally by a ridge, which continues further distally with keeping a constant distance from the anterior margin of the bone toward the presence of a distinct pit in at the middle of the lateral surface (Fig. 45C). The lateral surface of the deltopectoral crest is flat to slightly concave. Distally, a vertical flute emerges at the level of the distal extremity of the deltopectoral crest as in *Falcarius* and *Microvenator* (Zanno, 2006). The flute runs distally along the lateral ridge toward the pit, whereas it curves posteriorly to avoid a slight tabular protrusion emerging just proximal to the pit.

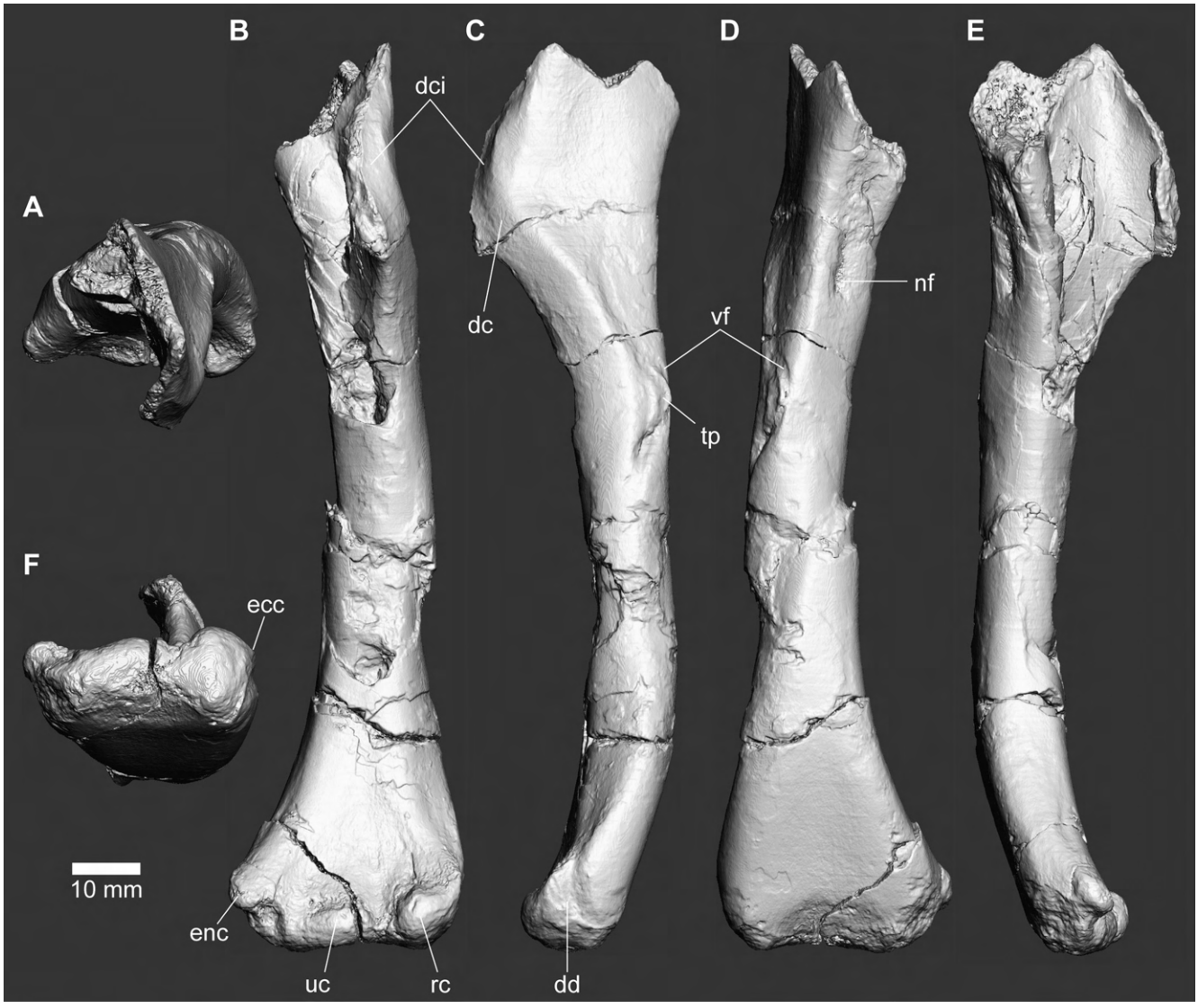

FIGURE 45. Humerus of FPDM-V-8461. Left humerus in proximal (**A**), anterior (**B**) lateral (**C**), posterior (**D**), medial (**E**) and distal (**F**) views. Abbreviations: dc, deltopectoral crest; dci, m. deltoideus clavicularis insertion; dd, m. distolateral depression; ecc, ectepicondyle; enc, entepicondyle; nf, nutrient foramen; rc, radial condyle; tp, tabular process; uc, ulnar condyle; vf, vertical flute.

Distally, the humerus is expanded unusually medially in anterior view to form broad, slightly concave anterior and posterior surfaces in contrast to a narrow shaft (Fig. 45B). In anterior view, the distal margin is perpendicular to the long axis of the bone and its width (35 mm) is about three times greater than the minimum width of the shaft (14 mm). The distal articular condyles are bulbous and project more anteriorly than distally as in therizinosaurs and late-diverging alvarezsaurs (Turner et al., 2012). The radial condyle is expanded well proximally and anteroposteriorly so that it is apparently larger than the ulnar condyle in both anterior and distal views (Fig. 45B, F). However, the ulnar condyle is expanded further medially than the radial condyle laterally in distal view. The lateral surface of the distal end bears a distinct depression resembling the origin scar of M. extensor metacarpi radialis in avialans (Vanden Berge, 1975). The entepicondyle is spherical in anterior view and separated from the ulnar condyle by a distinct fossa on the anterodistal margin between them. The entepicondyle is located well medial to the ulnar condyle as in therizinosaurs (Zanno et al., 2009).

Ulna

The left ulna is nearly complete with missing the distal extremity (Fig. 46B, C, F, H, I, K). The right ulna is represented by the proximal half of the shaft lacking its posterior part of the proximal end. The ulna is relatively long as the preserved length

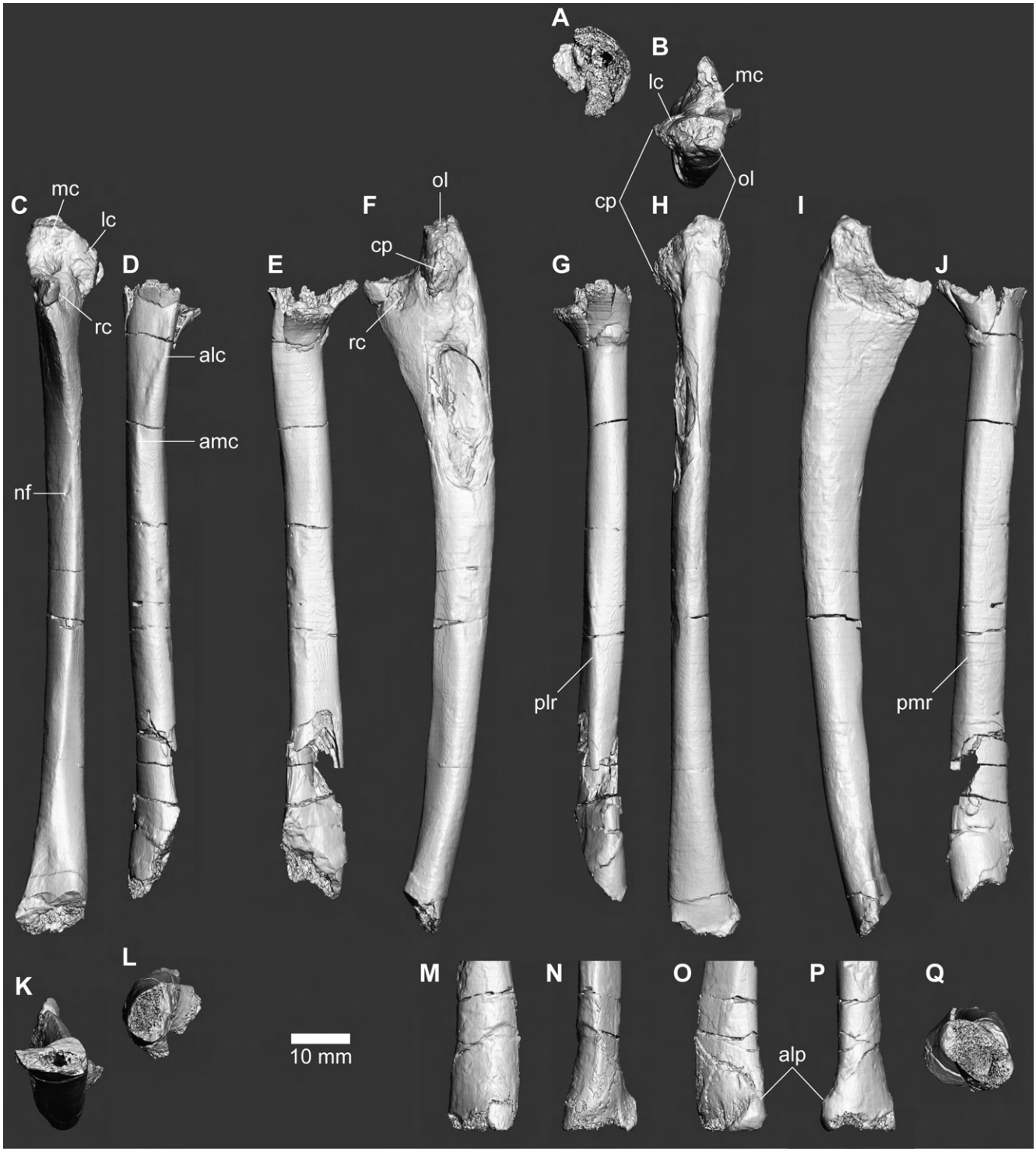

FIGURE 46. Radii and ulna of FPDM-V-8461. Proximal (**A**, **B**), anterior (**C**, **D**, **P**), lateral (**E**, **F**, **O**), posterior (**G**, **H**, **N**), medial (**I**, **J**, **M**) and distal (**K**, **L**, **Q**) views of left radius (A, D, E, G, J, L), left ulna (B, C, F, H, I, K) and distal part of right radius (M–Q). Abbreviations: alc, anterolateral crest; alp, anterolateral process; amc, anteromedial crest; cp, coronoid process; lc, lateral cotyla; mc, medial cotyla; nf, nutrient foramen; ol, olecranon; plr, posterolateral ridge; pmr, posteromedial ridge; rc, radius contact.

exceeds 90% of the humerus (Table 7) like those of alvarezsaurs and some paravians (Clark et al., 2006; Turner et al., 2012), while it is less than 70% in length of the femur.

In lateral view, the shaft is bowed posteriorly (Fig. 46F) as in maniraptorans except for alvarezsaurs, therizinosauroids and some oviraptorosaurs (Gauthier, 1986; Maryańska et al., 2002, Brusatte et al., 2014) so that the ulna is well separated from the radius along their length except both ends when in articulation. The shaft is proximally expanded anteriorly to bear smooth triangular surfaces on the lateral and medial aspects (Fig. 46F, I). The proximal end is anteroposteriorly higher than the mediolaterally wide, whereas the olecranon is slightly wider than high (Fig. 46B). The proximal end bears a prominent coronoid process anterolateral to the large olecranon, which are separated by a faint depression on the posterolateral aspect (Fig. 46F, H) and not hypertrophied as those of *Compsognathus* (Ostrom, 1978), *Sinosauropteryx* (Hwang et al., 2004) and alvarezsaurs (Choiniere et al., 2010b). The lateral surface just dorsal to the coronoid process bears a faint depression to contact with the radius (Fig. 46C, F) and lacks the bicipital scar that is seen in most paravians (Turner et al., 2012). The lateral cotyla situated proximally on the coronoid process is small and convex, whereas the medial cotyla on the main shaft is large and concave; these cotylae are not clearly separated and rather form a continuous surface (Fig. 46B, C). The distal end is expanded mediolaterally to reach the width (12.2 mm) twice as large as the one of the midshaft (6.1 mm). The anterior margin of the shaft is formed by a distinct longitudinal ridge through its length, and it distally forms the lateral margin of the triangular depression facing anteromedially. The lateral margin of this flat surface contacts the posteromedial margin of the radius when in articulation.

Radius

Although both radii are well preserved, the left lacks its distal end (Fig. 46A, D, E, G, J) and the right has somewhat damaged proximal and distal surfaces (Fig. 46M, N). The nearly complete length of the right radius reaches about 80% of the humerus (Table 7).

The shaft of the radius is approximately straight in both anterior and lateral views (Fig. 46D, E, M, N). The proximal end is unusually flared posterolaterally to separate the shaft from the ulna. The proximal surface is deeply concave in both left and right radii so that the proximal end is notably funnel-shaped. The shaft has a smooth medial surface which is anteroposteriorly broader in the middle part (Fig. 46J). Middle parts of the antero- and posteromedial margins are formed by blunt longitudinal ridges, except for a short longitudinal crest in the former at the proximal fourth of the shaft (Fig. 46D). Proximal to this crest, another prominent crest emerges on the dorsal margin and extends toward the anterolateral margin of the proximal end. The lateral surface is flat with the proximal portion slightly twisted anteriorly (Fig. 46E). The posterolateral margin of the distal shaft is formed by a distinct ridge (Fig. 46G). The posterior surface between the posteromedial and posterolateral ridges are also flat, so that the cross section of the mid-shaft exhibits a sub-quadrangular profile. The distal end is flared anteroposteriorly to bear a broad articular surface for the carpals (Fig. 46M–Q). In addition, a distinct process is present in the anterolateral margin of the distal end.

Metacarpus

While carpal elements are missing, the complete left metacarpus (Fig. 47A, G, O) and right metacarpal I are preserved. Metacarpals exhibit no sign of fusion with any distal carpal.

Metacarpal I is considerably shorter than other metacarpals unlike those of ornithomimids (Pérez-Moreno et al., 1994), with its length about the half of metacarpal II and 60% of metacarpal III, while its length being greater than the width (Table 7). The element is dorsoventrally thin and mediolaterally wide in contrast to metacarpal III (Fig. 48Y). Additionally, it is roughly hourglass-shaped in dorsal view due to medially-expanded proximal and distal ends (Fig. 47A). Even in the narrowest point, the mediolateral width of metacarpal I is greater than that of the midshaft of metacarpal II. The dorsal surface appears slightly concave and faces somewhat medially. The proximal end is triradiate in proximal view, with its sharpest apex directed medially (Fig. 48V). The lateral surface of the proximal third is concave (Fig. 47Y) to receive the convexity in the proximoventral part of the medial surface of metacarpal II (Fig. 48AF). The lateroventral margin of metacarpal I bears a small process partially underlying the metacarpal II (Fig. 48Z) to a lesser extent than the rectangular buttress of therizinosaurs (Russell and Dong, 1993). The distal end is marked by a highly ginglymoid joint through well developed distal condyles, among which the medial condyle is slightly larger than the lateral (Fig. 47D)

Metacarpal II is the longest among three metacarpals and longer than the longest manual phalanx (I-1), while it is substantially shorter than the combined length of phalanges II1 and 2 (Fig. 47G–I) unlike those of therizinosauroids (Zanno, 2006). The nearly straight shaft bows slightly medially in dorsal view (Fig. 47G). The proximal fifth of the dorsal surface and the proximodorsal end of the medial surface are shallowly concave (Figs. 47G, 48AF). The laterodorsal margin of the shaft is formed by a blunt longitudinal ridge, which has a tiny protuberance laterodistal to the concavity on the dorsal surface (Fig. 47G). While the reminder of the dorsal, medial and lateral surfaces of the shaft are convex, the ventral surface is notably flat and is laterally demarcated by a longitudinal ridge (Fig. 48K). In proximal view, the well-preserved dorsal part exhibits a convex articular surface (Fig. 48O). The distal end exhibits a ginglymoid joint (Fig. 47K), which is less developed than the one in metacarpal I whereas unlike the rounded ones of ornithomimids (Turner et al., 2012). The lateral collateral ligament fossa is much shallower than the medial one (Figs. 47AB, 48AF).

Metacarpal III is the slenderest among the three metacarpals, being dorsoventrally thick and mediolaterally narrow (Fig. 47O, AF) in contrast to metacarpal I. Both the proximodistal length and the dorsoventral thickness are slightly less than those of

FIGURE 47. Metacarpus and manual phalanges of FPDM-V-8461. Dorsal (**A–C**, **G–J**, **O–S**), distal (**D–F**, **K–N**, **T–X**) and lateral (**Y–AJ**) views of left metacarpals I (A, D, Y), II (G, K, AB) and III (O, T, AF), left phalanges I-1 (B, E, Z), I-2 (C, F, AA), II-1 (H, L, AC), II-2 (I, M, AD), II-3 (J, N, AE), III-1 (P, U, AG), III-2 (Q, V, AH) and III-3 (R, W, AI), and mirrored right phalanx III-4 (S, X, AJ). Abbreviations: ft, flexor tubercle; ldp, laterodorsal protuberance; pl, proximodorsal lip.

FIGURE 48. Metacarpus and manual phalanges of FPDM-V-8461. Ventral (**A–E**, **K–N**, **S–U**, **Z**), proximal (**F–J**, **O–R**, **V–Y**) and medial (**AA–AL**) views of left metacarpals I (S, V, AJ), II (K, O, AF) and III (A, F, AA), proximal part of left metacarpus in articulation (Y, Z), left phalanges I-1 (T, W, AK), I-2 (U, X, AL), II-1 (L, P, AG), II-2 (M, Q, AH), II-3 (N, R, AI), III-1 (B, G, AB), III-2 (C, H, AC) and III-3 (D, I, AD), and mirrored right phalanx III-4 (E, J, AE). Metacarpals II and III in Z are shaded to highlight the lateroventral process of the metacarpal I. Abbreviations: ft, flexor tubercle; lp, lateroventral process; pc, proximal concavity; plr, proximolaterally-directed ridge; pvc, proximoventral concavity.

TABLE 7. Measurements on the forelimbs of FPDM-V-8461.

Element	Proximodistal length (mm)	Mediolateral width (mm)	Anteroposterior/ dorsoventral depth (mm)
Humerus (L)	133.6*	34.7*	31.0*
Humerus (R)	35.7*	28.4*	20.0*
Radius (L)	105.6*	13.5*	15.6*
Radius (R)	106.2*	15.4*	14.7*
Ulna (L)	122.7*	15.1*	22.6
Ulna (R)	72.2*	8.1*	22.7
Metacarpal I (L)	31.1	13.6*	11.1
Metacarpal I (R)	31.1	14.2	11.1
Metacarpal II (L)	62.8	12.8	12.3
Metacarpal III (L)	50.4*	7.6*	10.5*
Manual phalanx I-1 (L)	47.0	12.7	13.0
Manual phalanx I-2 (L)	35.4	8.3	32.4*
Manual phalanx II-1 (L)	42.3	11.0	13.5
Manual phalanx II-2 (L)	46.5	8.4	13.3
Manual phalanx II-2 (R)	46.9	8.8	13.6
Manual phalanx II-3 (L)	44.5	8.3	38.3
Manual phalanx III-1 (L)	20.3	8.8	10.0
Manual phalanx III-1 (R)	18.8	8.6	9.8
Manual phalanx III-2 (L)	16.7	7.3	10.5
Manual phalanx III-3 (L)	36.1	7.3	9.8
Manual phalanx III-4 (R)	37.0	4.6	17.5

*Specimen incomplete in measured dimension.

metacarpal II (Table 7). The proximal end is triangular in proximal view with its apex directed dorsally, and the proximal surface forms a deep concavity (Fig. 47F) as in *Mononykus* and *Shuvuuia* (Brusatte et al., 2014). Distally, the ventral surface becomes narrow (Fig. 48A) while the dorsal surface widens to form a flat surface in distal two-thirds of the shaft (Fig. 47O). The distal end is dorsoventrally taller than mediolaterally wide and is less ginglymoid than other metacarpals (Fig. 47T). The condyles are discrete ventrally and merged dorsally. The lateral collateral ligament fossa is substantially broader than the medial one (Figs. 47AF, 48AA).

Manual phalanges

As in the metacarpus, the left manual phalanges are nearly complete except for the missing third ungual (III-4), which is preserved in the right (Figs. 47–48). Additional right elements include only II-2 and III-1. All non-ungual phalanges bear deep collateral ligament fossae in medial and lateral sides of the distal trochleae. In the penultimate phalanx, the collateral ligament fossae are located very close to the proximodorsal extremity of the distal articular surface, which is more dorsally than those of other non-ungual phalanges. The distal articular surface of the penultimate phalanx extends more proximally in the ventral side than the dorsal side so that the surface faces somewhat distoventrally.

I-1 is the largest among non-ungual phalanges, in which the shaft is subcircular in cross section due to the flat ventral surface (Fig. 48T) and its diameter is approximately equal to that of the radius. Proximally, the ventral surface becomes concave so that the medio- and lateroventral margins form longitudinal ridges, which are less prominent than the flexor processes seen in ornithomimosaurs and alvarezsaurids (Sereno, 2001). The shaft is twisted to turn the distal trochlea about 20 degrees clockwise in distal view of the left I-1 when the ventral surface of the proximal end is oriented horizontally (Fig. 47E). II-1 is essentially similar to I-1, except that it is shorter proximodistally and narrower lateromedially so that the shaft of II-1 is subcylindrical in cross section. The ventral surface of the shaft is flat except for proximolaterally-directed ridge emerging at about the center of the midshaft to join with the lateroventral margin at the proximal fourth of the bone (Fig. 48L). II-2 is about 10% longer than II-1 (Table 7). Phalanges of digit III are mediolaterally narrower than those of digits I and II. In addition, III-1 and 2 are notably short in contrast to III-3, which is longer than the combined length of III-1 and 2. In dorsal view, the medial margin of III-1 is strongly concave (Fig. 47P), apparently to avoid the contact with the metacarpophalangeal joint of the digit II when in articulation.

All unguals are strongly recurved (Fig. 47AA, AE, AJ) unlike those of ornithomimosaurs and alvarezsaurids (Brusatte et al., 2014) and lateromedially narrow (Fig. 47C, J, S). The proximodistal length of each ungual is approximately the same with its penultimate phalanx (Table 7). All medial and lateral grooves are shallow (Figs. 47AA, AR, AJ, 48AE, AI, AL). Each ungual has a large flexor tubercle (Fig. 47AA, AE, AJ) unlike small ones of tyrannosauroids and ornithomimosaurs (Brusatte et al., 2010), and is located substantially distal to the proximal end unlike proximally located ones of pennaraptorans and late-diverging therizinosauroids (Nicholls and Russell, 1985; Xu et al., 2011; Brusatte et al., 2014). The first ungual is dorsoventrally deeper and mediolaterally thicker than others and the most strongly recurved in lateral view (Fig. 47AA). However, the proximodistal length of the first ungual is slightly shorter than the second. The second ungual is relatively elongated proximodistally and bears a prominent proximodorsal lip (Fig. 47AE) as in alvarezsaurs and maniraptorans (Currie and Russell, 1988; Zanno et al., 2009). The third ungual is the thinnest and shortest among the unguals, while it is more strongly recurved than the second (Fig. 47S, AJ).

Pubis

Although both ilia and ischia are missing, nearly complete shaft of the right pubis is preserved (Fig. 49). The shaft is straight excepting that the proximal end is slightly bowed laterally (Fig. 49B, C). Proximally, the cross section of the shaft is anteroposteriorly elongated and thin lateromedially. The shaft

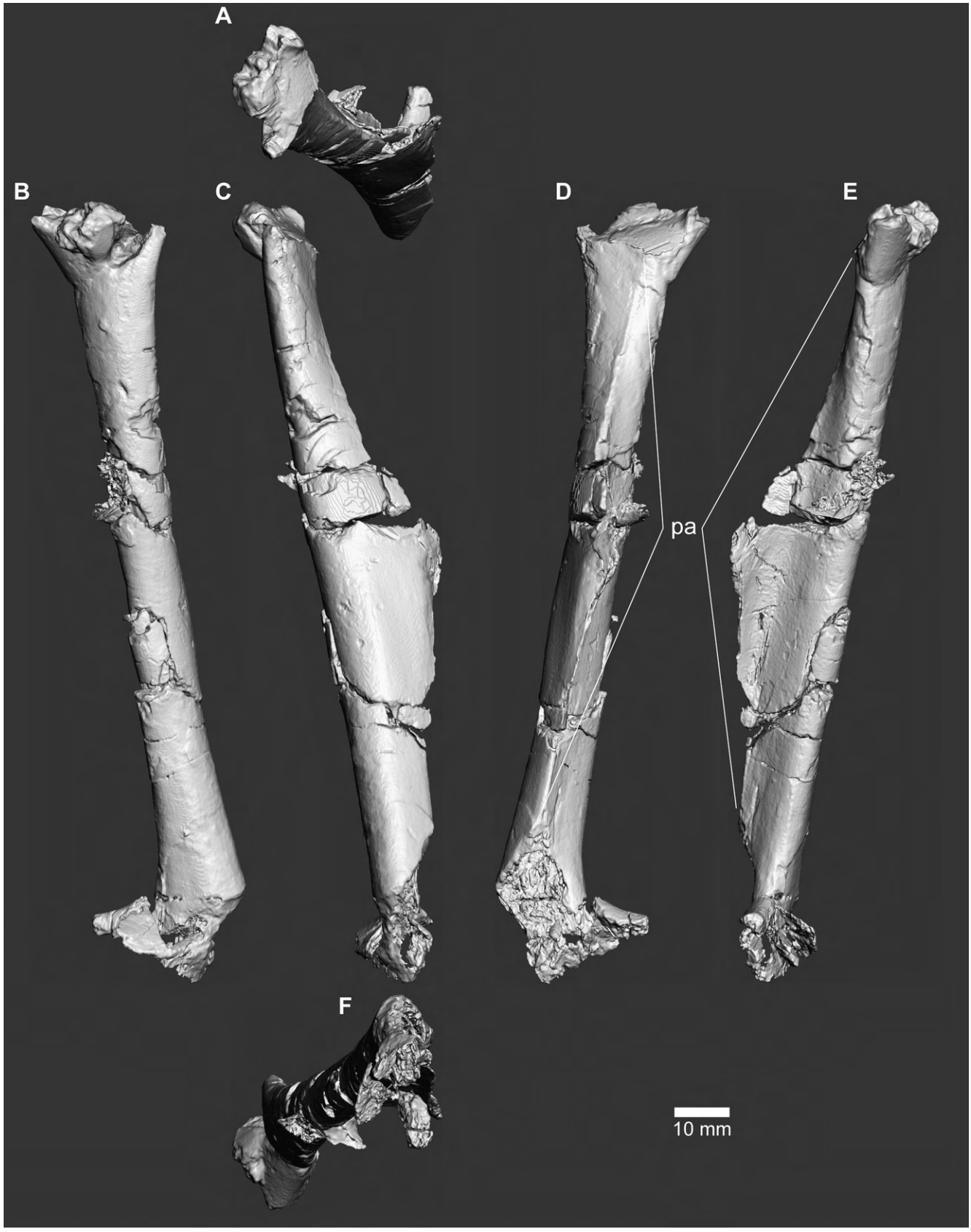

FIGURE 49. Pubis of FPDM-V-8461. Right pubis in proximal (**A**), lateral (**B**), anterior (**C**), medial (**D**), posterior (**E**) and distal (**F**) views. Abbreviation: pa, pubic apron.

FIGURE 50. Femur of FPDM-V-8461. Left femur in proximal (**A**), medial (**B**), anterior (**C**), lateral (**D**), posterior (**E**) and distal (**F**) views. Abbreviations: at, accessory trochanter; fc, fovea capitis; fh, femoral head; fo, fossa; ft, fourth trochanter; gt, greater trochanter; hlp, hook-like process; hr, horizontal ridge; lr, lateral ridge; lt, lesser trochanter; nf, nutrient foramen; pt, posterior trochanter; tf, trochanteric fossa; ts, trochanteric shelf.

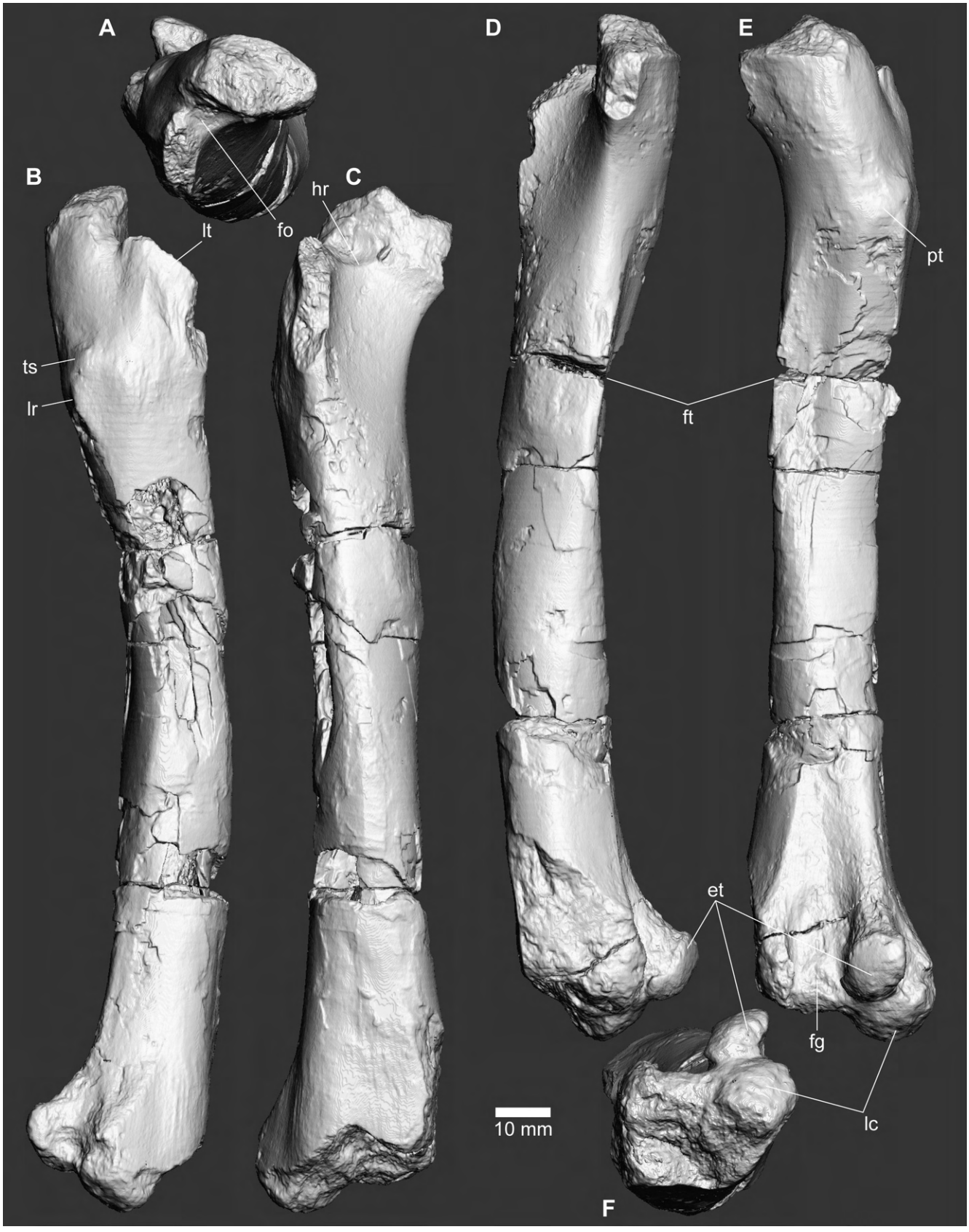

FIGURE 51. Femur of FPDM-V-8461. Right femur in proximal (**A**), lateral (**B**), anterior (**C**), medial (**D**), posterior (**C**) and distal (**F**) views. Abbreviations: et, ectocondylar tubercle; fg, flexor groove; fo, fossa; ft, fourth trochanter; hr, horizontal ridge; lc, lateral condyle; lr, lateral ridge; lt, lesser trochanter; pt, posterior trochanter; ts, trochanteric shelf.

distally becomes thicker so that the cross section is subcircular, except for the pubic apron. The pubic apron emerges as a low ridge from the middle of the medial surface of the proximal end (Fig. 49D). The ridge extends anterodistally and becomes more prominent to form a thin flange-like apron projected from the anteromedial margin of the shaft. The mediolateral width of the apron reaches its apex at the midlength of the preserved shaft and then diminishes distally (Fig. 49E). Distal to the apex, the medial margin of the apron is rough possibly due to the contact with the opposing pubis. However, the distalmost part of the apron turns to a low ridge with a smooth surface, indicating absence of a contact with the opposing pubis at least in the distal fourth of the shaft. The preserved distal end of the shaft exhibits a slight expansion in anteroposterior orientation indicating the presence of a pubic boot.

Femur

Both femora are preserved with both the proximal and distal ends damaged. However, the proximal end is better preserved in the left (Fig. 50) and the distal end better in the right (Fig. 51), so that the original length of the femur can be estimated as 190 mm by mirroring the one and superimposing on the other.

In anterior view, the proximal margin of the femoral head is straight and perpendicular to the long axis of the shaft (Fig. 50C). The head bears a blunt, small hook-like process protruding distally at its mediodistal margin. In medial view, the fovea capitis is present as a slight depression on the proximoventral margin (Fig. 50B) and posteriorly continuous with the trochanteric fossa on the posterior surface of the head (Fig. 50E). Although the presence of this trochanteric fossa makes a partial constriction on the region bridging the head and the greater trochanter in proximal view (Fig. 50A), the constriction is not as prominent as those of some oviraptorosaurs (Balanoff and Norell, 2012) and therizinosauroids (Zanno et al., 2009). In addition, the anterior margin of the proximal end is straight in proximal view as in other maniraptorans (Brusatte et al., 2014).

The greater and lesser trochanters are separated from each other by a deep cleft (Fig. 50D). The cleft is continuous with a fossa on the anterior surface just below the greater trochanter and is ventrally demarcated by a horizontal ridge (Fig. 50A, C). The lesser trochanter is largely damaged so that the original dorsal height is unknown, whereas it projects anteroproximally as a broad flange that is anteroposteriorly wider than the greater trochanter; i.e. the alariform shape (Fig. 50D). There is a faint swelling on the anterodistal margin of the lesser trochanter probably representing the accessory trochanter.

At the level with the base of the lesser trochanter, the posterior trochanter forms a blunt swelling on the lateral half of the ventral aspect (Fig. 50E). In lateral view, a longitudinal ridge extends from the posteroventral termination of the lesser trochanter to the anterior margin of the trochanteric shelf (Fig. 50D). Another longitudinal ridge extends distally from the ventral end of the trochanteric shelf to demarcate the lateroventral margin of the shaft, possibly corresponding to the lateral ridge seen in many maniraptorans (Norell and Makovicky, 1999; Hutchinson, 2001). Slightly distal to the level of posterior trochanter, the fourth trochanter emerges as a longitudinal ridge on the posteromedial margin (Fig. 50E). The anterior surface near the distal end of the femur exhibits a flat surface (Fig. 51C). The medial part of the distal end is incompletely preserved and the presence of mediodistal crest is unknown. In the distal epiphysis, the ectocondylar tubercle is projected posterodistally and separated from the lateral condyle by a deep cleft in both lateral and distal views (Fig. 51B, F), while they are not as developed to form a trochlea seen in pygostylians (Clarke et al., 2006). The ectocondylar tubercle forms the lateral wall of the flexor groove that opens distally (Fig. 51E).

Tibia

Both tibiae are preserved (Fig. 52). The right tibia lacks the proximal end including most of the cnemial crests and the distal end. Despite the incompleteness, the left tibia is longer than the estimated length of the femur, indicating that the original length of the tibia is substantially longer than the femur (Table 8).

In anterior view, the shaft curves medially and expands mediolaterally toward the distal end (Fig. 52A). The fibular crest emerges at the level slightly above the distal extremity of the cnemial crest as a bulge of the ridge that runs distally from the proximal end (Fig. 52B). The fibular crest is positioned further away from the distal end indicating that the crest is proximally located and never extends to the midshaft of the tibia, contrasting with those of therizinosauroids (Xu et al., 2002c; Zanno et al., 2009; Zanno, 2010). Posteriorly, the preserved proximal end bears a shallow concavity, which probably corresponds to the remnant of the cleft between the medial and lateral proximal condyles (Fig. 52C). The distalmost part of the anterior surface is nearly entirely covered by the astragalus and calcaneum when in articulation (Fig. 52G). In addition, the laterodistal part of the anterior surface bears a blunt longitudinal ridge demarcating the lateral margin of the area covered by the ascending process of the astragalus (Fig. 52A). The narrow surface lateral to this ridge is flat to contact with the fibula and the calcaneum and faces anteriorly and slightly laterally as in *Falcarius* (UMNH VP 12362). The lateral margin of the distal shaft is kinked to form another distinct ridge. The distal extremity of this ridge diverges from the lateral margin due to the presence of the shoulder of the lateral malleolus. The shoulder and the distal margin of the medial malleolus are situated more proximally than those of lateral malleolus (Fig. 52A, G) as in *Falcarius* (Zanno, 2010). The posterior surface of the distal shaft bears a sharp longitudinal ridge demarcating the broad posterolateral and narrow posteromedial surfaces. This ridge is slightly curved distomedially, resulting in the posteromedial projection of the distal end located lateral to the medial edge by about one third of the mediolateral width (Fig. 52E).

Fibula

The proximal and distal parts of the right fibula are preserved (Fig. 52). The proximal part lacks the proximal end, while exhibiting the base of the proximomedial fossa as a proximally-shallow concavity that is expanded anteroposteriorly

FIGURE 52. Tibiae of FPDM-V-8461. Left (**A**–**F**) and distal half of right (**G**) tibiae in anterior (A, G), lateral (B), posterior (C), medial (D), proximal (E) and distal (F) views. Abbreviations: ac, astragalus contact; acm, ascending process contact margin; apc, ascending process contact; cc, calcaneum contact; fco, fibula contact; fcr, fibular crest; ic, probable remnant of the intercondylar cleft between the medial and lateral proximal condyles; lm, lateral malleolus; lms, shoulder of lateral malleolus; mm, medial malleolus; mms, shoulder of medial malleolus; pp, posteromedial projection.

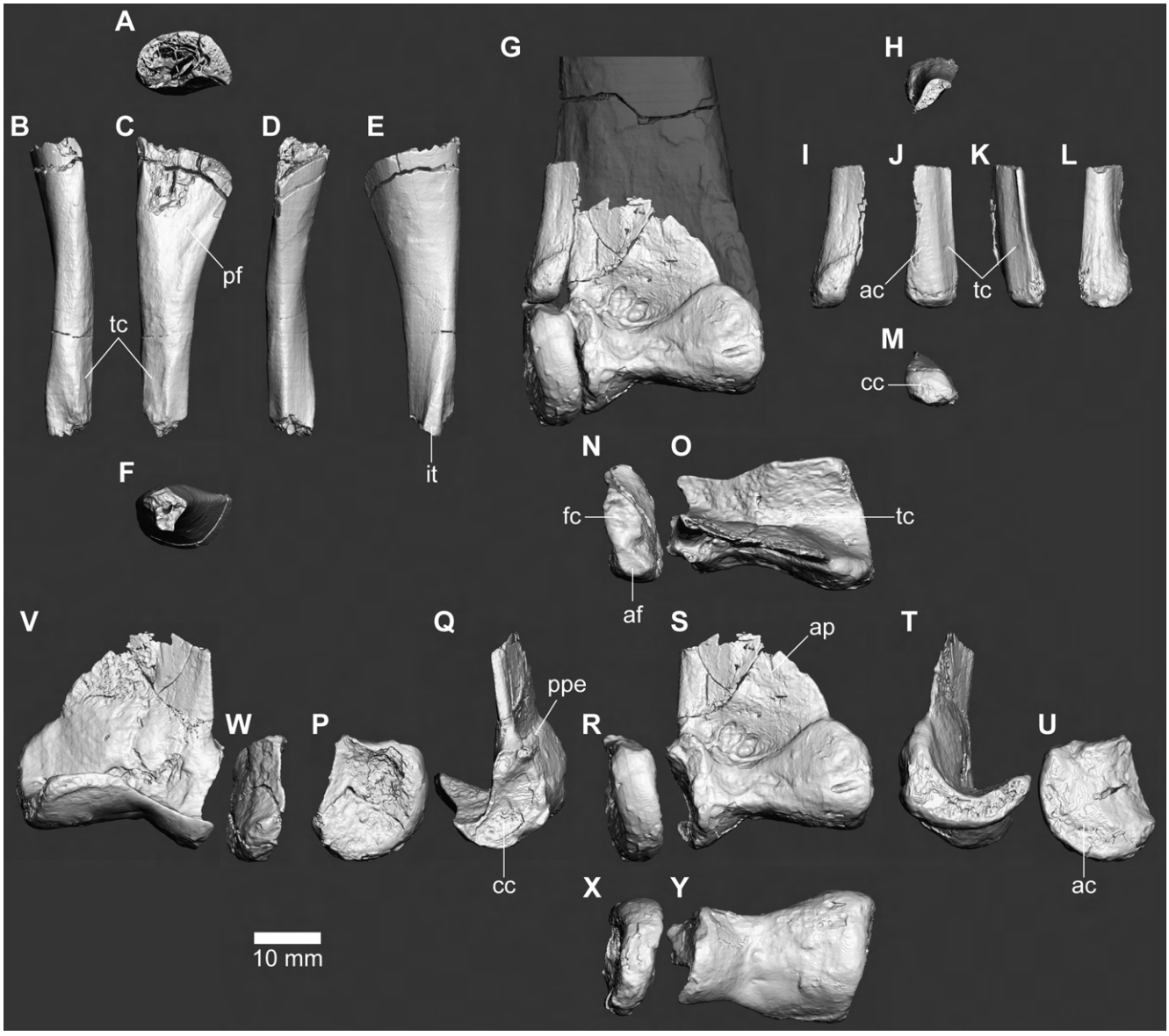

FIGURE 53. Fibula, astragalus and calcaneum of FPDM-V-8461. Proximal part of right fibula (**A**–**F**), distal parts of right fibula and mirrored left tibia (shaded) in articulation with right astragalus and calcaneum (**G**), distal part of right fibula (**H**–**M**), right calcaneum (**N**, **W**, **P**, **R**, **U**, **X**) and astragalus (**O**, **V**, **Q**, **S**, **T**, **Y**) in proximal (A, H, N, O), anterior (B, G, I, R, S), medial (C, J, T, U), posterior (D, K, V, W) lateral (E, L, P, Q) and distal (F, M, X, Y) views. Abbreviations: ac, astragalus contact; af, anteroproximal facet; ap, ascending process; cc, calcaneum contact; fc, fibula contact; it, iliofibularis tubercle; pf, proximomedial fossa; ppe, proximally-pointed eminence; tc, tibia contact.

(Fig. 53C). The anterior, ventral and posterior margins of the proximomedial fossa are indistinct unlike well-defined ones of tyrannosaurs and ornithomimosaurs (Brusatte et al., 2014). Distal to the proximomedial fossa, a rough surface occurs as a contact with the fibular crest of the tibia, demarcated by the anterior margin of the fibula and a longitudinal ridge along the midline of the medial surface. In lateral view, the proximal end of the iliofibularis tubercle is preserved as a stout ridge forming the lateral margin of the fibula accompanying a rough, slightly concave anterior surface (Fig. 53B, E). When in articulation with the tibia, the tubercle is situated at the midheight of the fibular crest, which, in turn, is situated much proximal to the midshaft of the tibia. The distal part of the fibula has a distal articular surface for the proximal tarsals (Fig. 53G) indicating that the fibula originally has the length subequal to that of the tibia. The articular surface extends well proximally along the anterior margin so that it contributes a concave surface with the anteroproximal facet of the calcaneum when in articulation (Fig. 53G).

Tarsus

Both astragali, right calcaneum and right distal tarsal III are present (Figs. 53, 54). Unlike those of some maniraptorans, there is no sign for the fusion of tarsal bones. When the astragalus and calcaneum are articulated, both the lateral and medial condyles are similar in size and the former projects more distally than the latter in anterior view (Fig. 53G).

The ascending process of the astragalus is tall and broad to cover most of the anterior surface of the distal end of the tibia (Fig. 53G). The anterior surface of the ascending process bears a broad fossa that becomes deeper in its distal part and distinctly demarcated by the dorsal margin of the distal condyles (Fig. 53S). Within the fossa, just proximal to the intercondylar sulcus, two distinct circular pits are present. The anteroproximal end of the lateral condyle forms a proximally-pointed eminence (Fig. 53Q). In contrast to the anterior side, there is no proximal expansion on the posterior side (Fig. 53V). Distally, the medial and lateral condyles are separated by a broad and distinct sulcus in anterior view, while it becomes indefinite in distal view unlike the distinct ones of alvarezsaurs, troodontids and avialans (Turner et al., 2012). The anterior surface of the intercondylar sulcus bears a shallow horizontal groove. In distal view, the mediolateral width of the medial condyle is slightly greater than that of the that of the lateral condyle and anteroposterior depths of both condyles (Fig. 53Y). Both condyles mesially constricted anteroposteriorly in distal view.

The proximal surface of distal tarsal III is convex (Fig. 55F) whereas the distal one is concave with an anteroposteriorly oriented ridge separating the facet for metatarsals II and III mediolaterally (Fig. 54R). Distal tarsal III is proximodistally thin and thickens posteriorly in lateral view (Fig. 55N). The posterior margin of the bone bears a large swelling protruding posteriorly in the middle to lateral part, as well as a slight depression in the medial part (Fig. 55H).

Metatarsus

The right metatarsus is mostly complete whereas the left lacks metatarsal IV (Figs. 54, 55). No trace for the fusion is observable between the metatarsal elements. When in articulation, metatarsals II–IV are proximodistally elongated as a whole in anterior view. In addition, metatarsals II–IV are closely appressed only at their proximal ends and distally diverged from each other as in therizinosaurs (Zanno et al., 2009).

Metatarsal I bears a triangular shape in anterior view with a sharp point directed proximally (Fig. 54F). The lateral side bears a broad concave surface in the proximal half to contact with metatarsal II (Fig. 55S). The distal half of the lateral surface is mostly occupied by the collateral ligament fossa, which is much deeper than the medial one (Fig. 54L).

Metatarsal II is nearly straight in anterior view. In proximal view, the bone has a semicircular profile with a straight medial margin and the posterior two-thirds of the proximal surface is depressed for the contact with distal tarsal III (Fig. 55B). The proximal end is expanded anteroposteriorly in lateral view and exhibits a flat lateral surface facing slightly posteriorly for the contact with metatarsal III. The proximal end bears a posterior projection with a narrow rugose surface (Fig. 55I). The proximalmost part of the anteromedial margin forms a sharp angle, although it abruptly becomes blunt due to the presence of a small boss (Fig. 55R) which probably corresponds to the tuberositas m. tibialis cranialis of extant birds (Baumel and Witmer, 1993). As in most non-avian theropods, definite signs of articulation with metatarsal I are absent in both medial and posterior surfaces. However, at the level slightly distal to the midshaft, the medial surface bears a posterodistally directed groove (Fig. 54H). The intercondylar sulcus is slightly visible within the distal margin in anterior view (Fig. 54E), while it is not as specialized as those of dromaeosaurids (Norell and Makovicky, 1997). The mediolateral width of the distal trochlea (15.8 mm) is approximately the same with those of metatarsals III (15.0 mm) and IV (14.7 mm).

Metatarsal III bears a stout shaft exposed both anteriorly and posteriorly when in articulation with other metatarsals through its entire length, unlike the arctometatarsalian condition seen in some coelurosaurs (Holtz, 1995). The proximal end exhibits a flat medial surface for the contact with metatarsal II (Fig. 54I) and a lateral projection followed posteriorly by a concavity for the contact with metatarsal IV (Fig. 55Q). Other than these, no obvious contact surface for neighboring metatarsals is observed. In lateral view, the shaft is proximally expanded anteroposteriorly in the proximal half, whereas it is anteroposteriorly thin in the distal half. The proximal half of the shaft having a convex anterior surface with a small boss at the middle of the proximal fifth (Fig. 54D), which probably corresponds to the tuberositas m. tibialis cranialis of extant birds (Baumel and Witmer, 1993). In contrast, the distal half of the shaft forms a flat anterior surface. The distal margin of metatarsal III is approximately flat in anterior view and not ginglymoid. In anterior view, the distal articular surface is expanded more proximally above the medial condyle than the lateral condyle.

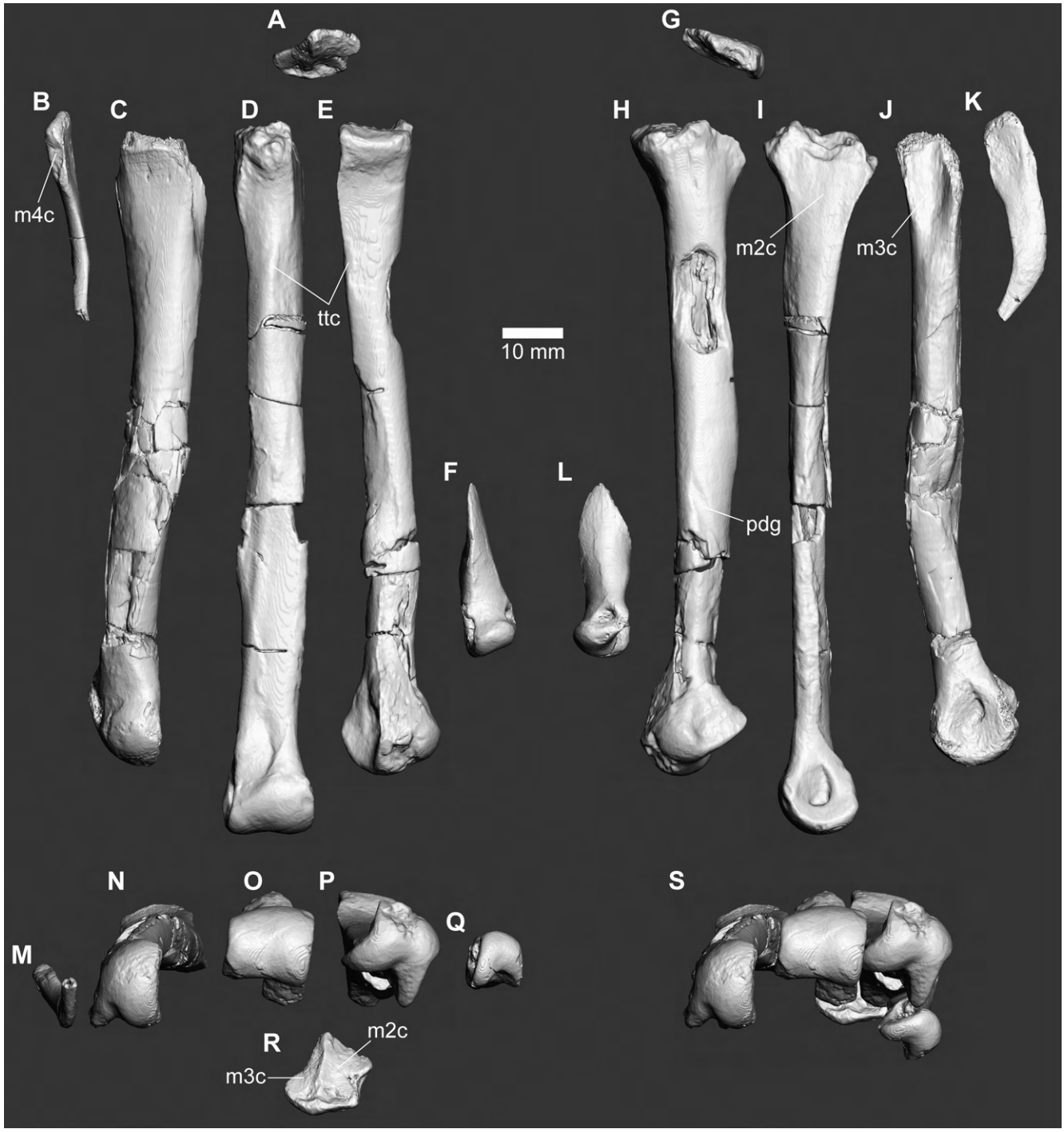

FIGURE 54. Distal tarsal III and metatarsus of FPDM-V-8461. Anterior (**A**–**F**), medial (**G**–**L**) and distal (**M**–**S**) views of right distal tarsal III (A, G, R), mirrored left metatarsal I (F, L, Q), right metatarsals II (E, H, P), III (D, I, O), and IV (C, J, N), mirrored left metatarsal V (B, K, M) and right distal tarsal III in articulation with metatarsus incorporating mirrored left metatarsals I and V (S). Abbreviations: m2c, metatarsal II contact; m3c, metatarsal III contact; m4c, metatarsal IV contact; pdg, posterodistally-directed groove; ttc, tuberositas m. tibialis cranialis.

FIGURE 55. Distal tarsal III and metatarsus of FPDM-V-8461. Proximal (**A**–**G**), posterior (**H**–**M**) and lateral (**N**–**S**) views of right distal tarsal III (F, H, N), mirrored left metatarsal I (A, M, S), right metatarsals II (B, I, R), III (C, J, Q) and IV (D, K, P), mirrored left metatarsal V (E, L, O), and right distal tarsal III in articulation with metatarsus incorporating mirrored left metatarsals I and V (G). Abbreviations: d3c, distal tarsal III contact; m2c, metatarsal II contact; m3c, metatarsal III contact; m4c, metatarsal IV contact; ttc, tuberositas m. tibialis cranialis.

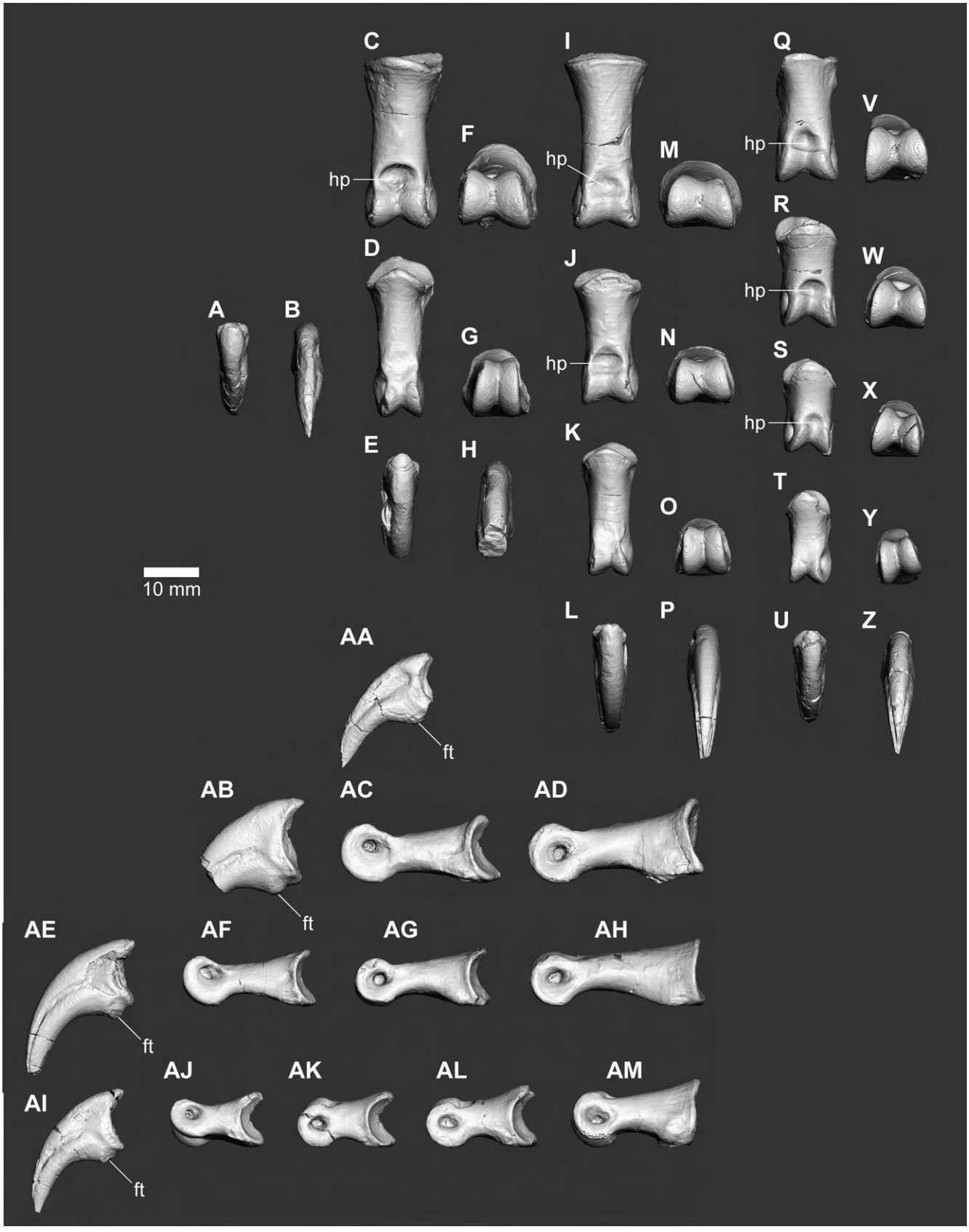

FIGURE 56. Pedal phalanges of FPDM-V-8461. Dorsal (**A**, **C**–**E**, **I**–**L**, **Q**–**U**), distal (**B**, **F**–**H**, **M**–**P**, **V**–**Z**) and lateral (**AA**–**AM**) views of left phalanges I-2 (A, B, AA), II-1 (C, F, AD), II-2 (D, G, AC), II-3 (E, H, AB), III-1 (I, M, AH), III-2 (J, N, AG), III-3 (K, O, AF), III-4 (L, P, AE), IV-1 (Q, V, AM), IV-2 (R, W, AL), IV-3 (S, X, AK) and IV-4 (T, Y, AJ), IV-5 (U, Z, AI). Abbreviations: ft, flexor tubercle; hp, hyperextensor pit.

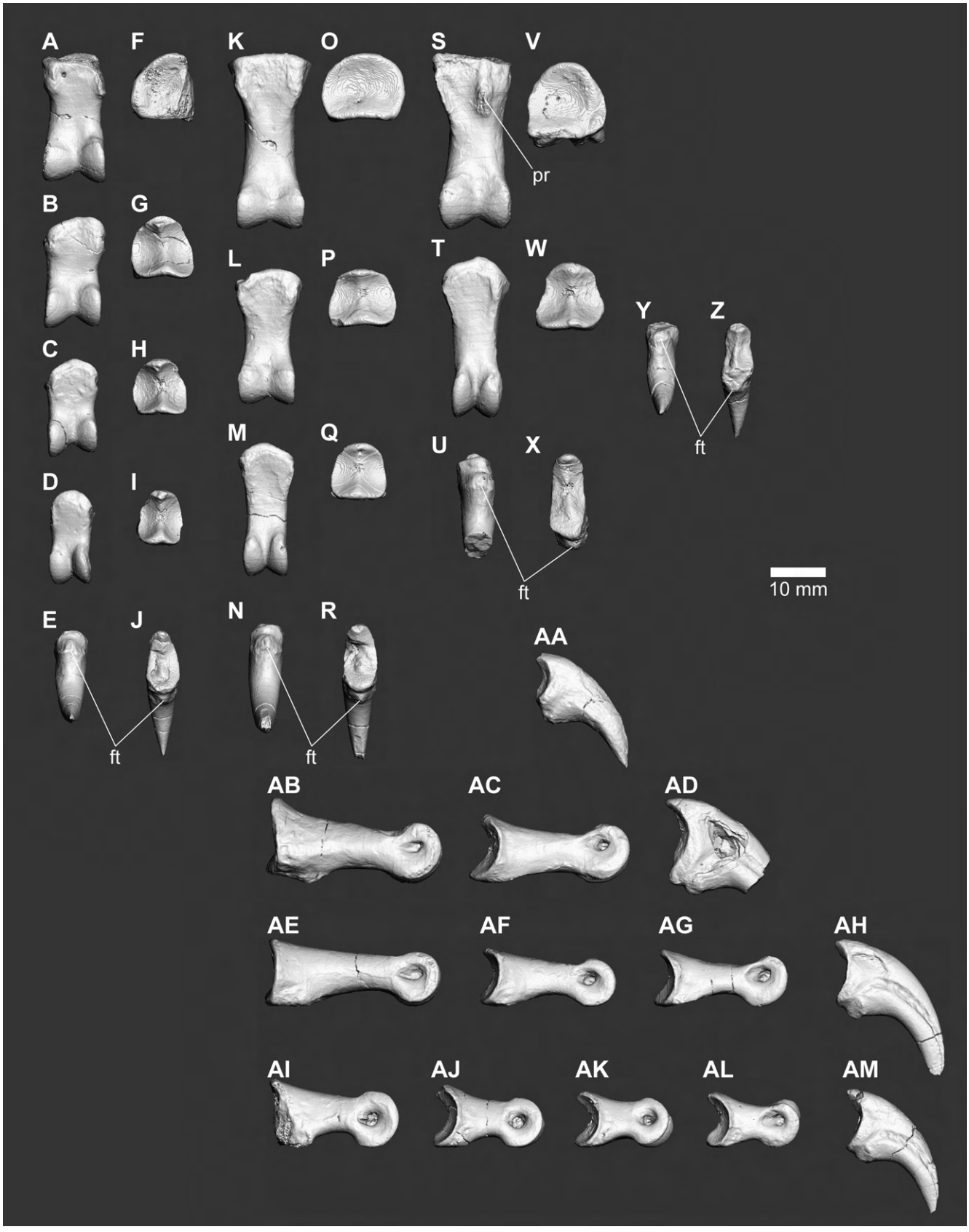

FIGURE 57. Pedal phalanges of FPDM-V-8461. Ventral (**A**–**E**, **K**–**N**, **S**–**U**, **Y**), proximal (**F**–**J**, **O**–**R**, **V**–**X**, **Z**) and medial (**AA**–**AM**) views of left phalanges I-2 (Y–AA), II-1 (S, V, AB), II-2 (T, W, AC), II-3 (U, X, AD), III1 (K, O, AE), III-2 (L, P, AF), III-3 (M, Q, AG), III-4 (N, R, AH), IV-1 (A, F, AI), IV-2 (B, G, AJ), IV-3 (C, H, AK) and IV-4 (D, I, AL), IV-5 (E, J, AM). Abbreviation: ft, flexor tubercle; pr, proximomedial ridge.

TABLE 8. Measurements on the pubis and hindlimbs of FPDM-V-8461.

Element	Proximodistal length (mm)	Mediolateral width (mm)	Anteroposterior/ dorsoventral depth (mm)
Pubis (R)	146.3*	25.0*	30.4*
Femur (L)	164.1*	51.0*	34.2*
Femur (R)	186.7*	35.9*	37.7*
Tibia (L)	204.9*	37.8	31.3*
Tibia (R)	187.7*	26.5*	29.0*
Fibula (L)	21.9*	8.9*	7.8*
Fibula (R)	45.2*	9.8*	14.6*
Astragalus (L)	29.2*	32.6	23.4
Astragalus (R)	32.6	31.5	20.1
Calcaneum (R)	19.1	9.3	17.8
Distal tarsal III (R)	8.4	14.7	13.7
Metatarsal I (L)	28.8	9.5	9.7
Metatarsal I (R)	30.1*	10.2	10.4
Metatarsal II (L)	104.9*	25.0*	22.8
Metatarsal II (R)	108.6*	17.2*	19.4
Metatarsal III (L)	104.8*	15.0*	12.8*
Metatarsal III (R)	118.3	15.4	19.0
Metatarsal IV (R)	105.1	19.8	20.6
Metatarsal V (L)	34.9	7.5	10.6
Pedal phalanx I-2 (L)	16.9	6.1	20.9
Pedal phalanx II-1 (L)	32.1	14.5	15.6
Pedal phalanx II-1 (R)	33.2	14.5	10.9*
Pedal phalanx II-2 (L)	29.3	12.5	12.5
Pedal phalanx II-3 (L)	19.1*	7.1	17.7*
Pedal phalanx III-1 (L)	31.9	15.0	12.4
Pedal phalanx III-1 (R)	32.3	15.6	13.2
Pedal phalanx III-2 (L)	24.7	12.4	10.7
Pedal phalanx III-3 (L)	24.3	10.3	10.5
Pedal phalanx III-3 (R)	24.2	10.0	10.7
Pedal phalanx III-4 (L)	19.9	6.5	24.7
Pedal phalanx IV-1 (L)	23.5	11.6	12.5
Pedal phalanx IV-1 (R)	23.7	12.2	13.0
Pedal phalanx IV-2 (L)	20.2	11.4	11.4
Pedal phalanx IV-3 (L)	17.8	9.8	10.3
Pedal phalanx IV-3 (R)	18.1	10.0	10.3
Pedal phalanx IV-4 (L)	17.1	8.5	10.1
Pedal phalanx IV-4 (R)	17.7	8.4	10.3
Pedal phalanx IV-5 (L)	16.8	6.3	22.6
Pedal phalanx IV-5 (R)	17.1	6.0	20.7

*Specimen incomplete in measured dimension.

Metatarsal IV exhibits a stout shaft as in metatarsals II and III. The proximal part is slightly expanded posteroproximally unlike those of metatarsals II and III (Fig. 54J). The medial surface of the proximal end is occupied by a broad longitudinal groove, which roughly fits with the lateral projection in the proximal end of metatarsal III. The shaft of metatarsal IV bears convex anterior and flat posterior surfaces to form a semicircular shape in cross-section. In addition, the shaft is slightly mediolaterally wider than dorsoventrally deep. In distal view, however, the anteroposterior depth (15.0 mm) of the distal end is subequal to the mediolateral width (14.7 mm) in metatarsal IV (Fig. 54N).

Metatarsal V is crescent-shaped in lateral view with a distinctive proximal articular surface and a pointed distal end without articular surface (Fig. 55O). The bone is lateromedially thin through its entire length (Fig. 54B). The medial surface constitutes a shallow concavity to contact with metatarsal IV in the proximal third of the element. The posterior margin of the distal half is thick and rugose in contrast to a thin, sharp margin of the proximal half (Fig. 55L).

Pedal phalanges

Pedal phalanges are almost completely known in the left pes except for I-1 and the distal end of the second ungual (Figs. 56, 57). The right pedal phalanges are represented by I2, II-1, III-1, III-3, IV-1, IV-3, IV-4 and IV-5.

All non-ungual phalanges share a proximodistally-elongated slender shape in dorsal view unlike the square-shaped non-ungual phalanges in most large-bodied theropods. Particularly, those of digits II and III are three times longer or more proximodistally than wide lateromedially (Fig. 56C–E, I–L). In ventral view, phalanx II-1 bears a short ridge laterally demarcating a narrow rugose surface in the proximomedial margin (Fig. 57S). In contrast, phalanx III-1 and IV-1 exhibit two ridges in medial and lateral margins near the proximal end (Fig. 57A, K). Proximodorsal to the distal articular surface, each non-ungual phalanx is excavated by the hyperextensor pit except for the penultimate one (Fig. 56C, I, J, Q–S). In each distal trochlea, the lateral condyle is larger than the medial one in the second digit (Fig. 56F, G), whereas the condition is reversed in the fourth digit (Fig. 56V–Y). The dorsoventral depth of the distal articular surface of pedal phalanx II-2 is approximately equal to that of the proximal articular surface (Fig. 55AD) unlike those of some troodontids (Turner et al., 2012).

Pedal unguals essentially resemble those of most other theropods. Each pedal ungual is distally recurved, pointed ventrally and lateromedially thin with a small lip overhanging the proximal articular surface dorsally. Just below the dorsoventrally-elongated articular surface, a tuber for the attachment of the flexor tendon is present (Fig. 56AA, AB, AE, AI). Among four pedal unguals, the first is the smallest and the second is the largest in size, although it is not significantly larger than the third unlike those of deinonychosaurs (Turner et al., 2012).

DISCUSSION

Phylogenetic position of *Fukuivenator*

A theropod genus *Fukuivenator* was erected in Azuma et al. (2016) with 14 autapomorpies as a basal member of Maniraptora. Maniraptora originally established by Gauthier (1986) is defined as a stem-based clade containing *Passer domesticus* and all coelurosaurs closer to it than to *Ornithomimus velox* (Maryańska et al., 2002). The phylogenetic position of *Fukuivenator* proposed by Azuma et al. (2016) within a polytomy of Ornithomimosauria and other clades leaves maniraptoran affinity of this genus uncertain.

The phylogenetic analysis performed in this study recovered 62 MPTs with a length of 3453 steps (consistency index = 0.313; retention index = 0.772). Additional TBR branch swapping on these MPTs resulted in >10000 total MPTs. In the resulted strict consensus tree, *Fukuivenator* is recovered as an unambiguous member of Maniraptora, and in total of 12 autapomorpies of the genus are proposed within the clade in the present study (see "Emendation of diagnosis" for detail). As a result, *Fukuivenator* is placed at the base of the clade Therizinosauria (Fig. 58), although the robustness of this placement should be accepted with caution because statistical supports for the clade are not strong. Nevertheless, the result indicates a slightly more crownward position of *Fukuivenator* than previously proposed in Azuma et al. (2016), in which no positive relationship with Therizinosauria is suggested. In addition, the polytomy unresolved in Nesbitt et al. (2019) composed of Compsognathidae, Ornithomimosauria, Therizinosauria, Alvarezsauria and Paraves is resolved in the reduced consensus tree of the present study.

According to the analysis, the monophyly of Maniraptora was supported by 19 unambiguous synapomorphies and *Fukuivenator* presents two of them:

780(2) foramen magnum larger than occipital condyle;
840(1) straight anterior margin of femur in proximal view (also in some tyrannosauroids).

Fukuivenator also presents four unambiguous synapomorphies for maniraptorans diverging later than Alvarezsauria:

150(1) proximodorsal lip of manual unguals (also in *Bicentenaria*);
488(1) wide maxillary fenestra (also in some tyrannosauroids, some compsognathids and *Garudimimus*);
688(0) bowed ulnar shaft (also in Zuolong, some early-diverging tyrannosauroids, *Ornitholestes* and *Archaeornithomimus*);
839(1) longer scapula contribution to the glenoid (also in some tyrannosauroids).

In addition, *Fukuivenator* exhibits eight unambiguous synapomorphies for Therizinosauria:

8(1) subotic recess on braincase (also in ornithomimids and some troodontids);
90(1) 11 or more cervical vertebrae (also in *Citipati*, *Jinfengopteryx* and some avialans);
98(1) two pneumatic foramina on each side of cervical vertebrae (also in some oviraptorosaurs, *Sinovenator* and some avialans);
117(0) distal caudal neural spines present as low ridges (also in *Zuolong*, tyrannosauroids, ornithomimosaurs and some oviraptorosaurs);
309(1) 11 dorsal vertebrae (also in *Patagopteryx*);
366(1) distal articular condyles present on anterior surface of humerus (also in alvarezsaurids and most avialans);
789(1) deep dorsal neural arches;
824(0) metatarsals II–IV divergent from each other.

The unusual morphological condition of *Fukuivenator* resulted in 46 diagnostic features, which is the largest in number among all taxa in the reduced consensus tree. Among them, nine diagnostic features are autapomorphic within Maniraptora:

25(0) short anteromedial process of maxilla;
103(1) zygapophyses of dorsal vertebrae situated lateral to the neural canal and hyposphenes connected by an inset web (also in Ornithomimosauria and some tyrannosauroids);
526(1) pneumatic posterior process of lacrimal (also in late-diverging tyrannosauroids);
613(1) posteroventrally facing basisphenoid recess (also in some tyrannosauroids);
661(1) well-developed posterior centrodiapophyseal laminae in anterior-middle cervicals (also in Tyrannosaurinae);
664(1) nearly horizontal posterior centrodiapophyseal lamina in anterior-middle cervicals (also in basal tyrannosauroids);
680(0) relatively short scapula (also in Ornithomimosauria, some compsognathids, some basal tyrannosauroids);
843(0) laterally-displaced medial ridge on posterior surface of distal tibia;
844(1) fossa on lateral surface of scapula immediately above glenoid (also in *Coelurus* and *Tanycolagreus*).

Remaining 37 diagnostic features of *Fukuivenator* are homoplastic within Maniraptora:

10(1) basisphenoid recess divided into two foramina (also in *Citipati*, *Chirostenotes* and some eudromaeosaurs);
14(0) solid basipterygoid processes (also in Paraves);
19(2) exits for cranial nerves X–XII located in a shallow depression (also in some eudromaeosaurs, late-diverging avialans and *Incisivosaurus*);
27(2) large maxillary fenestra (also in troodontids diverging later than *Almas* and IGM 100/1126);
38(1) lacrimal foramen (or fenestra) (also in *Citipati* and *Rinchenia*);
39(2) small posterodorsal process of lacrimal (also in troodontids diverging later than *Jinfengopteryx* and *Mei*,

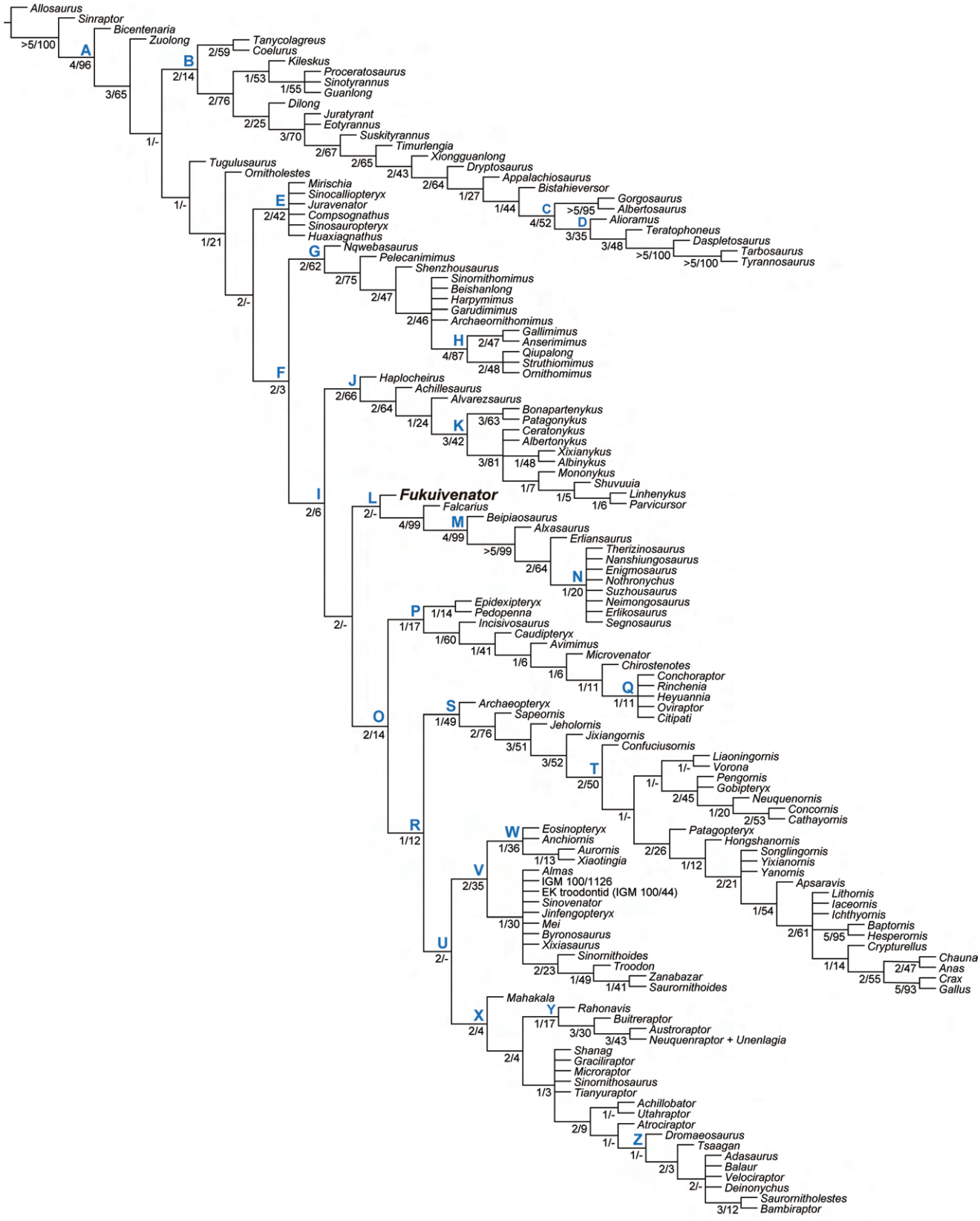

FIGURE 58. Strict consensus tree of coelurosaurs including *Fukuivenator paradoxus*. A, Coelurosauria; B, Tyrannosauroidea; C, Tyrannosauridae; D, Tyrannosaurinae; E, Compsognathidae; F, Maniraptoriformes; G, Ornithomimosauria; H, Ornithomimidae; I, Maniraptora; J, Alvarezsauria; K, Alvarezsauridae; L, Therizinosauria; M, Therizinosauroidea; N, Therizinosauridae; O, Pennaraptora; P, Oviraptorosauria; Q, Oviraptoridae; R, Paraves; S, Avialae, T, Pygostylia; U, Deinonychosauria; V, Troodontidae; W, Anchiornithinae; X, Dromaeosauridae; Y, Unenlagiinae; Z, Eudromaeosauria. Numbers at the bottom left of each node represent the decay index (Bremer support; left) and the bootstrapping score (right) for the node. Hyphen (-) indicates that the node has not been recovered for the respective test.

Austroraptor and some alvarezsaurs);

42(1) sinusoidal anterior emargination of supratemporal fossa on frontal (also in most dromaeosaurids);

44(1) notched lacrimal suture on frontal (also in some dromaeosaurids and *Ichthyornis*);

46(0) unfused parietals (also in Avialae and Eudromaeosauria);

56(1) twisted paroccipital process (also in Dromaeosauridae and *Haplocheirus*);

91(1) large epipophyses of axis (also in Eudromaeosauria, *Mei* and some avialans);

100(0) absence of hypapophyses in anterior dorsal vertebrae (also in *Alvarezsaurus*, *Microvenator*, *Microraptor*, *Sinovenator* and basal avialans);

101(1) distinctly projected parapophyses in posterior dorsal vertebrae (also in Alvarezsauria, Dromaeosauridae, *Mei* and *Confuciusornis*);

107(1) interspinous ligament scar terminating below apex of dorsal neural spine (also in Deinonychosauria and *Conchoraptor*);

116(1) caudal neural spines separated anteroposteriorly (also in *Rahonavis* and *Jeholornis*);

118(0) relatively short prezygapophyses of distal caudals (also in avialans diverging later than *Archeopteryx* and some troodontids);

146(1) metacarpal I longer than the half of metacarpal II (also in Ornithomimosauria and a late-diverging avialan *Chauna*);

241(1) lateral lamina of maxilla reduced to small triangle (also in some dromaeosaurids, Anchiornithinae, some troodontids and *Jeholornis*);

318(1) fused distal caudal vertebrae (also in Pygostylia, *Citipati*, *Conchoraptor*, *Beipiaosaurus* and *Sapeornis*);

337(1) flat or convex dorsal suture on coracoid against scapula (also in alvarezsaurs diverging later than *Ceratonykus*, *Albertonykus*, *Xixianykus* and *Albinykus*, and some avialans);

345(1) flat medial surface around coracoid foramen (also in Parvicursorinae, *Sinovenator*, and some avialans);

351(1) ulna approximately long as humerus (also in Alvarezsauria, *Microraptor*, *Aurornis*, *Eosinopteryx* and avialans diverging later than *Archaeopteryx*);

359(1) deltopectoral crest dorsoventrally thick as humeral shaft (also in Unenlagiinae, some avialans, *Oviraptor*, *Heyuannia*, *Mononykus* and *Shuvuuia*);

373(1) pit on distolateral margin of humerus (also in Ornithurae);

377(0) indistinct dorsal cotyla of ulna (also in *Citipati*);

409(0) slightly developed posterior trochanter (also in Paraves);

448(1) anterior tympanic recess confluent with prootic recess (also in late-diverging troodontids);

607(1) ventral flange at distal end of paroccipital process (also in Dromaeosauridae);

630(1) dorsoventrally shallow meckelian groove (also in *Zanabazar*);

687(1) medial condyle of humerus expanded well medially (also in *Patagonykus*);

713(1) distally situated fourth trochanter (also in therizinosauroids diverging later than *Erliansaurus*);

766(1) deeply concave proximal articular surface on metacarpal III (also in *Mononykus* and *Shuvuuia*);

777(0) horizontal groove separating distal condyles from ascending process of astragalus (also in *Alvarezsaurus*);

797(1) expanded medial aspect of distal humerus (also in therizinosauroids diverging later than *Alxasaurus*);

829(0) meckelian groove centered at midheight of dentary (also in *Austroraptor* and *Erlikosaurus*);

837(0) antorbital fossa occupying almost entire lateral surface of lacrimal body (also in *Sapeornis* and Oviraptorosauria);

841(1) horizontal ridge between femoral head and neck (also in *Linhenykus*).

Azuma et al. (2016) previously argued that these features highlight unusual mosaic condition of *Fukuivenator*. Revised features of *Fukuivenator* and its position in the current phylogenetic analyses in the present study seem to support the previous hypothesis.

Emendation of diagnosis

With aids of CT analyses in the present study, 5 of 14 characters are retracted from the original diagnosis in Azuma et al. (2016). Particularly, those on the premaxilla and the postorbital (the first and fifth of the original diagnoses) are withdrawn due to misidentification of the elements. The large promaxillary fenestra subequal in size to maxillary fenestra, the second of the original diagnosis (Azuma et al., 2016), is in fact the dorsal part of the maxillary fenestra (Fig. 4C). In relation to the lacrimal, the element originally described as the left lacrimal is re-identified as the right lacrimal, where the anterior and descending rami being identified conversely in Azuma et al. (2016). The present study identifies the groove present between the lateral and medial laminae of the descending ramus (Fig. 6K), and the ridge on the laterodorsal margin of the anterior ramus (Fig. 6J) as in most theropods. Contrary to Azuma et al. (2016), no additional projection on the posterior surface of basal tubera of the braincase is present except for the ridges extending mediodorsally from it (Fig. 12D). Such feature is shared with other theropod such as *Piatnitzkysaurus* (Rauhut, 2004) and *Velociraptor* (Norell et al., 2004), although it is more distinctive in *Fukuivenator*.

Two additional diagnostic characters of *Fukuivenator* within maniraptorans are also identified: unusually thick dorsal margin of the jugal and bifid posterior end of the ectopterygoid. The pronounced thickness results from the inflation of the bone by a large jugal sinus. Although the jugal sinus is also present in tyrannosauroids and *Pelecanimimus* (Gold et al., 2013) among coelurosaurs, such thickness at the dorsal margin of the suborbital part is unknown with most maniraptorans completely lacking the sinus. Therefore, this character highlights an unusual pneumaticity of the jugal of *Fukuivenator* within the clade. In the ectopterygoid, the posterior margin of the main body is

bifurcated by a notch in lateral view. This notch is adjacent to the medial margin of the main body of ectopterygoid that is usually attached to the pterygoid, so that a complex, relatively robust connection may have been present between the two bones in *Fukuivenator*.

Remarks on maniraptoran anatomy

Maxillary fenestra and other openings on antorbital fossa

One of the notable characters of *Fukuivenator*, the large maxillary fenestra occupying more than half the area between the anterior margins of the antorbital fossa and fenestra, is also present in most troodontids (character 27). Such condition of the maxillary fenestra is scored as a second derived state for Troodontidae by Currie and Varricchio (2004; character 22(2)) and incorporated into the TWiG dataset by Turner et al. (2012; character 27). However, this character scoring was modified in the latter study into the first derived state (state 1) for most troodontids as possessing the smaller maxillary fenestra, except for jinfengopterygines, although the maxillary fenestra is apparently larger also in other troodontids (Norell et al., 2009; Pei et al., 2017). To assess the phylogenetic affinity of *Fukuivenator*, scorings of the character in troodontids were revised in the present study based on published descriptions and figured photographs. Specifically, scorings for the following taxa are modified from the first (Turner et al., 2012) to the second derived states (state 2): *Saurornithoides* (Norell et al., 2009), *Zanabazar* (Norell et al., 2009), *Xixiasaurus* (Lü et al., 2010), *Byronosaurus* (Makovicky et al., 2003; Bever and Norell, 2009), *Aurornis* (Godefroit et al., 2013) and *Sinovenator* (Xu et al., 2002b). In addition, the scorings for *Troodon* (interpreted as a composite of *Stenonychosaurus* and *Latenivenatrix* after van der Reest and Currie, 2017) is modified into unknown due to insufficient description in the literature referred in Turner et al. (2012).

In addition, the scorings for the location of maxillary fenestra (character 28) are revised for some troodontids. The locations of the maxillary fenestra in *Jinfengopteryx* and *Almas* is apparently situated posterior to the border (Shuan and Qiang, 2007:fig. 2; Pei et al., 2017) and their condition is scored as the derived state (state 1) in the present study, contra to Turner et al. (2012) that scores them as the primitive state (state 0).

Fukuivenator and some late-diverging troodontids such as *Saurornithoides* and *Zanabazar* exhibit similarly large maxillary fenestra located anteriorly in antorbital fossa (Norell et al., 2009). Yet, despite the apparent resemblance, the phylogenetic position of *Fukuivenator* is recovered somewhat distant from Troodontidae. Indeed, the maxillary fenestra of *Fukuivenator* is rather quadrangular than elliptical, unlike those in the late-diverging troodontids. In addition, the maxilla of *Fukuivenator* bears a large pneumatic excavation (excavatio pneumatica *sensu* Witmer, 1997) posterodorsal to the maxillary fenestra as well as a small promaxillary fenestra, both of which are absent in troodontids. The antorbital fossa of *Fukuivenator* is strikingly similar to a hatchling of allosauroid IPFUB Gui Th 4 (Rauhut and Fechner, 2005) in exhibiting both the quadrangular maxillary fenestra and the excavatio pneumatica. Therefore, it is hypothesized that such features of antorbital fossa in *Fukuivenator* possibly resulted from the retention of a paedomorphic condition widely shared among avetheropods including basal maniraptorans.

Incisiform tooth and loss of denticles

Fukuivenator exhibits highly heterodont condition with four morphotypes of teeth within one individual, all of which are unserrated and approximately conical. As mentioned by Azuma et al. (2016), the mesialmost tooth is somewhat similar to the incisor-like teeth of *Incisivosaurus* (Xu et al., 2002a; Balanoff et al., 2009) in having subcircular section at the base and the lingual surface becoming flatter apically. However, the incisiform tooth of *Fukuivenator* does not exhibit apparent wear surface nor large size, features that are extensive in *Incisivosaurus*. According to Hendrickx et al. (2019), such incisiform teeth are also seen in *Ornitholestes*, *Falcarius* and *Pelecanimimus*. Therefore, such condition is possibly plesiomorphic to a clade containing *Ornitholestes* and Maniraptoriformes and inherited in basal ornithomimosaur *Pelecanimimus* and basal therizinosaurs *Fukuivenator* and *Falcarius*.

The loss of denticles in the whole dentition is another dental feature of *Fukuivenator*. Hendrickx et al. (2019) hypothesizes that the complete loss of the denticles is apomorphy of Paraves so that the denticles are plesiomorphically present in Therizinosauria. However, the present phylogenetic position of *Fukuivenator* suggests an alternative hypothesis where the teeth of Therizinosauria are plesiomorphically unserrated and their denticles are re-acquired within the clade. In the reduced strict consensus tree of the present study, unserrated conditions for both the mesial (character 81(2)) and lateral (character 782(1)) dentitions are optimized as ancestral for Maniraptoriformes. In this scenario, the unserrated dentitions are inherited to basal paravians, so that the partially serrated (character 81(1)) and serrated lateral dentitions are acquired in *Haplocheirus* and within Therizinosauria, respectively (gained twice). This scenario is more plausible than the alternative in accordance with Hendrickx et al. (2019), in which the loss of the serration independently occurs in *Fukuivenator*, Oviraptorosauria and basal paravians (lost three times). On the other hand, the shared conidont/folidont tooth condition in basal therizinosaurs *Fukuivenator* and *Falcarius* and basal oviraptorosaurs suggests that such dentition is synapomorphic to the clade Therizinosauria + Pennaraptora in support of Hendrickx et al. (2019).

Fused posteriormost caudals

Fused posteriormost caudals is generally known as a shared trait in avialan pygostylians. On the other hand, such feature is also known in the ornithomimosaur *Deinocheirus* (Lee et al., 2014), therizinosaur *Beipiaosaurus* (Xu et al., 2003), and oviraptorosaurs *Nomingia* (Barsbold et al., 2000b), *Similicaudipteryx* (He et al., 2008), *Citipati* and *Conchoraptor* (Persons et al., 2014), as well as the non-pygostylian avialan

TABLE 9. Encephalization quotients (REQs) of *Fukuivenator* and other selected theropods.

Taxon	REQ (37%)	REQ (50%)	REQ (100%)
Carnotaurus[1]	1.4–1.6	1.9–2.2	3.9–4.3
Majungasaurus[1]	1.14	1.54	3.08
Ceratosaurus[2]	1.22	1.66	3.31
Allosaurus[1]	1.3	1.8	3.28
Allosaurus[1]	1.8	2.4	3.68
Gigantosaurus[1]	1.07	1.4	2.9
Sinraptor[1]	0.81	1.1	2.19
Murusraptor[1]	1.33	1.8	3.6
Tyrannosaurus[1]	1.8	2.5	4.4
Tyrannosaurus[1]	1.6	2.2	4.49
Troodon[3]	2.61	3.53	7.07
Dromiceiomimus[3]	3.14	4.31	8.6
Dromiceiomimus[3]	2.61	3.58	7.15
Erlikosaurus[4]	1.03	1.39	2.79
Fukuivenator	1.08	1.46	2.92

Note: [1]Cerroni & Paulina-Carabajal (2019); [2]Franzosa (2004); [3]Hurlburt (1996); [4]Lautenshlager et al. (2012).

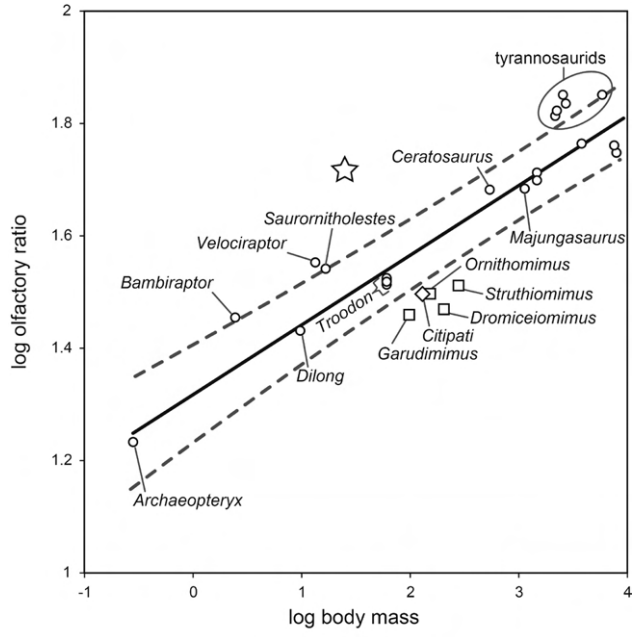

FIGURE 59. Relationship between olfactory ratio and body mass for selected dinosaurs. Bold and dashed lines represent independent contrast least-squares regression and 95% CI, respectively. Star, *Fukuivenator*; diamond, oviraptorid; squares, ornithomimosaurs; circles, other theropods. Modified from Zelenitsky et al. (2009).

Fukuipteryx (Imai et al., 2019). This feature appears to be convergently acquired at least in Therizinosauria and Oviraptorosauria because it is absent in their basal members (Persons et al., 2014) and anatomically different between the two clades (Wang and O'Connor, 2017). The number of caudal vertebrae contributing to the structure varies from two to five. As in *Similicaudipteryx* and possibly *Deinocheirus*, the fused posteriormost caudal vertebrae in *Fukuivenator* are composed of two. However, the anatomy of the structure as a whole is rather similar to the one in *Beipiaosaurus* than to the ones in oviraptorosaurs and *Fukuipteryx* in exhibiting the concave ventral margin and a blunt posterior end in lateral view. Although it is assumed that the pygostyle functioned to maneuver fan-forming rectrices in oviraptorosaurs, the presence of such rectrices is only known in the taxa lacking the fused posteriormost caudals (Ji et al., 1998) and rectrices are evidently absent in the posterior end of the tail in *Beipiaosaurus* (Xu et al., 2003). Therefore, there is no evidence that the fused posteriormost caudals of *Fukuivenator* supported the rectrices in life. In addition, the large total number of caudal vertebrae in *Fukuivenator* suggests that the fusion of the posteriormost vertebrae is not associated with the reduction of the tail in contrast to the pygostyle of most avialans. With lacking a modern analogue possessing a long tail ending with fused vertebrae, and highly convergent nature of the feature, functional role of the fused posteriormost caudal vertebrae in non-pygostylian theropods remains unknown.

Paleobiology of *Fukuivenator*

Calculations of Sensory and Cognitive Capabilities

The preserved portion of the brain endocast of *Fukuivenator* measures 7.94 cm^3 in volume, and the minimum volume of the complete endocast is estimated 12.24 cm^3 based on the existing part. Following Hurlburt et al. (2013), the reptile encephalization quotients (REQs) at 100%, 70%, and 50% of the endocranial volume of *Fukuivenator* was calculated using the following equation: $REQ = MBr/ (0.0155 \times MBd^{0.553})$, where MBr is the brain mass and MBd is the body mass (Hurlburt et al., 2013). In the present analysis, MBr was calculated from the estimated minimum volume of the complete endocast (12.24 g), and MBd was adopted from Azuma et al. (2016) as 2,500 g. It turns out that the REQ of *Fukuivenator* is barely different from those of basal maniraptorans (Table 9), and close to the REQ of a late-diverging therizinosaurid *Erlikosaurus*. The similar REQs between an early-diverging therizinosaur *Fukuivenator* and a late-diverging therizinosaurid *Erlikosaurus* suggest that therizinosaurs did not acquire a large brain throughout their evolution.

The size of the olfactory bulb relative to the width of the cerebrum is considered an indicator of olfactory acuity (Zelenitsky et al., 2009, 2011). The maximum width of the

cerebrum and the length of the olfactory bulb were measured on *Fukuivenator* and the relative size of the olfactory bulb was calculated. Then, following Zelenitsky et al. (2009), a regression analysis was conducted between the relative olfactory bulb size and the body weight for theropods (Fig. 59), which suggests that *Fukuivenator* had the most acute sense of smell among them. Presence of the relatively large olfactory bulb with unusually acute sense of smell in early-diverging therizinosaur *Fukuivenator* supports Lautenschlager et al. (2012) arguing that therizinosaurs had a well-developed sense of olfaction as a plesiomorphic feature.

As demonstrated by Azuma et al. (2016), the semicircular canals of *Fukuivenator* are also quite sophisticated among theropods, indicating an acute sense of balance equilibrium of the animal. Following Gleich et al. (2005), the best frequency of hearing range and highfrequency hearing limit were estimated 1477 Hz and 3766 Hz, respectively, based on the length of the cochlear duct. These values are within the range of values calculated for other therizinosaurs. These values are close to those of a tyrannosaurid *Gorgosaurus* (Witmer and Ridgely, 2009; Sakagami and Kawabe, 2020), indicating that *Fukuivenator* was able to perceive a wide range of sound among dinosaurs.

Omnivory of *Fukuivenator*

As noted by Azuma et al. (2016), *Fukuivenator* exhibits the heterodont dentition with incisiform mesialmost teeth, unserrated mesial teeth, symmetrical lateral teeth and non-ziphodont whole dentition. Such dental features, as well as the increased number of cervical vertebrae, are consistent with the traits correlated with herbivory (Zanno and Makovicky, 2011). The elongated cervical region is indeed common in purportedly herbivorous therizinosaurs (*Falcarius*, *Nanshiungosaurus*, *Neimongosaurus*), oviraptorosaurs (Osmólska et al., 2004; Balanoff and Norell, 2012), *Jinfengopteryx* (Ji et al., 2005), and numerous avialans. On the other hand, the recurved, well-pointed posterior maxillary teeth of *Fukuivenator* are somewhat reminiscent of carnivorous theropods, despite the lack of denticles. Additionally, many herbivorous dental traits, such as elongate premaxillary teeth, lack of mesial teeth, lanceolate lateral teeth, and densely packed dentition, are absent in the dentition of *Fukuivenator*. These lines of evidence probably indicate the omnivorous diet of the animal. If such condition reflects the dietary shift from the carnivory (Azuma et al., 2016), the carnivory is likely plesiomorphic in the clade Therizinosauria + Pennaraptora and possibly retained in Deinonychosauria, while the omnivory and herbivory are acquired in the rest of the clade.

The higher olfactory ratios seen in carnivorous tyrannosaurids and dromaeosaurids suggest that they largely relied on olfaction than in other theropods, probably to accommodate for the diminished vision effectiveness in low-light conditions, to locate food sources, and/or to navigate larger home ranges (Zelenitsky et al., 2009). On the contrary, ornithomimosaurs and oviraptorids exhibit lower olfactory ratios suggesting that they relied more on sight than on olfaction, possibly reflecting adaptations for the omnivorous diet (Zelenitsky et al., 2009), although herbivory is inferred in some of them (Zanno and Makovicky, 2011). The large olfactory acuity is also known in *Erlikosaurus* and is hypothesized as an ancestral feature of Therizinosauria, which is widely regarded as herbivorous (Lautenschlager et al., 2012). The unusually large olfactory ratio of *Fukuivenator* not only supports the idea, but also suggests that the exceptional olfactory ability is a synapomorphic feature of Therizinosauria, possibly evolved as a response to a dietary shift.

CONCLUSIONS

Description of the holotype specimen of *Fukuivenator paradoxus* with aids of CT techniques clarifies its notable morphological features unknown in the original description. Among them, re-identification of some cranial elements causes both the retraction of previously suggested diagnostic characters as well as the discovery of additional ones. The phylogenetic analyses using an additional set of morphological features of *Fukuivenator* reveals that the animal is an unambiguous member of Maniraptora placed at the base of Therizinosauria. Along with some therizinosaurian synapomorphies, *Fukuivenator* exhibits morphological features related to the herbivorous diet while retaining reminiscence of the carnivorous diet, indicating that the animal is likely adapted to the omnivory as a transitional stage of the dietary shift that occurred at the earliest stage of therizinosaurian evolution. In addition, the revised brain endocast with newly identified parietals reveals the highest olfactory ratio of *Fukuivenator* among theropods, indicating that the exceptional olfactory ability could be a synapomorphy of Therizinosauria.

Although dinosaurs are widely popular in Japan among the public, their fossils are fairly limited in quality and quantity compared with dinosaur-rich areas in the world such as North America, China and Argentina. Among the dinosaur remains from Japan, the occurrence of *Fukuivenator* is notable due to its outstanding preservation, unusually unique morphological features and its unexpected phylogenetic position within theropods. Due to its close relationship to the stem-lineage, future studies on *Fukuivenator* will substantially contribute to understand the evolutionary history of maniraptoran theropods toward birds in numerous perspectives, including the functional, ecological and biogeographical aspects. Additionally, this study highlights the importance of further exploration at the Kitadani Dinosaur Quarry to comprehend the evolutionary history of dinosaurs in the Early Cretaceous.

ACKNOWLEDGEMENTS

The authors thank all people who contributed to the first through fourth Dinosaur Excavation Projects in Fukui since 1989, as well as to the preparators at FPDM for their patient and skillful work. The authors are grateful to the late Junchang Lü for his considerable support to the earlier phase of the investigation on the specimen. The authors also thank Stephen Brusatte (University of Edinburgh, UK) and an anonymous

reviewer who provided detailed and insightful reviews that greatly improved this manuscript.

APPENDIX

Character-state codings for *Fukuivenator paradoxus* for the character-taxon matrix of Brusatte et al. (2014) updated by Nesbitt et al. (2019).

??????11101010011011?????00201??????0012??10100?????00
00110??0?????000????????0?0200??0??0110000111001111001
01100001100100102?????000200101020?0???10001???????????
?????????????100?000100?00?00?010000000?0?000??00???0
?00?0?0???0?????001?0000?10??00??0???0?????010200???0??
0?0??00????0??????00?000????????????00100100000120?????
????????20010?000001010101??????1100???010000001000?0
00???00000??00000??????????0?000000000000000000000?0
?1000000?0001201000?00???0010????????000000?????????
0110100?0000000?000???0???00??000001111???10??0??01
000?0?????????????????????0?00???000?0000000?0000?0011
00?000???0??10100010100???????????01?????????????????01
0?00100000010110000 1?00100000000010?10?0100????????0
??????0?001???0?01?00000020000???00101?00??01?10??1??0
000100?0?100000????00002??1??000110000001000?????????
0000??000000000000?0??100?000111?0100?????01

REFERENCES

Azuma, Y. 2003. Early Cretaceous vertebrate remains from Katsuyama City, Fukui Prefecture, Japan. Memoir of the Fukui Prefectural Dinosaur Museum 21:17–21.

Azuma, Y., and P. J. Currie. 2000. A new carnosaur (Dinosauria: Theropoda) from the Lower Cretaceous of Japan. Canadian Journal of Earth Sciences 37:1735–1753.

Azuma, Y., and M. Shibata. 2010. *Fukuititan nipponensis*, a new titanosauriform sauropod from the Early Cretaceous Tetori Group of Fukui Prefecture, Japan. Acta Geologica Sinica - English Edition 84:454–462.

Azuma, Y., X. Xu, M. Shibata, S. Kawabe, K. Miyata and T. Imai. 2016. A bizarre theropod from the Early Cretaceous of Japan highlighting mosaic evolution among coelurosaurians. Scientific Reports 6:20478.

Balanoff, A. M., and M. A. Norell. 2012. Osteology of Khaan mckennai (Oviraptorosauria: Theropoda). Bulletin of the American Museum of Natural History 372:1–36.

Balanoff, A. M., M. A. Norell, A. V. C. Hogan and G. S. Bever. 2018. The endocranial cavity of oviraptorosaur dinosaurs and the increasingly complex, deep history of the avian brain. Brain, Behavior and Evolution 91:125–135.

Balanoff, A. M., X. Xu, Y. Kobayashi, Y. Matsufune and M. A. Norell. 2009. Cranial osteology of the theropod dinosaur *Incisivosaurus gauthieri* (Theropoda: Oviraptorosauria). American Museum Novitates 3651:1–35.

Barsbold, R. 1974. Saurornithoididae, a new family of small theropod dinosaurs from Central Asia and North America. Palaeontologia Polonica 30:5–22.

Barsbold, R. 1981. Toothless dinosaurs of Mongolia. Trudy Sovmestnoi SovetskoMongol'skoi Paleontologicheskoi Ekspeditsii 15:28–39.

Barsbold, R., H. Osmólska, M. Watabe, P. J. Currie and K. Tsogtbaatar. 2000b. A new oviraptorosaur (Dinosauria, Theropoda) from Mongolia: The first dinosaur with a pygostyle. Acta Palaeontologica Polonica 45:97–106.

Barsbold, R., P. J. Currie, N. P. Myhrvold, H. Osmólska, K. Tsogtbaatar and M. Watabe. 2000a. A pygostyle from a non-avian theropod. Nature 403:155–156.

Baumel, J. J., and L. M. Witmer. 1993. Osteologia; pp. 45–132 *in* J. J. Baumel, A. S. King, J. E. Breazile, H. E. Evans, and J. C. Vanden Berge (eds.), Handbook of Avian Anatomy: Nomina Anatomica Avium. Nuttal Ornithological Club, Cambridge, Massachusetts.

Bever, G. S., and M. A. Norell. 2009. The perinate skull of *Byronosaurus* (Troodontidae) with observations on the cranial ontogeny of paravian theropods. American Museum Novitates 3657:1–52.

Bever, G. S., S. L. Brusatte, T. D. Carr, X. Xu, A. M. Balanoff and M. A. Norell. 2013. The braincase anatomy of the Late Cretaceous dinosaur *Alioramus* (Theropoda: Tyrannosauroidea). Bulletin of the American Museum of Natural History 376:1–72.

Bronzati, M., R. B. J. Benson, S. W. Evers, M. D. Ezcurra, S. F. Cabreira, J. Choiniere, K. N. Dollman, A. Paulina-Carabajal, V. J. Radermacher, L. Roberto-da-Silva, G. Sobral, M. R. Stocker, L. M. Witmer, M. C. Langer and S. J. Nesbitt. 2021. Deep evolutionary diversification of semicircular canals in archosaurs. Current Biology 31:2520-2529.e6.

Brochu, C. A. 2003. Osteology of *Tyrannosaurus rex*: Insights from a nearly complete skeleton and high-resolution computed tomographic analysis of the skull. Journal of Vertebrate Paleontology 22:1–138.

Brusatte, S. L., M. A. Norell, T. D. Carr, G. M. Erickson, J. R. Hutchinson, A. M. Balanoff, G. S. Bever, J. N. Choiniere, P. J. Makovicky and X. Xu. 2010. Tyrannosaur paleobiology: new research on ancient exemplar organisms. Science 329:1481–1485.

Brusatte, S. L., G. T. Lloyd, S. C. Wang and M. A. Norell. 2014. Gradual assembly of avian body plan culminated in rapid rates of evolution across the dinosaur-bird transition. Current Biology 24:2386–2392.

Burch, S. H. 2014. Complete forelimb myology of the basal theropod dinosaur *Tawa hallae* based on a novel robust muscle reconstruction method. Journal of Anatomy 225:271–297.

Carr, T. D. 2005. Phylogeny of Tyrannosauroidea (Dinosauria: Coelurosauria) with special reference to North American Forms. University of Toronto, 1170 pp.

Cerroni, M. A., and A. Paulina-Carabajal. 2019. Novel information on the endocranial morphology of the abelisaurid theropod Carnotaurus sastrei. Comptes Rendus Palevol 18:985–995.

Choiniere, J. N., J. M. Clark and M. A. Norell. 2014. Cranial osteology of *Haplocheirus sollers* Choiniere et al., 2010

(Theropoda: Alvarezsauroidea). American Museum Novitates 2010:1–44.

Choiniere, J. N., C. A. Forster and W. J. de Klerk. 2012. New information on *Nqwebasaurus thwazi*, a coelurosaurian theropod from the Early Cretaceous Kirkwood Formation in South Africa. Journal of African Earth Sciences 71–72:1–17.

Choiniere, J. N., J. M. Clark, C. A. Forster and X. Xu. 2010a. A basal coelurosaur (Dinosauria: Theropoda) from the Late Jurassic (Oxfordian) of the Shishugou Formation in Wucaiwan, People's Republic of China. Journal of Vertebrate Paleontology 30:1773–1796.

Choiniere, J. N., X. Xu, J. M. Clark, C. A. Forster, Y. Guo and F. Han. 2010b. A basal alvarezsauroid theropod from the early Late Jurassic of Xinjiang, China. Science 327:571–574.

Clarke, J. A., Z. Zhou and F. Zhang. 2006. Insight into the evolution of avian flight from a new clade of Early Cretaceous ornithurines from China and the morphology of *Yixianornis grabaui*. Journal of Anatomy 208:287–308.

Claessens, L. P. A. M. 2004. Dinosaur gastralia; origin, morphology, and function. Journal of Vertebrate Paleontology 24:89–106.

Colbert, E. H., and D. A. Russell. 1969. The small Cretaceous dinosaur *Dromaeosaurus*. American Museum Novitates 2380:1–49.

Currie, P. J. 1985. Cranial anatomy of *Stenonychosaurus inequalis* (Saurischia, Theropoda) and its bearing on the origin of birds. Canadian Journal of Earth Sciences 22:1643–1658.

Currie, P. J. 1987. Bird-like characteristics of the jaws and teeth of troodontid theropods (Dinosauria, Saurischia). Journal of Vertebrate Paleontology 7:72–81.

Currie, P. J. 1995. New information on the anatomy and relationships of *Dromaeosaurus albertensis* (Dinosauria: Theropoda). Journal of Vertebrate Paleontology 15:576–591.

Currie, P. J., and D. A. Russell. 1988. Osteology and relationships of *Chirostenotes pergracilis* (Saurischia, Theropoda) from the Judith River (Oldman) Formation of Alberta, Canada. Canadian Journal of Earth Sciences 25:972–986.

Currie, P. J., and D. J. Varricchio. 2004. A new dromaeosaurid from the Horseshoe Canyon Formation (Upper Cretaceous) of Alberta, Canada; pp. 112–132 *in* P. J. Currie, E. B. Koppelhus, M. A. Shugar, and J. L. Wright (eds.), Feathered Dragons: Studies on the Transition from Dinosaurs to Birds. Indiana University Press, Bloomington.

Currie, P. J., and X. Zhao. 1993a. A new carnosaur (Dinosauria, Theropoda) from the Jurassic of Xinjiang, People's Republic of China. Canadian Journal of Earth Sciences 30:2037–2081.

Currie, P. J., and X. Zhao. 1993b. A new troodontid (Dinosauria, Theropoda) braincase from the Dinosaur Park Formation (Campanian) of Alberta. Canadian Journal of Earth Sciences 30:2231–2247.

Daqing, L., P. Cuo, Y. Hailu, M. C. Lamanna, J. D. Harris, K. J. Lacovara and Z. Jianping. 2007. A large therizinosauroid (Dinosauria: Theropoda) from the Early Cretaceous of Northwestern China. Acta Geologica Sinica - English Edition 81:539–549.

Domínguez Alonso, P., A. C. Milner, R. A. Ketcham, M. J. Cookson and T. B. Rowe. 2004. The avian nature of the brain and inner ear of *Archaeopteryx*. Nature 430:666–669.

Dong, Z. 1979. Dinosaurs from the Cretaceous of South China; pp. 342–350 *in* Institute of Vertebrate Paleontology and Paleoanthropology and Nanjing Institute of Paleontology (eds.), Mesozoic and Cenozoic Red Beds of South China: Selected Papers from the Cretaceous-Tertiary Workshop, Nanxiong, Guangdong Province. Science Press, Beijing.

Eddy, D. R., and J. A. Clarke. 2011. New information on the cranial anatomy of *Acrocanthosaurus atokensis* and its implications for the phylogeny of Allosauroidea (Dinosauria: Theropoda). PLOS ONE 6:e17932.

Franzosa, J. W. 2004. Evolution of the brain in Theropoda (Dinosauria). Ph.D. dissertation, The University of Texas at Austin, Austin, Texas, 357 pp.

Gauthier, J. A. 1986. Saurischian monophyly and the origin of birds. Memoirs of the California Academy of Sciences 8:1–55.

Gleich, O., R. J. Dooling and G. A. Manley. 2005. Audiogram, body mass, and basilar papilla length: correlations in birds and predictions for extinct archosaurs. Naturwissenschaften 92:595–598.

Godefroit, P., A. Cau, H. Dong-Yu, F. Escuillié, W. Wenhao and G. Dyke. 2013. A Jurassic avialan dinosaur from China resolves the early phylogenetic history of birds. Nature 498:359–62.

Gold, M. E. L., S. L. Brusatte and M. A. Norell. 2013. The cranial pneumatic sinuses of the tyrannosaurid *Alioramus* (Dinosauria: Theropoda) and the evolution of cranial pneumaticity in theropod dinosaurs. American Museum Novitates 3790:1–46.

Goloboff, P. A., and S. A. Catalano. 2016. TNT version 1.5, including a full implementation of phylogenetic morphometrics. Cladistics 32:221–238.

Goto, M., A. Yabe and S. Sano. 2002. The research report of the Dinosaur Fossil Exploratory Excavation held by Fukui Prefecture in 2001. Memoir of the Fukui Prefectural Dinosaur Museum 1:102–118.

Hanson, M., E. A. Hoffman, M. A. Norell and B. S. Bhullar. 2021. The early origin of a birdlike inner ear and the evolution of dinosaurian movement and vocalization. Science 372:601–609.

He, T., X. Wang and Z. Zhou. 2008. A new genus and species of caudipterid dinosaur from the Lower Cretaceous Jiufotang Formation of western Liaoning, China. Vertebrata Palasiatica 46:178–189.

Hendrickx, C., and O. Mateus. 2014. *Torvosaurus gurneyi* n. sp., the largest terrestrial predator from Europe, and a proposed terminology of the maxilla anatomy in nonavian theropods. PLOS ONE 9:e88905.

Hendrickx, C., O. Mateus and R. Araújo. 2015. A proposed terminology of theropod teeth (Dinosauria, Saurischia).

Journal of Vertebrate Paleontology 35:e982797.
Hendrickx, C., O. Mateus, R. Araújo and J. Choiniere. 2019. The distribution of dental features in non-avian theropod dinosaurs: Taxonomic potential, degree of homoplasy, and major evolutionary trends. Palaeontologia Electronica 22:1–110.
Holtz, T. R., Jr., 1995. The arctometatarsalian pes, an unusual structure of the metatarsus of Cretaceous Theropoda (Dinosauria: Saurischia). Journal of Vertebrate Paleontology 14:480–519.
Holtz, T. R., Jr., 2001. The Phylogeny and Taxonomy of the Tyrannosauridae; pp. 64–83 *in* D. H. Tanke and K. Carpenter (eds.), Mesozoic Vertebrate Life. Indiana University Press, Bloomington.
von Huene, F. 1914. Das natürliche system der Saurischia. Zentralblatt für Mineralogie, Geologie und Paläontologie Abteilung B 5:154–158.
Hurlburt, G. R. 1996. Relative brain size in Recent and fossil amniotes: determination and interpretation. Ph.D. dissertation, University of Toronto, Toronto, Ontario, 250 pp.
Hurlburt, G. R., R. C. Ridgely and L. M. Witmer. 2013. Relative size of brain and cerebrum in tyrannosaurid dinosaurs: an analysis using brain-endocast quantitative relationships in extant alligators; pp. 134–154 *in* J. M. Parrish, M. Henderson, P. J. Currie, and E. Koppelhus (eds.), Tyrannosaurid Paleobiology. Indiana University Press, Bloomington.
Hutchinson, J. R. 2001. The evolution of femoral osteology and soft tissues on the line to extant birds (Neornithes). Zoological Journal of the Linnean Society 131:169–197.
Hwang, S. H., M. A. Norell, Q. Ji and K. Gao. 2002. New Specimens of *Microraptor zhaoianus* (Theropoda: Dromaeosauridae) from Northeastern China. American Museum Novitates 3381:1–44.
Hwang, S. H., M. A. Norell, Q. Ji and K. Gao. 2004. A large compsognathid from the Early Cretaceous Yixian Formation of China. Journal of Systematic Palaeontology 2:13–30.
Imai, T., Y. Azuma, S. Kawabe, M. Shibata, K. Miyata, M. Wang and Z. Zhou. 2019. An unusual bird (Theropoda, Avialae) from the Early Cretaceous of Japan suggests complex evolutionary history of basal birds. Communications Biology 2:399.
Ji, Q., P. J. Currie, M. A. Norell, and S. Ji. 1998. Two feathered dinosaurs from northeastern China. Nature 393:753–761.
Ji, Q. Q., S. S. Ji, J. Lü, H. You, W. Chen, Y. Y. Liu and Y. Y. Liu. 2005. First avialian bird from China. Geological Bulletin of China 24:197–210.
Kirkland, J. I., and D. G. Wolfe. 2001. First definitive therizinosaurid (Dinosauria; Theropoda) from North America. Journal of Vertebrate Paleontology 21:410–414.
Kobayashi, Y., and Y. Azuma. 2003. A new iguanodontian (Dinosauria: Ornithopoda) from the Lower Cretaceous Kitadani Formation of Fukui Prefecture, Japan. Journal of Vertebrate Paleontology 23:166–175.
Kobayashi, Y., and R. Barsbold. 2005. Reexamination of a primitive ornithomimosaur, *Garudimimus brevipes* Barsbold, 1981 (Dinosauria: Theropoda), from the Late Cretaceous of Mongolia. Canadian Journal of Earth Sciences 42:1501–1521.
Kobayashi, Y., and R. Barsbold. 2005. Anatomy of *Harpymimus okladnikovi* Barsbold and Perle 1984 (Dinosauria; Theropoda) of Mongolia; pp. 97–126 in K. Carpenter (ed.), The Carnivorous Dinosaurs. Indiana University Press.
Kobayashi, Y., and J. Lü. 2003. A new ornithomimid dinosaur with gregarious habits Bloomington from the Late Cretaceous of China. Acta Palaeontologica Polonica 48:235–259.
Kubota, K. 2005. Charophyte gyrogonites from the Lower Cretaceous Kitadani Formation of the Tetori Group in the Takinamigawa area, Katsuyama City, Fukui Prefecture, central Japan. Paleontological Research 9:203–213.
Kundrát, M. 2007. Avian-like attributes of a virtual brain model of the oviraptorid theropod *Conchoraptor gracilis*. Naturwissenschaften 94:499–504.
Kundrát, M., and J. Janáček. 2007. Cranial pneumatization and auditory perceptions of the oviraptorid dinosaur *Conchoraptor gracilis* (Theropoda, Maniraptora) from the Late Cretaceous of Mongolia. Naturwissenschaften 94:769–778.
Kundrát, M., X. Xu, M. Hančová, A. Gajdoš, Y. Guo and D. Chen. 2020. Evolutionary disparity in the endoneurocranial configuration between small and gigantic tyrannosauroids. Historical Biology 32:620–634.
Kurzanov, S. M. 1981. An unusual theropod from the Upper Cretaceous of Mongolia. Trudy Sovmestnoi Sovetsko-Mongol'skoi Paleontologicheskoi Ekspeditsii 15:39–50.
Lautenschlager, S., E. J. Rayfield, P. Altangerel, L. E. Zanno and L. M. Witmer. 2012. The endocranial anatomy of Therizinosauria and its implications for sensory and cognitive function. PLOS ONE 7:e52289.
Lautenschlager, S., L. M. Witmer, P. Altangerel, L. E. Zanno and E. J. Rayfield. 2014. Cranial anatomy of *Erlikosaurus andrewsi* (Dinosauria, Therizinosauria): new insights based on digital reconstruction. Journal of Vertebrate Paleontology 34:1263–1291.
Lee, Y., R. Barsbold, P. J. Currie, Y. Kobayashi, H. Lee, P. Godefroit, F. Escuillié and T. Chinzorig. 2014. Resolving the long-standing enigmas of a giant ornithomimosaur *Deinocheirus mirificus*. Nature 515:257–260.
Liao, C., L. E. Zanno, S. Wang and X. Xu. 2021. Postcranial osteology of *Beipiaosaurus inexpectus* (Theropoda: Therizinosauria). PLOS ONE 16:e0257913.
Lü, J., L. Xu, Y. Liu, X. Zhang, S. Jia and Q. Ji. 2010. A new troodontid theropod from the Late Cretaceous of central China, and the radiation of Asian troodontids. Acta Palaeontologica Polonica 55:381–388.
Maddison, W. P., and D. R. Maddison. 2019. Mesquite: a modular system for evolutionary analysis. Version 3.61.
Makovicky, P. J., and M. A. Norell. 1998. A partial ornithomimid braincase from Ukhaa Tolgod (Upper Cretaceous, Mongolia). American Museum Novitates 3247:1–16.
Makovicky, P. J., and H.D. Sues. 1998. Anatomy and

phylogenetic relationships of the theropod dinosaur *Microvenator celer* from the Lower Cretaceous of Montana. American Museum Novitates 3240:1–15.

Makovicky, P. J., S. Apesteguía and F. L. Agnolín. 2005. The earliest dromaeosaurid theropod from South America. Nature 437:1007–1011.

Makovicky, P. J., Y. Kobayashi and P. J. Currie. 2004. Ornithomimosauria; pp. 137–150 *in* D. B. Weishampel, P. Dodson, and H. Osmólska (eds.), The Dinosauria, 2nd ed. University of California Press, Berkeley.

Makovicky, P. J., M. A. Norell, J. M. Clark and T. Rowe. 2003. Osteology and relationships of *Byronosaurus jaffei* (Theropoda: Troodontidae). American Museum Novitates 3402:1–32.

Marsh, O. C. 1881. Principal characters of American dinosaurs, part V. American Journal of Science 16:417–423.

Maryańska, T., H. Osmólska and M. Wolsan. 2002. Avialan status for Oviraptorosauria. Acta Paleontologica Polonica 47:97–116.

Nesbitt, S. J., R. K. Denton, M. A. Loewen, S. L. Brusatte, N. D. Smith, A. H. Turner, J. I. Kirkland, A. T. McDonald and D. G. Wolfe. 2019. A mid-Cretaceous tyrannosauroid and the origin of North American end-Cretaceous dinosaur assemblages. Nature Ecology & Evolution 3: 892–899.

Nicholls, E. L., and A. P. Russell. 1985. Structure and function of the pectral girdle and forelimb of *Struthiomimus altus* (Theropoda: Ornithomimidae). Palaeontology 28:643–647.

Norell, M. A., and P. J. Makovicky. 1997. Important features of the dromaeosaur skeleton: information from a new specimen. American Museum Novitates 3215:1–28.

Norell, M. A., and P. J. Makovicky. 1999. Important features of the dromaeosaurid skeleton II: Information from newly collected specimens of *Velociraptor mongoliensis*. American Museum Novitates 3282:1–27.

Norell, M. A., and P. J. Makovicky. 2004. Dromaeosauridae; pp. 196–209 *in* D. B. Weishampel, P. Dodson, and H. Osmólska (eds.), The Dinosauria, 2nd ed. University of California Press, Berkeley.

Norell, M. A., P. J. Makovicky and J. M. Clark. 2000. A new troodontid theropod from ukhaa tolgod, Mongolia. Journal of Vertebrate Paleontology 20:7–11.

Norell, M. A., P. J. Makovicky and J. M. Clark. 2004. The braincase of *Velociraptor*; pp. 133–143 *in* P. J. Currie, E. B. Koppelhus, M. A. Shugar, and J. L. Wright (eds.), Feathered Dragons: Studies on the Transition from Dinosaurs to Birds. Indiana University Press, Bloomington.

Norell, M. A., J. M. Clark, A. H. Turner, P. J. Makovicky, R. Barsbold and T. Rowe. 2006. A new dromaeosaurid theropod from Ukhaa Tolgod (Ömnögov, Mongolia). American Museum Novitates 3545:1–51.

Norell, M. A., P. J. Makovicky, G. S. Bever, A. M. Balanoff, J. M. Clark, R. Barsbold and T. Rowe. 2009. A review of the Mongolian Cretaceous dinosaur *Saurornithoides* (Troodontidae: Theropoda). American Museum Novitates 3654:1–63.

Novas, F. E. 1997. Anatomy of *Patagonykus puertai* (Theropoda, Avialae, Alvarezsauridae), from the Late Cretaceous of Patagonia. Journal of Vertebrate Paleontology 17:137–166.

Osmólska, H., E. Roniewicz and R. Barsbold. 1972. A new dinosaur, *Gallimimus bullatus* n. gen., n. sp. (Ornithomimidae) from the Upper Cretaceous of Mongolia. Palaeontologia Polonica 27:103–143.

Osmólska, H., P. J. Currie and R. Barsbold. 2004. Oviraptorosauria; pp. 165–183 *in* D. B. Weishampel, P. Dodson, and H. Osmólska (eds.), The Dinosauria, 2nd ed. University of California Press, Berkeley.

Ostrom, J. H. 1969. Osteology of *Deinonychus antirrhopus*, an unusual theropod from the Lower Cretaceous of Montana. Peabody Museum of Natural History Bulletin 30:1–165.

Ostrom, J. H. 1978. The osteology of *Compsognathus longipes* Wagner. Zitteliana 4:73–118.

Owen, R. 1842. Report on British fossil reptiles, part II. Reports of the British Association for the Advancement of Science 11:60–204.

Pei, R., M. A. Norell, D. E. Barta, G. S. Bever, M. Pittman and X. Xu. 2017. Osteology of a new Late Cretaceous troodontid specimen from Ukhaa Tolgod, Ömnögovi Aimag, Mongolia. American Museum Novitates 3889:1–47.

Pérez-Moreno, B. P., J. L. Sanz, A. D. Buscalloni, J. J. Moratalla, F. Ortega and D. Rasskin-Gutman. 1994. A unique multitoothed ornithomimosaur dinosaur from the Lower Cretaceous of Spain. Nature 370:363–367.

Perle, A., L. M. Chiappe, R. Barsbold, J. M. Clark and M. A. Norell. 1994. Skeletal morphology of *Mononykus olecranus* (Theropoda: Avialae) from the Late Cretaceous of Mongolia. American Museum Novitates 3105:1–29.

Persons, W. S., P. J. Currie and M. A. Norell. 2014. Oviraptorosaur tail forms and functions. Acta Palaeontologica Polonica 59:553–567.

Pu, H., Y. Kobayashi, J. Lü, L. Xu, Y. Wu, H. Chang, J. Zhang and S. Jia. 2013. An unusual basal therizinosaur dinosaur with an ornithischian dental arrangement from Northeastern China. PLOS ONE 8:e63423.

Rauhut, O. W. M. 2003. The interrelationships and evolution of basal theropod dinosaurs. Special Papers in Palaeontology 69:1–213.

Rauhut, O. W. M. 2004. Braincase structure of the Middle Jurassic theropod dinosaur *Piatnitzkysaurus*. Canadian Journal of Earth Sciences 41:1109–1122.

Rauhut, O. W. M., and R. Fechner. 2005. Early development of the facial region in a non-avian theropod dinosaur. Proceedings of the Royal Society B: Biological Sciences 272:1179–1183.

van der Reest, A. J., and P. J. Currie. 2017. Troodontids (Theropoda) from the Dinosaur Park Formation, Alberta, with a description of a unique new taxon: implications for deinonychosaur diversity in North America. Canadian Journal of Earth Sciences 935:919–935.

Russell, D. A., and Z. Dong. 1993. The affinities of a new

theropod from the Alxa Desert, Inner Mongolia, People's Republic of China. Canadian Journal of Earth Sciences 30:2107–2127.

Sakagami, R., and S. Kawabe. 2020. Endocranial anatomy of the ceratopsid dinosaur *Triceratops* and interpretations of sensory and motor function. PeerJ 8:e9888.

Sakai, Y., Y. Tsutsumi, N. Kusuhashi, T. Sonoda, K. Horie and A. Matsuoka. 2019. Zircon LA-ICP-MS U-Pb age of a tuff from the Akaiwa Formation of the Tetori Group in the Shiramine area, Ishikawa Prefecture, central Japan. The Journal of the Geological Society of Japan 125:255–260.

Sano, S. 2015. New view of the stratigraphy of the Tetori Group in Central Japan. Memoir of the Fukui Prefectural Dinosaur Museum 14:25–61.

Sano, S., and A. Yabe. 2017. Fauna and flora of Early Cretaceous Tetori Group in Central Japan: The clues to revealing the evolution of Cretaceous terrestrial ecosystem in East Asia. Palaeoworld 26:253–267.

Sereno, P. C. 2001. Alvarezsaurids: birds or ornithomimosaurs?; pp. 69–98 *in* J. Gauthier and L. F. Gall (eds.), New Perspectives on the Origin and Early Evolution of Birds. Yale University Press, New Haven.

Sereno, P. C. 2017. Early Cretaceous Ornithomimosaurs (Dinosauria: Coelurosauria) from Africa. Ameghiniana 54:576–616.

Shibata, M., and Y. Azuma. 2015. New basal hadrosauroid (Dinosauria: Ornithopoda) from the Lower Cretaceous Kitadani Formation, Fukui, central Japan. Zootaxa 3914:421–440.

Shibata, M., and M. Goto. 2008. Report of the 3rd Dinosaur Excavation Project in Katsuyama, Fukui, 2007. Memoir of the Fukui Prefectural Dinosaur Museum 7:109–116.

Shuan, J., and J. Qiang. 2007. *Jinfengopteryx* compared to *Archaeopteryx*, with comments on the mosaic evolution of long-tailed avialan birds. Acta Geologica Sinica - English Edition 81:337–343.

Smith, D. K. 2014. The braincase of the North American therizinosaurian *Nothronychus mckinleyi* (Dinosauria, Theropoda). Journal of Vertebrate Paleontology 34:635–646.

Smith, D. K., R. K. Sanders and D. G. Wolfe. 2018. A re-evaluation of the basicranial soft tissues and pneumaticity of the therizinosaurian *Nothronychus mckinleyi* (Theropoda; Maniraptora). PLOS ONE 13:e0198155.

Smith, D. K., L. E. Zanno, R. K. Sanders, D. D. Deblieux and J. I. Kirkland. 2011. New information on the braincase of the North American therizinosaurian (Theropoda, Maniraptora) *Falcarius utahensis*. Journal of Vertebrate Paleontology 31:387–404.

Tahara, R., and H. C. E. Larsson. 2011. Cranial pneumatic anatomy of *Ornithomimus edmontonicus* (Ornithomimidae: Theropoda). Journal of Vertebrate Paleontology 31:127–143.

Turner, A. H., P. J. Makovicky and M. A. Norell. 2012. A review of dromaeosaurid systematics and paravian phylogeny. Bulletin of the American Museum of Natural History 371:1–206.

Vanden Berge, J. C. 1975. Aves Myology; pp. 1802–1848 *in* R. Getty (ed.), The Anatomy of the Domestic Animals, 5th ed. W. B. Saunders, Philadelphia.

Wang, W., and J. K. O'Connor. 2017. Morphological coevolution of the pygostyle and tail feathers in Early Cretaceous birds. Vertebrata PalAsiatica 55:289–314.

Wilson, J. A. 1999. A nomenclature for vertebral laminae in sauropods and other saurischian dinosaurs. Journal of Vertebrate Paleontology 19:639–653.

Wilson, J. A. 2012. New vertebral laminae and patterns of serial variation in vertebral laminae of sauropod dinosaurs. Contributions from the Museum of Paleontology University of Michigan 32:91–110.

Wilson, J. A., M. D. D' Emic, T. Ikejiri, E. M. Moacdieh and J. A. Whitlock. 2011. A nomenclature for vertebral fossae in sauropods and other saurischian dinosaurs. PLOS ONE 6:e17114.

Witmer, L. M. 1997. The evolution of the antorbital cavity of archosaurs: a study in soft-tissue reconstruction in the fossil record with an analysis of the function of pneumaticity. Journal of Vertebrate Paleontology 17:1–76.

Witmer, L. M., and R. C. Ridgely. 2009. New insights into the brain, braincase, and ear region of tyrannosaurs (Dinosauria, Theropoda), with implications for sensory organization and behavior. Anatomical Record 292:1266–1296.

Xu, L., Y. Kobayashi, J. Lü, Y. Lee, Y. Liu, K. Tanaka, X. Zhang, S. Jia and J. Zhang. 2011. A new ornithomimid dinosaur with North American affinities from the Late Cretaceous Qiupa Formation in Henan Province of China. Cretaceous Research 32:213–222.

Xu, X., Y. Cheng, X. Wang and C. Chang. 2002a. An unusual oviraptorosaurian dinosaur from China. Nature 685:291–293.

Xu, X., Y. Cheng, X. Wang and C. Chang. 2003. Pygostyle-like structure from *Beipiaosaurus* (Theropoda, Therizinosauroidea) from the Lower Cretaceous Yixian Formation of Liaoning, China. Acta Geologica Sinica - English Edition 77:294–298.

Xu, X., M. A. Norell, X. Wang, P. J. Makovicky and X. Wu. 2002b. A basal troodontid from the Early Cretaceous of China. Nature 415:780–784.

Xu, X., X. Zhang, P. C. Sereno, X. Zhao, U. Kuang, J. Han and L. Tan. 2002c. A new therizinosauroid (Dinosauria, Theropoda) from the Upper Cretaceous Iren Dabasu Formation of Nei Mongol. Vertebrata PalAsiatica 40:228–240.

Xu, X., M. Pittman, C. Sullivan, J. N. Choiniere, Q. Tan, J. M. Clark, M. A. Norell and S. Wang. 2015. The taxonomic status of the Late Cretaceous dromaeosaurid *Linheraptor exquisitus* and its implications for dromaeosaurid systematics. Vertebrata PalAsiatica 53:29–62.

Xu, X., J. Choiniere, Q. Tan, R. B. J. Benson, J. Clark, C. Sullivan, Q. Zhao, F. Han, Q. Ma, Y. He, S. Wang, H. Xing and L. Tan. 2018. Two Early Cretaceous fossils document transitional stages in alvarezsaurian dinosaur evolution. Current Biology 28:2853-2860.e3.

Yin, Y., R. Pei and C. Zhou. 2018. Cranial morphology of

Sinovenator changii (Theropoda: Troodontidae) on the new material from the Yixian Formation of western Liaoning, China. PeerJ 6:e4977.

Zanno, L. E. 2006. The pectoral girdle and forelimb of the primitive therizinosauroid *Falcarius utahensis* (Theropoda, Maniraptora): analyzing evolutionary trends within Therizinosauroidea. Journal of Vertebrate Paleontology 26:636–650.

Zanno, L. E. 2010. Osteology of *Falcarius utahensis* (Dinosauria: Theropoda): characterizing the anatomy of basal therizinosaurs. Zoological Journal of the Linnean Society 158:196–230.

Zanno, L. E., and P. J. Makovicky. 2011. Herbivorous ecomorphology and specialization patterns in theropod dinosaur evolution. Proceedings of the National Academy of Sciences 108:232–237.

Zanno, L. E., D. D. Gillette, L. B. Albright and A. L. Titus. 2009. A new North American therizinosaurid and the role of herbivory in "predatory" dinosaur evolution. Proceedings of the Royal Society B: Biological Sciences 276:3505–3511.

Zelenitsky, D. K., F. Therrien and Y. Kobayashi. 2009. Olfactory acuity in theropods: palaeobiological and evolutionary implications. Proceedings of the Royal Society B: Biological Sciences 276:667–673.

Zelenitsky, D. K., F. Therrien, R. C. Ridgely, A. R. McGee and L. M. Witmer. 2011. Evolution of olfaction in non-avian theropod dinosaurs and birds. Proceedings of the Royal Society B: Biological Sciences 278:3625–3634.